

I N T W O P A R T S

P A R T O N E

pp. 1 - 51

E N E R G Y R A T I O O F T H E S E I S M I C
W A V E S R E F L E C T E D A N D R E F R A C T E D
A T A R O C K W A T E R B O U N D A R Y

Thesis by

Kazim Ergin

In Partial Fulfillment of the Requirements
For the Degree of
Doctor of Philosophy

California Institute of Technology

Pasadena , California

1960

ACKNOWLEDGMENT

The writer owes a debt of gratitude to Dr. B. Gutenberg who supervised the work and gave generous constructive criticism at its different stages. He also wishes to express his thanks to Dr. C. F. Richter who made very valuable suggestions.

ABSTRACT

Using the Knott-Zoeppritz equations, the general behavior, zero points and extreme points of the energy ratio that goes into reflected and refracted waves upon the incidence of a wave at either side of the rock-water boundary at the bottom of the ocean are computed as a function of the angle of incidence, for a possible range of values of the parameters involved, namely, Poisson's ratio, the ratio of the longitudinal wave velocities in two media, and the density ratio.

From the computed results it is found that:

1. Poisson's ratio of the solid medium is a dominating factor in the general behavior, zero points and extreme points of the reflected and refracted waves that travel in the solid.
2. Any change in the ratio of the two longitudinal velocities produces pronounced results in the refracted wave energy.
3. The effect of changing the density ratio is very slight.
4. Peculiar behavior occurs just before and right after the critical angle of incidences.
5. At a critical angle of incidence, all of the incident energy goes into the reflected wave of the same kind as the incident wave.
6. Most of the incident energy is reflected either as P or as S wave depending upon the angle of incidence.

TABLE OF CONTENTS

TITLE	PAGE
Introduction	1
Symbols Used	2
Equation Used for Computation	3
Extreme Points	5
Computed Values	7
Summary and Conclusions	13
References	15
Tables	
Figures	

INTRODUCTION

The subject of energy ratios of seismic waves reflected and refracted at a discontinuity has been studied by various authors in the past. A list of references is given at the end of this paper. They deal mostly with the theory and computations concerning the cases where a wave is incident at a boundary between two solid media. Reflection at the surface of the earth has been studied by Zeppritz, Geiger and Gutenberg (18), Geiger and Gutenberg (17), Gutenberg (7) and by Jeffreys (8). The case of the mantle-core boundary has been computed by Dana (3). The present paper deals with the case of the ocean floor. We are particularly interested in zero points and extreme points of energy ratios of waves resulting from the incidence of a wave at either side of the discontinuity.

Since this work began a few years ago, a great deal of progress has been accomplished in the study of microseisms and their use as a hurricane detecting device. In this connection we hope that the results obtained in this paper may furnish some material for further studies concerning the passage of a wave, set up in the water by a storm, to the solid crustal layers.

SYMBOLS USED IN THIS PAPER:

P	Longitudinal Wave
S	Transverse Wave
SV	Component of S in the plane of propagation
SH	" " " perpendicular to the plane of propagation

Incident	Reflected		Refracted		
P	S	P	S	P	S
A	B	C	D	E	F
		e	d	e	f
α	β	α	β	γ	ζ
					Amplitudes
					Square root of energy ratio
					Angle of incidence
		v_{1p}	v_{1s}	v_{2p}	v_{2s}
		ρ_1		ρ_2	Velocity
					Density

σ Poisson's ratio

$$n = v_{1p} / v_{1s} = f(\sigma)$$

$$n = v_{2p} / v_{1p}$$

$$r = \rho_2 / \rho_1$$

EQUATIONS USED FOR COMPUTATION

Snell's law:

$$\sin \alpha : \sin \beta : \sin \gamma : \sin \xi = v_{1p} : v_{1s} : v_{2p} : v_{2s} \quad (1)$$

Blut's energy equations:

P wave incident in the solid against the water:

$$\frac{C^2}{A^2} + \frac{D^2}{A^2} \frac{\sin 2\beta}{\sin 2\alpha} + \frac{E^2}{A^2} \frac{\rho_2}{\rho_1} \frac{\sin 2\gamma}{\sin 2\alpha} = 1 \quad (2)$$

or

$$c^2 + d^2 + e^2 = 1$$

P wave incident in the water against the solid:

$$\frac{C^2}{A^2} + \frac{E^2}{A^2} \frac{\rho_2}{\rho_1} \frac{\sin 2\gamma}{\sin 2\alpha} + \frac{F^2}{A^2} \frac{\rho_2}{\rho_1} \frac{\sin 2\xi}{\sin 2\alpha} = 1 \quad (3)$$

or

$$c^2 + e^2 + f^2 = 1$$

SV wave incident in the solid against the water:

$$\frac{D^2}{B^2} + \frac{C^2}{B^2} \frac{\sin 2\alpha}{\sin 2\beta} + \frac{E^2}{B^2} \frac{\rho_2}{\rho_1} \frac{\sin 2\gamma}{\sin 2\beta} = 1 \quad (4)$$

or

$$d^2 + c^2 + e^2 = 1$$

Relation between σ and m

$$\sigma = \frac{1}{2} \left(1 - \frac{1}{m^2-1} \right) \quad (5)$$

The amplitude ratios $\frac{C}{A}$, $\frac{D}{A}$, $\frac{E}{A}$ and $\frac{F}{A}$ are computed from the following Zoeppritz equations:

P wave incident in the solid against the water:

$$A \cos \alpha - C \cos \alpha + D \sin \beta - E \cos \gamma = 0 \quad (6a)$$

$$- A \cos 2\beta - C \cos 2\beta + D/m, \sin 2\beta + E \cos \alpha = 0 \quad (6b)$$

$$- A \sin 2\alpha + C \sin 2\alpha + D m, \cos 2\beta = 0 \quad (6c)$$

Solving these three equations and making use of equation (2),

and also making use of the identity $m, \cos 2\beta \cos \alpha - \sin 2\alpha \sin 2\beta = m, \cos \alpha$, we

get for the square root of the energy ratios, c , d , and e :

$$c = \frac{\cos \gamma (m, \cos^2 2\beta - 1/m, \sin 2\alpha \sin 2\beta) - m, \cos \alpha \cos \gamma}{\cos \gamma (m, \cos^2 2\beta + 1/m, \sin 2\alpha \sin 2\beta) + m, \cos \alpha \cos \gamma} \quad (7)$$

$$d = \frac{2 \sqrt{\sin 2\alpha \sin 2\beta} \cos 2\beta \cos \gamma}{\cos \gamma (m, \cos^2 2\beta + 1/m, \sin 2\alpha \sin 2\beta) + m, \cos \alpha \cos \gamma} \quad (8)$$

$$e = \frac{2m_1 \sqrt{nr \cos \alpha \cos \gamma} \cos 2\beta}{\cos \gamma (m_1 \cos^2 2\beta + \gamma m_1 \sin 2\alpha \sin 2\beta) + m_1 nr \cos \alpha} \quad (9)$$

11. P. P wave incident in the water against the solid:

$$A \cos \alpha - C \cos \alpha - E \cos \gamma - F \sin \gamma = 0 \quad (10a)$$

$$-A - C + E nr \cos 2\beta + F \frac{\gamma n}{m_2} \sin 2\beta = 0 \quad (10b)$$

$$+ E \sin 2\gamma - F m_2 \cos 2\beta = 0 \quad (10c)$$

Solving these three equations and making use of equation (3), we get for the square root of the energy ratios, c, e and f:

$$c = \frac{\cos \gamma - nr \cos \alpha [1 - 2 \sin \beta \sin 2\beta (\cos \beta - \gamma m_2 \cos \gamma)]}{\cos \gamma + nr \cos \alpha [1 - 2 \sin \beta \sin 2\beta (\cos \beta - \gamma m_2 \cos \gamma)]} \quad (11)$$

$$e = \frac{2 \sqrt{nr \cos \alpha \cos \gamma} \cos 2\beta}{\cos \gamma + nr \cos \alpha [1 - 2 \sin \beta \sin 2\beta (\cos \beta - \gamma m_2 \cos \gamma)]} \quad (12)$$

$$f = \frac{2 \frac{\gamma n}{m_2} \sqrt{r \sin 2\alpha \sin 2\beta} \cos \gamma}{\cos \gamma + nr \cos \alpha [1 - 2 \sin \beta \sin 2\beta (\cos \beta - \gamma m_2 \cos \gamma)]} \quad (13)$$

SV wave incident in the solid against the water. (Note that in this case angle of incidence is β):

$$-B \sin \beta - C \cos \alpha + D \sin \beta - E \cos \gamma = 0 \quad (14a)$$

$$B \sin 2\beta - C m_1 \cos 2\beta + D \sin 2\beta + E m_1 nr = 0 \quad (14b)$$

$$-B \cos 2\beta + C \gamma m_1 \sin 2\alpha + D \cos 2\beta = 0 \quad (14c)$$

Solving these three equations and making use of equation (4), and again making use of the identity $m_1 \cos 2\beta \cos \alpha - \sin 2\alpha \sin \beta = m_1 \cos \alpha$, we get for the square root of the energy ratios, c, d and f:

$$d = \frac{\cos \gamma (m_1 \cos^2 2\beta - \gamma m_1 \sin 2\alpha \sin 2\beta) + m_1 nr \cos \alpha}{\cos \gamma (m_1 \cos^2 2\beta + \gamma m_1 \sin 2\alpha \sin 2\beta) + m_1 nr \cos \alpha} \quad (15)$$

$$c = \frac{2 \sqrt{\sin 2\alpha \sin 2\beta} \cos \alpha}{\cos \gamma (m_1 \cos^2 2\beta + \gamma m_1 \sin 2\alpha \sin 2\beta) + m_1 nr \cos \alpha} \quad (16)$$

$$e = \frac{2 \sqrt{r \sin \beta \sin 2\gamma} \cos \alpha}{\cos \gamma (m_1 \cos^2 2\beta + \gamma m_1 \sin 2\alpha \sin 2\beta) + m_1 nr \cos \alpha} \quad (17)$$

11. 4. SH wave incident in the solid against the water. For this particular case Zoeppritz equations reduce to

$$B = D$$

so that all of the energy is reflected as SH wave for all angles of incidence.

EXTREME POINTS OF $\sqrt{E_{refl} p / E_{inc} p}$ AND $\sqrt{E_{refl} s / E_{inc} s}$

Differentiating (7) with respect to β and putting $\frac{\partial e}{\partial \beta} = 0$, we get

$$2(1-m^2) \sin^4 \beta + (3m^2-1) \sin^2 \beta - 2 + \frac{nr}{1-2\sin^2 \beta} (1-m^2 \sin^2 \beta)^{\frac{3}{2}} (1-\sin^2 \beta) = 0 \quad (7a)$$

The value of β that satisfies this equation is the angle of incidence of the reflected S wave at which the reflected P wave has its extreme value. The corresponding value of α can be computed from Snell's law

$$\sin \alpha : \sin \beta = v_{lp} / v_{ls}$$

When a P wave is incident at the surface of the earth, then $n = 0$, and the following equation gives the extreme points of the energy ratio of the P wave reflected at the surface of the earth,

$$2(1-m^2) \sin^4 \beta + (3m^2-1) \sin^2 \beta - 2 = 0 \quad (7b)$$

Last term of the equation (7a) is very small compared to the rest of the terms. The same statement is also true for the equation (7). This fact can be used to explain the similarity in the behavior of the reflected wave that is of the same type as the incident wave, in both cases, i.e., the rock water boundary and the surface of the earth.

In the case of an SV wave is incident in the rock against the solid, we get similar expression for the extreme points of the reflected SV wave, the only difference being that the sign of the last term is negative.

$$2(1-m^2) \sin^4 \beta + (3m^2-1) \sin^2 \beta - 2 - \frac{nr}{1-2\sin^2 \beta} (1-m^2 \sin^2 \beta)^{\frac{3}{2}} (1-\sin^2 \beta) = 0 \quad (15a)$$

When an SV wave is incident at the surface of the earth we again get the equation (7b). This result should be expected,

because for the surface of the earth, the expression giving

$\sqrt{\frac{Erefl\ p}{Einc\ p}}$ is the same as the expression giving
 $\sqrt{\frac{Erefl\ s}{Einc\ s}}$. (See Gutenberg (6)).

COMPUTED VALUES

In general, computation falls into three groups: (1). The general behavior of the energy ratio for each case involves calculation of the square root of the energy ratio for a sufficient number of the angles of incidence. This was done with a slide rule to the third decimal place, using one of the equations (7), (8), (9), (11), (12), (13), (15), (16) and (17) as the case may be. (2). Determination of the angle of incidence (if any) at which an energy ratio becomes zero. This was done by first determining this angle from the graphs showing the general behavior of the energy ratio approximately, and then computing more values with a calculating machine to the fourth decimal place in the neighborhood of the approximate value. The final value of the zero point was thus determined graphically. (3). The angle of incidence (if any) at which an energy ratio has an extreme value was also determined graphically.

The computation is carried out for possible values of three parameters, namely m , n and r . Results are tabulated and plotted against the angle of incidence and are given in the following pages. For the general case, according to Gutenberg (7), "the results of calculations are in good agreement with the observations. However, for a wave which travels almost tangent to the discontinuity and in the medium with higher velocity, the calculated energy may be much too small (Joes and Teltow (9), Ott (15)"). The same situation should be true for the special

cases considered here.

P wave incident in the solid against the water:

Using equations (7), (8) and (9) energy ratios are computed for the following values of parameters: $m=1.6, 1.7, 1.8$; $n=0.2, 0.3, 0.4$; $r=0.3, 0.4, 0.5$.

For different values of parameters values of c as a function of α are given in table 1, values of α_0 (for $c = 0$) in table 2, and values of α_{ext} (α for which c has an extreme value) in table 3. Fig. 1, 2, 3 and 4 show the general behavior of c . To show the effect of each parameter, in each figure two of the parameters are kept constant and three curves are drawn corresponding three different values of the third parameter. (m , is varied for two sets of values of n and r .) From these curves, it is easily seen that the effect of changing m , is greater than the effect of changing either n or r . In fig. 5 and 6, α_{01}, α_{02} and α_{ext} are plotted against m , for different values of n and r . Here we note that for all values of n and r , α_{02} approach 90° as m , approaches $\sqrt{2}$ ($\sigma = 0$). From these curves it is evident that theoretically α_0 curve intersects α_{ext} curve which means that there are some combination of values of parameters for which extreme value of c is zero. The following two examples are given to illustrate the possibility of such an incidence for actual values of densities and elastic constants:

Example 1. granite-sea water boundary.

$$V_{1p} = 5.55 \quad V_{1s} = 3.26 \quad V_{2p} = 1.5 \quad \rho_2 = 1.026 \quad \rho_1 = 2.9$$

$$\text{Hence} \quad \sigma = 0.24 \quad m = 1.70 \quad n = 0.27 \quad r = 0.354$$

These values of parameters are represented by the curves and corresponding values of α_1 , α_2 and α_{ext} can easily be obtained by interpolation. It is evident that for this example e has two distinct roots and one extreme value between them.

Example 2. ultrabasic rock-sea water boundary.

$$V_{1p} = 8.0 \quad V_{1s} = 4.4 \quad V_{2p} = 1.5 \quad \rho_2 = 1.026 \quad r = 3.3$$

$$\text{Hence} \quad \sigma = 0.28 \quad m_1 = 1.82 \quad n = 0.1875 \quad r = 0.311$$

From the curves it is evident that for these values of parameters e has no roots but it has an extreme value. Thus, we conclude that for a solid medium with seismic velocities and density lying between those for granite and an ultrabasic rock such as dunite, e may have an extreme point which is at the same time a double root of the equation.

In table 4, the values of d and α_{ext} for d are given for different values of parameters. These results are plotted in fig. 7 and 8. Changes in r produce very little change in d , so that it is not considered here necessary to plot it. d starts from zero at $\alpha = 0^\circ$ increases rapidly. For small values of m_1 it has two distinct maxima and a minimum inbetween. As m_1 increases the extreme points become less pronounced and for $m_1 = 1.8$ they are represented by a flat section between $\alpha = 60^\circ$ and $\alpha = 80^\circ$. α_{ext} are not affected very much as we vary n and r .

Table 5 and fig. 9 show the values of e for different values of parameters. e starts with a value $\frac{2\sqrt{nr}}{1+nr}$ at $\alpha=0$, as α increases it diminishes very slowly but in the neighborhood of $\alpha=90^\circ$ very sharply and becomes zero at $\alpha=90^\circ$. For smaller m_1 it shows a slight increase after $\alpha=75^\circ$ and around $\alpha=87^\circ$ it starts

decreasing sharply to zero at $\alpha=90^\circ$. As m_1 takes larger values, this tendency seems to disappear. Changes in n and r have negligible effect on these turning points. For larger values of n , e has larger values at all angles of incidence. This simply means that the less longitudinal velocity contrast we have, the more energy goes into the refracted P wave.

P wave incident in the water against the solid.

Using equations (11), (12 and (13), energy ratios are computed for the following values of parameters: $m_2 = 1.6, 1.7, 1.8$ ($\sigma = 0.18-0.277$); $n = 3.0, 4.0$; $r = 2.5, 3.0$.

For this particular case we have total reflections occurring twice, namely one at $\gamma=90^\circ$ and one at $\zeta=90^\circ$. We shall call corresponding angles of incidence $\alpha_{c\gamma}$ and $\alpha_{c\zeta}$ respectively in the following discussions. At these critical incidences all of the energy is reflected as P wave.

Values of c , e and f are given in tables 6, 7 and 8 respectively. α_{ext} are given in table 9. These results are plotted in fig. 10-16.

c starts with a value $\frac{1-nr}{1+nr}$ at $\alpha=0^\circ$, staying almost constant until near $\alpha_{c\gamma}$. As $\alpha_{c\gamma}$ is approached it rapidly increases and becomes one at $\alpha_{c\gamma}$. Right after that, it suddenly drops down to a value less than it has for $\alpha < \alpha_{c\gamma}$, then it starts increasing slowly, the rate of increase diminishing gradually, and as it gets close to $\alpha_{c\zeta}$ it starts increasing sharply and at $\alpha_{c\zeta}$, $c = 1$. Values of α at which the energy curve starts increasing right after $\alpha_{c\gamma}$ are given in table 9 and fig. 16.

e starts with a value $\frac{2\sqrt{nr}}{1+nr}$ at $\alpha = 0^\circ$, it decreases slowly until near α_{c_2} where it shows little increase before it drops to zero at α_{c_2} . For small values of m_1 , for instance $m = 1.3$ ($\sigma < 0$, given here just as an illustration), it has a zero between $\alpha = 0^\circ$ and $\alpha = \alpha_{c_2}$, and for large values of m_1 it is a smooth, continuously decreasing function of α . After α_{c_2} no refracted P wave exists. $e = 0$

f starts from zero at $\alpha = 0^\circ$, increases almost linearly for a while, as α approaches α_c , it turns down and decreases sharply to zero at α_{c_2} . Right after α_{c_2} it increases suddenly and attains a value larger than it has for $\alpha < \alpha_{c_2}$. Here it turns and decreases very slowly, the rate of decrease becoming smaller and as α_{c_3} is approached it decreases sharply and becomes zero at α_{c_3} . After α_{c_3} there is no refracted S wave either. Thus all of the energy goes into reflected P wave. Turning points occurring just before and right after α_c are given in table 9 and fig. 16.

It is evident that here in this particular case, critical angles of incidences are the governing factors. All peculiarities occur just before and right after these angles.

Here we notice that most of the energy goes into the reflected P wave. None of the energy ratios become zero except at a critical incidence. The turning points which we may call α_{ext} are not very much different for different values of r , but they depend on m_2 and n .

SV wave incident in the solid against the water.

Using equations (15), (16) and (17), energy ratios have been computed and their zeros and extreme points investigated for the

following values of parameters: $m_1 = 1.6, 1.7, 1.75$ ($\sigma = 0.18 - 0.2576$), $n = 0.2, 0.3, 0.4$, and β_{ext} were computed, in addition to these values for $m_1 = 1.8$ ($\sigma = 0.277$).

In this particular case there is only one total reflection at β_{ca} ($\alpha = 90^\circ$). At this critical angle of incidence $d = 1$, $e = 0$, $c = 0$. The parts of the curves for d and e that lie between $\beta = 0$ and $\beta = \beta_{ca}$ are similar to the curves of c and d for the case of a P wave incident in the solid against the water. The curve for e as a whole is similar to that of f for the case of a P wave incident in the water against the solid, between $\alpha = 0$ and $\alpha = \alpha_g$. The only difference between these similar curves being that in the case of incident SV wave, at normal incidence all of the energy is reflected as SV wave whereas in other cases, at normal incidence the energy is split between c and e .

Here again we notice that β_{ext} are not very much different for different values of n and r . Therefore for practical purposes β_{ext} may be considered as a function of m_1 only.

Summary and Conclusions

General behavior, zeros and extreme points of different type of waves incident at both sides of the ocean floor, for some values of parameters m , n and r which are considered to include actual values, are computed; computed values are tabulated and plotted.

The following general conclusions are drawn from the results:

1. Poisson's ratio σ of the solid medium is a dominating factor in the general behavior, roots and extreme points of the reflected and refracted waves that travel in the solid and are produced by any possible type of wave incident at either side of the solid-water boundary.

2. n dominates the behavior of refracted waves and also plays an important role on the behavior of all waves around the critical incidence for $\gamma = 90^\circ$.

3. General behavior of any wave that is produced by incidence of any type of wave at either side of the boundary is affected very little by changing r , the effect being negligibly small in most cases.

4. In all cases the values of α_{ext} or β_{ext} change very slightly by changing r . The same statement is true for n except where the occurrence of extreme value is due to a total reflection at $\gamma = 90^\circ$.

5. In all cases considered in this paper, peculiar behaviors are observed just before and right after the critical angles

of incidences.

6. At a critical angle of incidence the whole energy goes into the reflected wave of the same kind as the incident wave.

7. In all cases considered most of the energy goes into reflected P or S wave depending on the angle of incidence. This can be explained by large contrast between densities and velocities in two media. In the case of a P wave incident in the water against the solid, after α_7 the energy is split between reflected P wave and refracted S wave but still a larger part goes into the reflected P wave.

REFERENCES

1. Blut, H. : Ein Beitrag zur Theorie der Reflexion und Brechung elastischer Wellen an Unstetigkeitsflächen, Zeitschr. f. Geophysik, vol. 8 (1932), pp. 130-144, and 305-322.
2. Byerly, Perry : Elastic Waves, Seismology, 1942, pp. 152-178.
3. Dana, S. W. : The Partition of Energy among Seismic Waves Reflected and Refracted at the Earth's Core, Bull. Seism. Soc. Am., vol. 34 (1944), pp. 189-198.
4. Dix, C. H. : Refraction and Reflection of Seismic Waves, Geophysics, vol. 4 (1939), pp. 81-101.
5. Geiger, L., and Gutenberg, B. : Ueber Erdbebenwellen VI, Nachr. Gesel. d. Wiss. Göttingen, math.-phys. Kl. (1912), pp. 623-675.
6. Gutenberg, B. : Theorie der Erdbebenwellen, Handbuch der Geophysik, (1932), pp. 1-80.
7. " : Energy Ratio of Reflected and Refracted Seismic Waves, Bull. Seism. Soc. Am., vol. 34 (1944), pp. 85-102.
8. Jeffreys, H. : The Reflection and Refraction of Elastic Waves, Mon. Not. Roy. Astr. Soc., Geoph. Suppl., vol. 1 (1926), pp. 321-334.
9. Joos, G., and Teltow, J. : Zur Deutung der Knallwellenaus-

- bereitung an der Trennschicht zweier Medien, Phys. Zeits., vol. 40 (1939), pp. 289-293.
10. Knott, G. D. : Reflection and Refraction of Elastic Waves with Seismological Applications, Phil. Mag., 5 th Ser., vol. 48 (1899), pp. 64-97.
11. " : The Propagation of Earthquake Waves through the Earth and Connected Problems, Proc. Roy. Soc. Edinburgh, vol. 59, part 1 (1919), pp. 157-208.
12. Macelwane, J. B. : Reflection and Refraction of Earthquake Waves, Physics of the Earth, VI, Bull. Nat. Res. Council, No. 90 (1933). pp. 116-120.
13. " : Reflection and Refraction of Seismic Waves, Introd. Theoretical Seismology, (1936), pp. 147-179.
14. Muskat, M., and Meres, M. W. : Reflection and Transmission Coefficients for Plane waves in Elastic Media, Geophysics, vol. 5 (1940), pp. 115-148.
15. Ott, H. : Reflexion und Brechung von Kugelwellen, Ann. d. Physik, vol. 38 (1942), pp. 443-466.
16. Slichter, L. B., and Gabriel, G. : Studies in Reflected Seismic waves, Gerl. Beit. z. Geophys., vol. 38 (1933), pp. 228-238.
17. Wiechert, E. : Ueber Erdbebenwellen I, Nach. Gesell. d. Wiss. Göttingen, math.-phys. kl., (1907),

pp. 415-589.

18. Zeeppritz, L., Geiger, L., and Gutenberg, B. : Ueber Erdbebenwellen V, Nach. Gesell. d. Wiss. Göttingen, math.-phys. Kl., (1912), pp. 121-206.

Table 1. Incident P wave in the solid against the water.
 Square root of the energy ratio of the reflected P wave.

Table 2. Incident P wave in the solid against the water.
 Angles of incidence at which the energy ratio of the reflected
 P wave is zero.

	$r \rightarrow$	0.3	0.4	0.5			
n	m_1	α_{01}	α_{02}	α_{01}	α_{02}	α_{01}	α_{02}
0.2	1.60	45°58'	86°32'	45°10'	86°38'	44°30'	86°45'
	1.65	49°11'	84°27'	48°20'	84°50'	47°30'	84°40'
	1.70	52°48'	81°32'	52°00'	81°50'	51°04'	82°08'
	1.75	58°03'	77°19'	56°40'	77°52'	55°28'	78°23'
	1.785	64°5	72°0				
0.3	1.60	44°46'	86°41'	43°45'	86°51'	42°38'	86°57'
	1.65	47°49'	84°42'	46°36'	84°55'	45°41'	85°07'
	1.70	51°25'	82°02'	50°08'	82°13'	48°33'	82°41'
	1.75	56°04'	78°21'	54°05'	78°59'	52°24'	79°35'
0.4	1.60	43°34'	86°40'	42°12'	86°59'	40°52'	87°07'
	1.65	46°34'	85°20'	44°44'	85°22'	43°15'	85°27'
	1.70	49°49'	82°27'	47°50'	83°02'	46°13'	83°16'
	1.75	53°58'	78°54'	51°38'	79°52'	49°28'	80°40'
	1.80	59°41'	74°0	56°16'	75°45'	53°28'	77°03'

Table 3. Incident P wave in the solid against the water.
 Angles of incidence at which the energy ratio of the reflected
 P wave has its extreme value.

$n \rightarrow$	0.2	0.2	0.4
$r \rightarrow$	0.3	0.3	0.3
m_1	α_{ext}	α	α_{ext}
1.60	74°00'	-0.4725	
1.65	71°41'	-0.5280	
1.70	70°08'	-0.1975	
1.75	68°50'	-0.0830	68°45'
1.79	68°25'	+0.0000	68°36'
1.80	68°15'	+0.0185	

Table 4. Incident P wave in the solid against the water.

(a) The square root of the energy ratio of the reflected S wave.

$n \rightarrow$	0.2		0.4		0.2	
$r \rightarrow$	0.3		0.5		0.4	
$\frac{\alpha}{m_1} \rightarrow$	1.7	1.8	1.7	1.7	1.7	1.7
0°	0.000	0.000	0.000	0.000	0.000	0.000
10°	0.518	0.289	0.289	0.275	0.284	
20°	0.600	0.552	0.508	0.519	0.541	
30°	0.804	0.748	0.704	0.705	0.733	
40°	0.914	0.875	0.841	0.826	0.868	
50°	0.936	0.930	0.917	0.878	0.913	
60°	0.900	0.941	0.954	0.885	0.923	
70°	0.844	0.925	0.960	0.869	0.907	
75°	0.844	0.940		0.885	0.924	
80°	0.882	0.979	0.967	0.927	0.965	
85°	0.978	0.929	0.869	0.892	0.917	
87°	0.970					
90°	0.000	0.000	0.000	0.000	0.000	

(b) Angles of incidence at which the energy ratio of the reflected S wave has its extreme value.

$n \rightarrow$	0.2		
$r \rightarrow$	0.3		
m_1	α_{ext}		
1.60	48°.2	73°.2	86°.5
1.65	51°.7	71°.5	84°.2
1.70	56°.8	69°.5	81°.5
1.725	60°	66°	
1.75			76°

Table 5. Incident P wave in the solid against the water.
 Square root of the energy ratio of the refracted P wave.

$n \rightarrow$	0.2			0.4	0.6
$r \rightarrow$	0.3			0.5	0.4
$\sqrt{m_1} \rightarrow$	1.6	1.7	1.8	1.7	1.7
0°	0.462	0.462	0.462	0.618	0.453
10°	0.455	0.457	0.458	0.614	0.448
20°	0.432	0.440	0.442	0.593	0.431
30°	0.415	0.419	0.426	0.562	0.411
40°	0.370	0.387	0.402	0.517	0.380
50°	0.325	0.351	0.373	0.475	0.345
60°	0.284	0.321	0.352	0.433	0.315
70°	0.250	0.294	0.330	0.404	0.288
75°	0.242	0.292	0.322	0.400	0.287
80°	0.251	0.300	0.319	0.420	0.295
85°	0.271	0.279	0.285	0.406	0.276
87°	0.272	0.259	0.237		
90°	0.000	0.000	0.000	0.000	0.000

Table 6. Incident P wave in the water against the solid.
 Square root of the energy ratio of the reflected P wave.

n	$\frac{m_2}{r} \rightarrow$	1.6		1.7		1.8	
		2.5	3.0	2.5	3.0	2.5	3.0
1	0°	0.764	0.800	0.764	0.800	0.764	0.800
	5°	0.764	0.799	0.764	0.799	0.761	0.798
	10°	0.763	0.798	0.760	0.795	0.760	0.796
	15°	0.747	0.787	0.753	0.790	0.738	0.794
	18°	0.749	0.787	0.762	0.802	0.774	0.810
	19°	0.762	0.797	0.788	0.823	0.821	0.848
	3.0 19°28'16"	1.000	1.000	1.000	1.000	1.000	1.000
	25°	0.740	0.775	0.710	0.753	0.682	0.728
	30°	0.761	0.795	0.723	0.766	0.702	0.745
	31°	0.786	0.820				
	32°13'51"	1.000	1.000				
	33°			0.755	0.790		
	34°					0.750	
	34°31'05"			1.000	1.000		
	35°					0.725	0.765
	36°						0.808
	36°52'12"					1.000	1.000
4.0	0°	0.818	0.846	0.818	0.846	0.818	0.846
	5°	0.818	0.845	0.818	0.844	0.816	0.844
	10°	0.812	0.838	0.812	0.841	0.816	0.844
	13°	0.809	0.836	0.814	0.844	0.814	0.851
	14°	0.814	0.844	0.832	0.858	0.846	0.872
	14°28'39"	1.000	1.000	1.000	1.000	1.000	1.000
	15°	0.771	0.808	0.768	0.819	0.792	0.822
	20°	0.805	0.837	0.793	0.821	0.776	0.810
	22°	0.782	0.813				
	23°	0.828	0.870	0.800	0.793	0.782	0.816
	23°34'41"	1.000	1.000				
	25°			0.908	0.920	0.797	0.828
	25°09'02"			1.000	1.000		
	26°44'36"					1.000	1.000

Table 7. Incident P wave in the water against the solid.
 Square root of the energy ratio of the refracted P wave.

n	$\frac{m_2}{r} \rightarrow$	1.6		1.7		1.8	
		2.5	3.0	2.5	3.0	2.5	3.0
3.0	0°	0.645	0.600	0.645	0.600	0.645	0.600
	5°	0.626	0.584	0.628	0.584	0.644	0.587
	10°	0.572	0.532	0.579	0.537	0.589	0.549
	15°	0.513	0.424	0.490	0.457	0.520	0.485
	18°	0.405	0.338	0.420	0.391	0.480	0.434
	18°30'		0.327	0.427	0.398		0.430
	19°	0.352	0.328	0.420	0.389	0.465	0.429
	19°28'16"	0.000	0.000	0.000	0.000	0.000	0.000
4.0	0°	0.575	0.532	0.575	0.532	0.575	0.532
	5°	0.543	0.503	0.549	0.508	0.555	0.513
	10°	0.459	0.407	0.462	0.428	0.481	0.446
	13°	0.332	0.308	0.359	0.352	0.450	0.393
	14°	0.306	0.284	0.254	0.340	0.400	0.370
	14°28'39"	0.000	0.000	0.000	0.000	0.000	0.000

Table 8. Incident P wave in the water against the solid
Square root of the energy ratio of the refracted S wave.

n	$\frac{M_2}{r^2} \rightarrow$	1.6		1.7		1.8	
		2.5	3.0	2.5	3.0	2.5	3.0
3.0	0°	0.000	0.000	0.000	0.000	0.000	0.000
	5°	0.165	0.151	0.152	0.142	0.142	0.130
	10°	0.314	0.293	0.305	0.280	0.274	0.253
	15°	0.487	0.455	0.441	0.410	0.398	0.373
	18°	0.557	0.520	0.495	0.452	0.427	0.396
	19°	0.543	0.503	0.452	0.420	0.351	0.326
	19°28'16"	0.000	0.000	0.000	0.000	0.000	0.000
	25°	0.680	0.637	0.705	0.662	0.732	0.690
	30°	0.648	0.605	0.688	0.644	0.695	0.658
	31°	0.416	0.387				
	32°13'51"	0.000	0.000				
	33°			0.655	0.613		
	34°						0.662
	34°31'05"			0.000	0.000		
	35°					0.705	0.660
	36°						0.598
	36°52'12"					0.000	0.000
4.0	0°	0.000	0.000	0.000	0.000	0.000	0.000
	5°	0.197	0.183	0.181	0.168	0.164	0.153
	10°	0.391	0.361	0.345	0.320	0.323	0.299
	15°	0.465	0.430	0.438	0.407	0.403	0.352
	14°	0.488	0.458	0.417	0.385	0.351	0.325
	14°28'39"	0.000	0.000	0.000	0.000	0.000	0.000
	18°	0.630	0.579	0.580	0.513	0.611	0.566
	20°	0.587	0.546	0.612	0.566	0.635	0.590
	22°	0.623	0.580				
	23°	0.519	0.492	0.598	0.555	0.627	0.583
	23°34'41"	0.000	0.000				
	25°			0.484	0.390	0.609	0.565
	25°09'02"			0.000	0.000		
	26°44'36"					0.000	0.000

Table 9. Incident P wave in the water against the solid.
 Angles of incidence at which the energy ratio of the refracted S wave has its extreme value.

(a) For angles of incidence
 greater than the critical
 angle of incidence.

$\frac{r}{m_2 n}$	3.0	3.5	4.0
1.6	18°.3	16°.0	15°.7
1.7	18°.0	15°.5	15°.4
1.8	17°.2	15°.1	13°.0

(b) For angles of incidence
 less than the critical angle
 of incidence.

$\frac{r}{m_2 n}$	3.0	3.5	4.0
1.6	20°.3	17°.2	15°.0
1.7	20°.9	17°.8	15°.4
1.8	21°.8	18°.6	16°.0

Table 10. Incident SV wave in the solid against the water.
 Square root of the energy ratio of the reflected S wave.

$n \rightarrow$	0.2			0.2	0.4
$r \rightarrow$	0.3			0.4	0.5
$\beta \diagdown m_1 \rightarrow$	1.6	1.7	1.75	1.7	1.7
0°	1.000	1.000	1.000	1.000	1.000
10°	0.889	0.867	0.871	0.870	0.874
20°	0.870	0.853	0.822	0.812	0.830
30°	-0.061	0.026	0.077	0.044	0.085
34°	-0.086			-0.067	-0.024
34°51'00"			1.000		
35°			0.922		
36°01'55"		1.000		1.000	1.000
37°		0.872		0.844	0.749
38°40'56"	1.000				
40°	0.864	0.851	0.845	0.804	0.702
50°	0.878	0.869	0.867	0.829	0.727
60°	0.886	0.875	0.875	0.836	0.736
70°	0.895	0.882	0.880	0.848	0.744
80°	0.927	0.922	0.915	0.904	0.812
90°	1.000	1.000	1.000	1.000	1.000

Table 11. Incident SV wave in the solid against the water.
 Angles of incidence at which the energy ratio of the reflected S wave is zero.

		n →		0.2		0.3		0.4	
r →	m₁			β_{01}	β_{02}	β_{01}	β_{02}	β_{01}	β_{02}
0.3	1.60	28°51'	38°53'.5	29°25'	38°52'.2	30°02'	38°50'.9		
	1.65	29°36'	36°59'.1	30°12'	36°55'.7	30°51'	36°51'.6		
	1.70	30°35'	35°15'	31°19'	35°08'.8	32°15'	34°55'.1		
	1.725	31°26'	34°05'	32°46'	33°23'				
0.4	1.60	29°13'	38°32'.8	29°57'	38°30'.3	30°50'	38°29'.1		
	1.65	30°01'	36°57'.1	30°48'	36°52'.2	31°44'	36°46'.3		
	1.70	31°03'	35°11'.8	32°04'	34°55'.5	33°22'	34°40'.5		
	1.725	32°15'	33°50'						

Table 12. Incident SV wave in the solid against the water.
 Angles of incidence at which the energy ratio of the reflected S wave has its extreme value.

		0.2			0.3			0.4		
r →	m₁	β_{ext}	d	β_{ext}						
	1.60	37°00'	- .3572	36°56'	36°58'	37°00'	36°55'	36°57'	36°58'	
	1.65	35°10'	- .2142	35°16'	35°17'	35°18'				
	1.70	33°40'	- .0880	33°45'	33°44'	33°45'				
	1.7375	32°30'	± .0000							
	1.75	32°10'	+ .0250	32°19'	32°20'	32°21'				
	1.80	30°55'	+ .1850	31°06'	31°07'	31°08'				

Table 13. Incident SV wave in the solid against the water.
 Square root of the energy ratio of the reflected P wave.

$n \rightarrow$	0.2			0.2	0.4
$r \rightarrow$	0.3			0.4	0.3
$\beta \backslash m_1$	1.6	1.7	1.75	1.7	1.7
0°	0.000	0.000	0.000	0.000	0.000
10°	0.497	0.482	0.475	0.472	0.456
20°	0.847	0.831	0.822	0.814	0.783
25°	0.928	0.915	0.908		
28°	0.939	0.935	0.935		
30°	0.933	0.930	0.943	0.912	0.883
32°	0.909	0.938	0.929		
34°				0.920	0.898
34°51'00"			0.000		
35°	0.846	0.948			
36°	0.854				
36°01'56"		0.000		0.000	0.000
37°	0.857				
38°	0.887				
38°40'56"	0.000				

Table 14. Incident SV wave in the solid against the water.
 Square root of the energy ratio of the refracted P wave.

$n \rightarrow$	0.2			0.2	0.4
$r \rightarrow$	0.3			0.4	0.5
$m_1 \rightarrow$	1.6	1.7	1.75	1.7	1.7
60°	0.000	0.000	0.000	0.000	0.000
100°	0.128	0.122	0.120	0.139	0.191
200°	0.259	0.241	0.239	0.272	0.375
300°	0.357	0.338	0.324	0.382	0.535
340°		0.343		0.390	0.555
34° 51' 00"			0.000		
35°			0.260		
36° 01' 55"		0.000		0.000	0.000
37°		0.490		0.560	0.774
38° 40' 56"	0.000				
40°	0.511	0.528	0.543	0.590	0.818
50°	0.490	0.492	0.501	0.558	0.794
60°	0.468	0.482	0.480	0.545	0.788
70°	0.445	0.463	0.460	0.530	0.780
80°	0.375	0.396	0.407	0.444	0.665
90°	0.000	0.000	0.000	0.000	0.000

Table 15. Incident of SV wave in the solid against the water.
 Angles of incidence at which the energy ratio of the refracted
 P wave has its extreme value.

$n \rightarrow$	$r \rightarrow$	0.2	0.3	0.4
n	m_1	β_{ext}	β_{ext}	β_{ext}
0.2	1.60	36°12'	36°19'	36°26'
	1.70		39°45'	
	1.75		31°15'	
0.3	1.60	36°10'	36°16'	36°23'

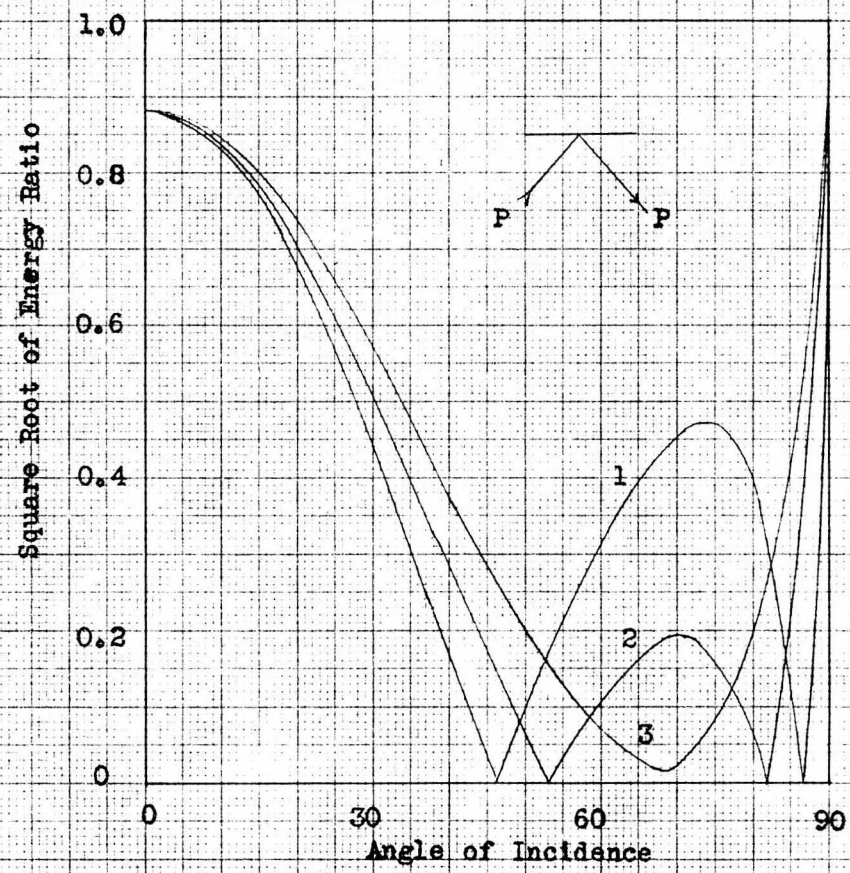


Fig. 1.- Incident P wave in the solid against the water
Square root of the energy ratio of the reflected P wave

Curve	$\frac{V_{p1}}{V_{s1}}$	$\frac{V_{p2}}{V_{p1}}$	$\frac{f_2}{f_1}$
(1)	1.6	0.2	0.3
(2)	1.7	0.2	0.3
(3)	1.8	0.2	0.3

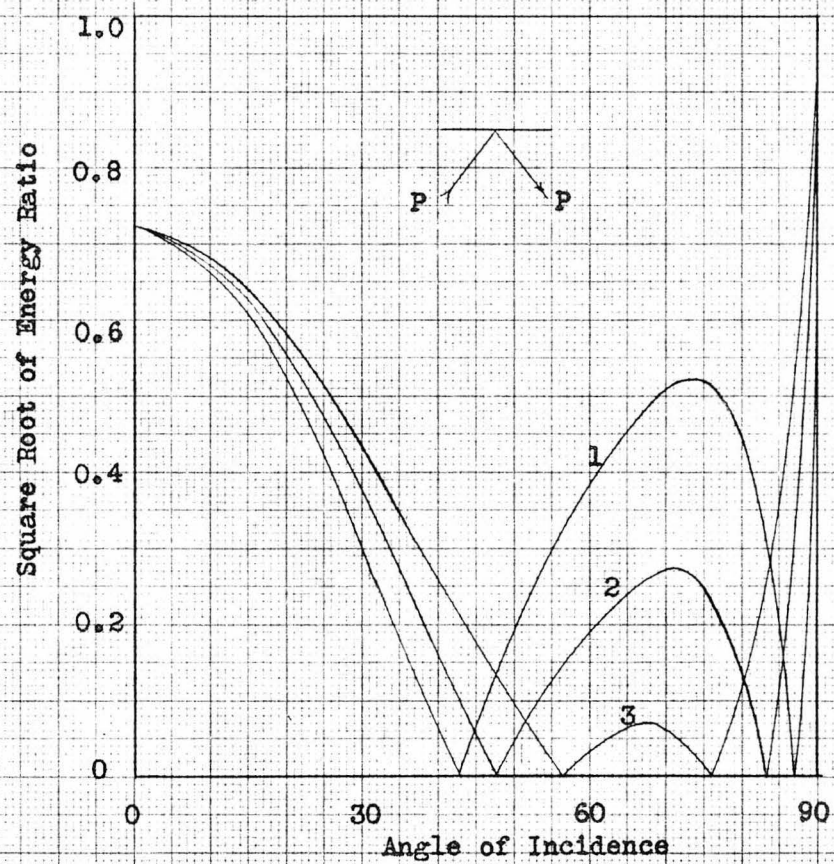


Fig. 2.- Incident P wave in the solid against the water
Square root of the energy ratio of the reflected P wave

Curve	$\frac{V_{PI}}{V_{sl}}$	$\frac{V_{p2}}{V_{pl}}$	$\frac{\rho_2}{\rho_1}$
(1)	1.6	0.4	0.4
(2)	1.7	0.4	0.4
(3)	1.8	0.4	0.4

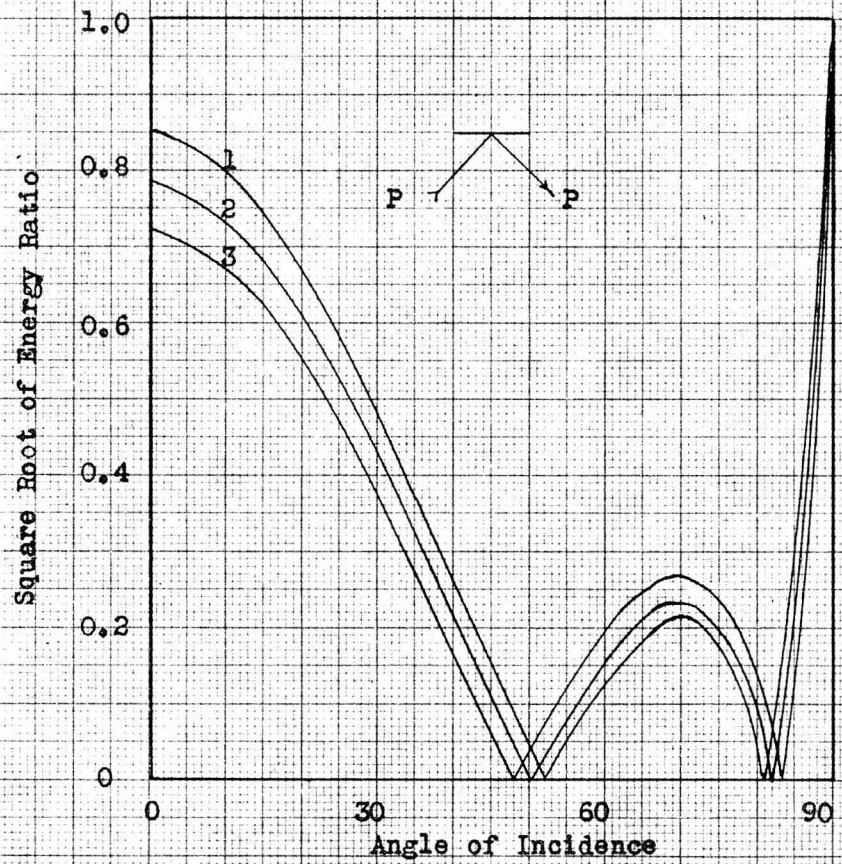


Fig. 3.- Incident P wave in the solid against the water
Square root of the energy ratio of the reflected P wave

Curve	V_{p1}/V_{s1}	V_{p2}/V_{p1}	ρ_2/ρ_1
(1)	1.7	0.2	0.4
(2)	1.7	0.3	0.4
(3)	1.7	0.4	0.4

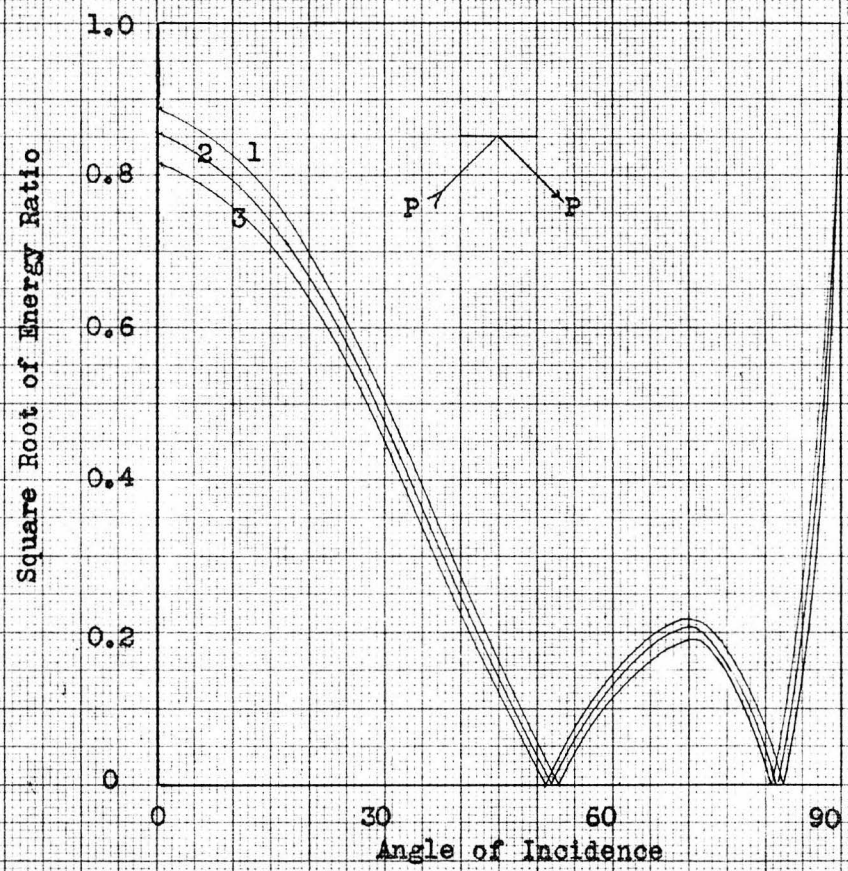
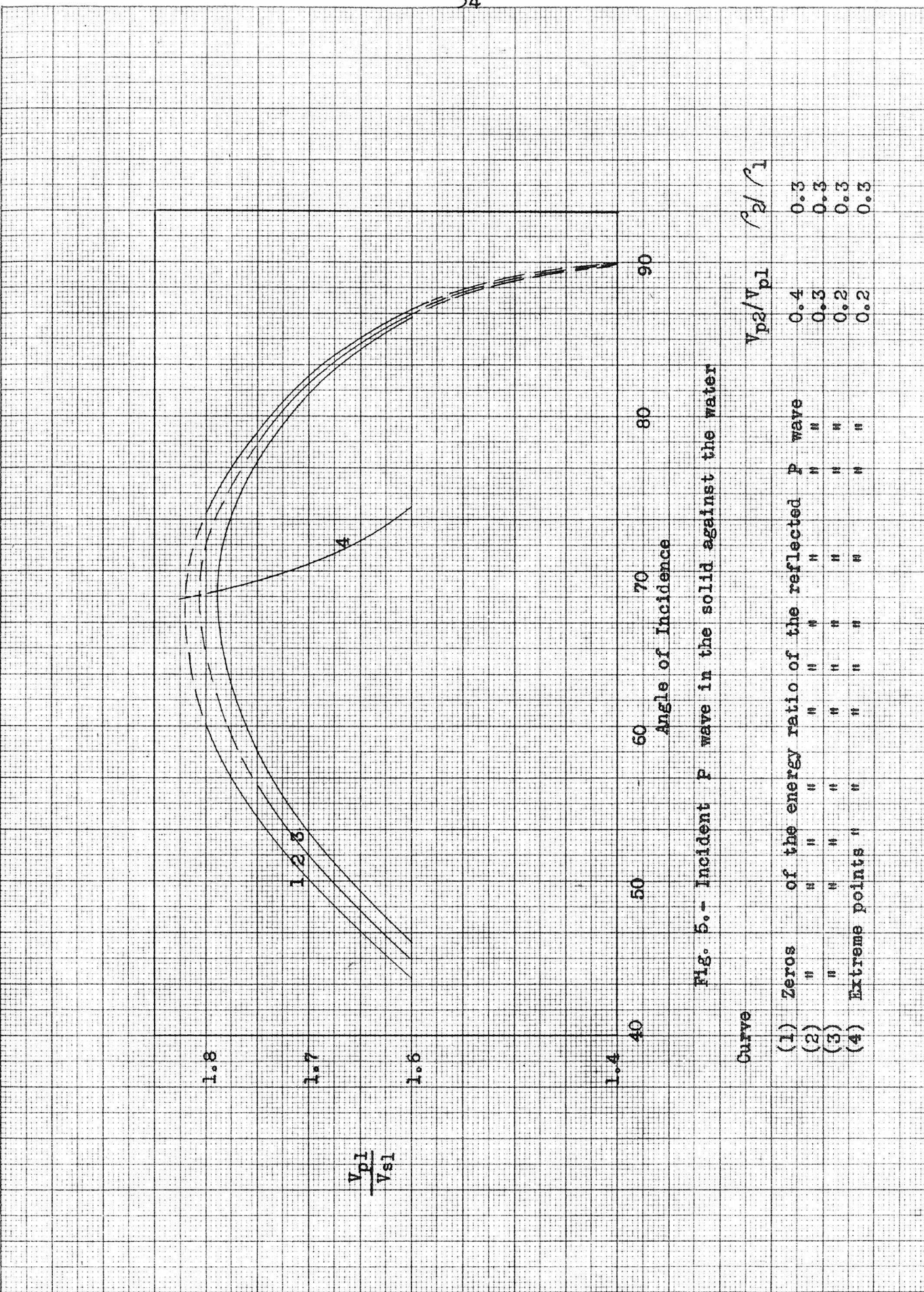
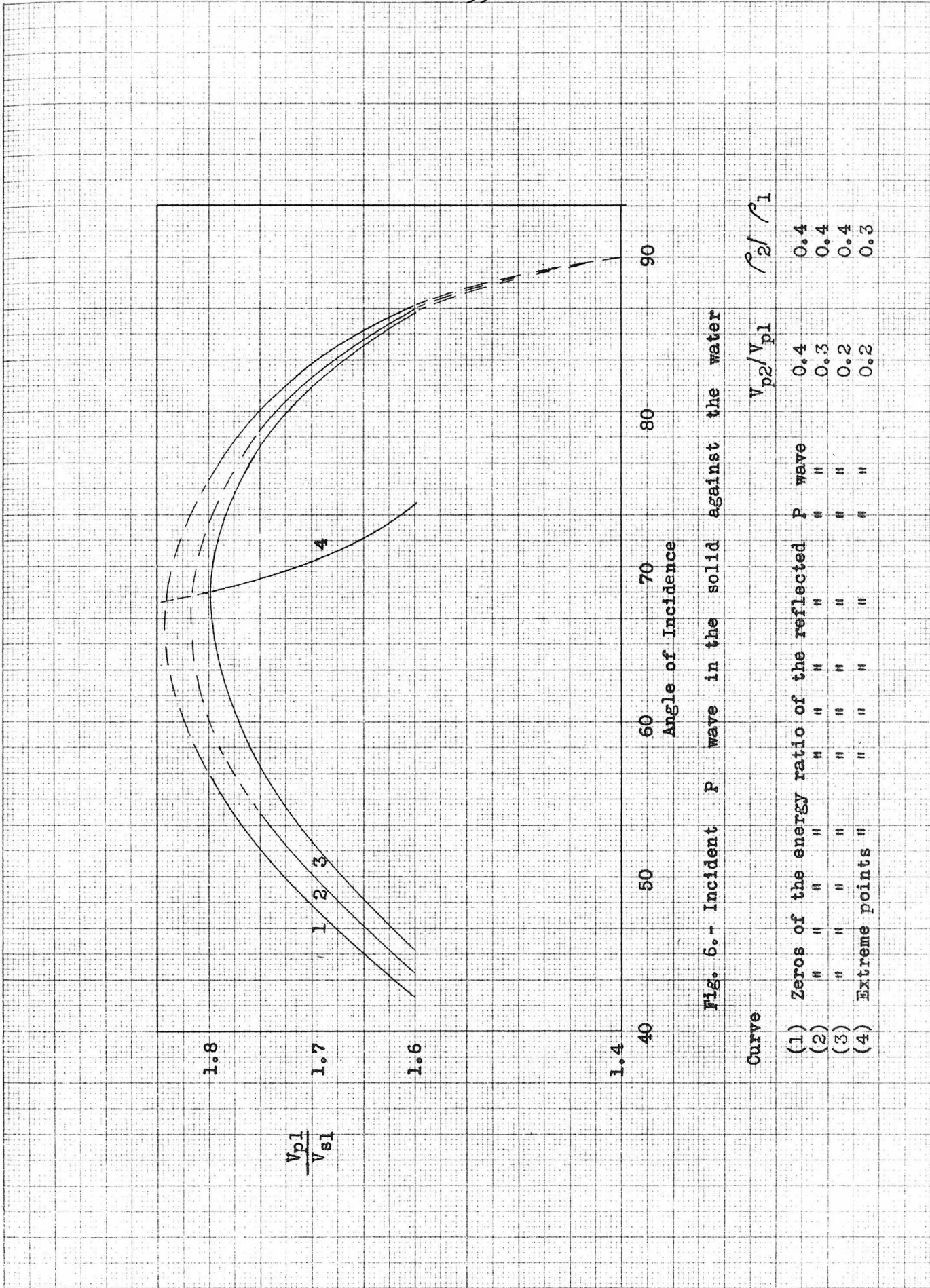
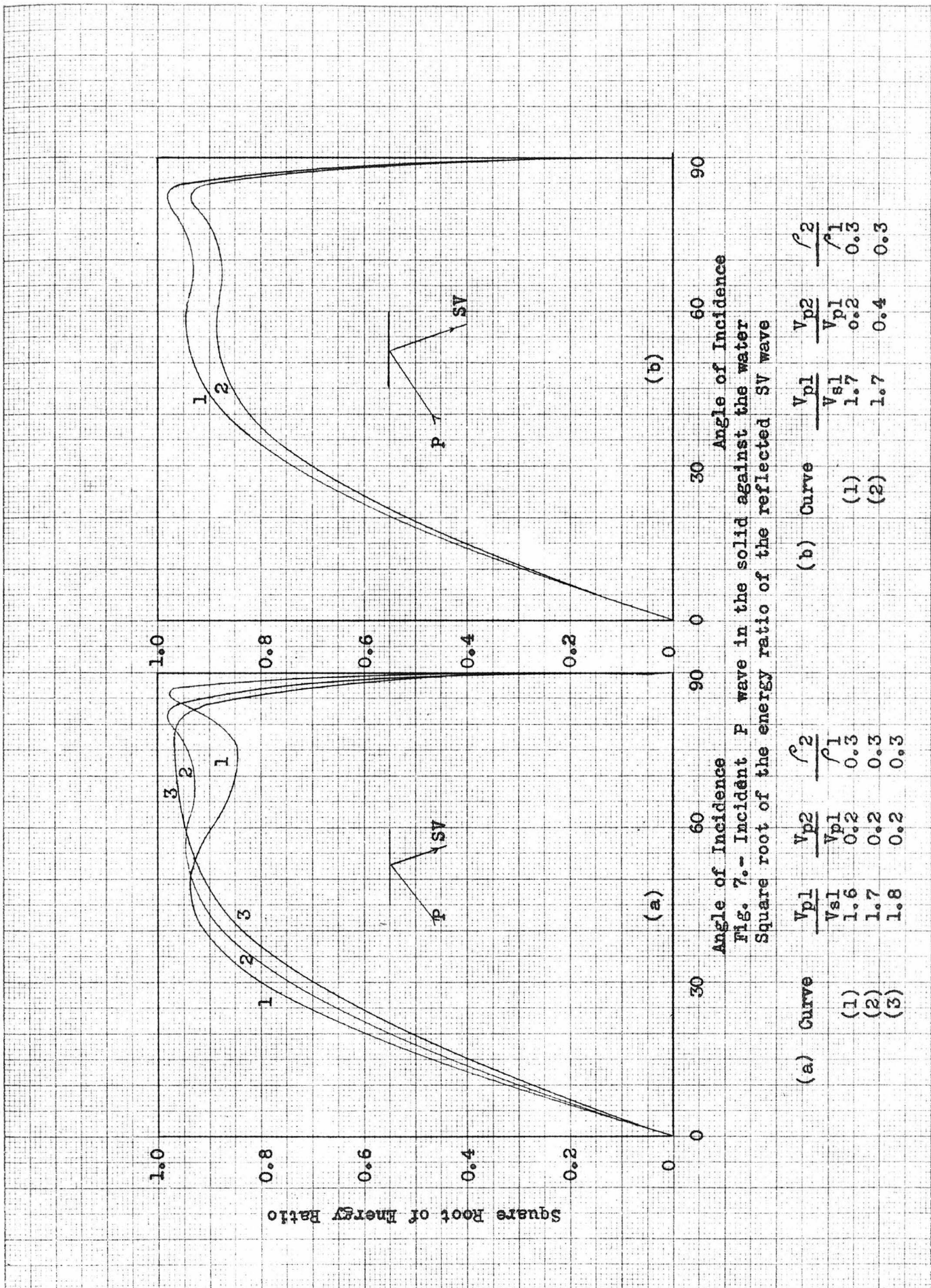


Fig. 4.- Incident P wave in the solid against the water
 Square root of the energy ratio of the reflected P wave

Curve	v_{p1}/v_{s1}	v_{p2}/v_{p1}	ρ_2/ρ_1
(1)	1.7	0.2	0.3
(2)	1.7	0.2	0.4
(3)	1.7	0.2	0.5







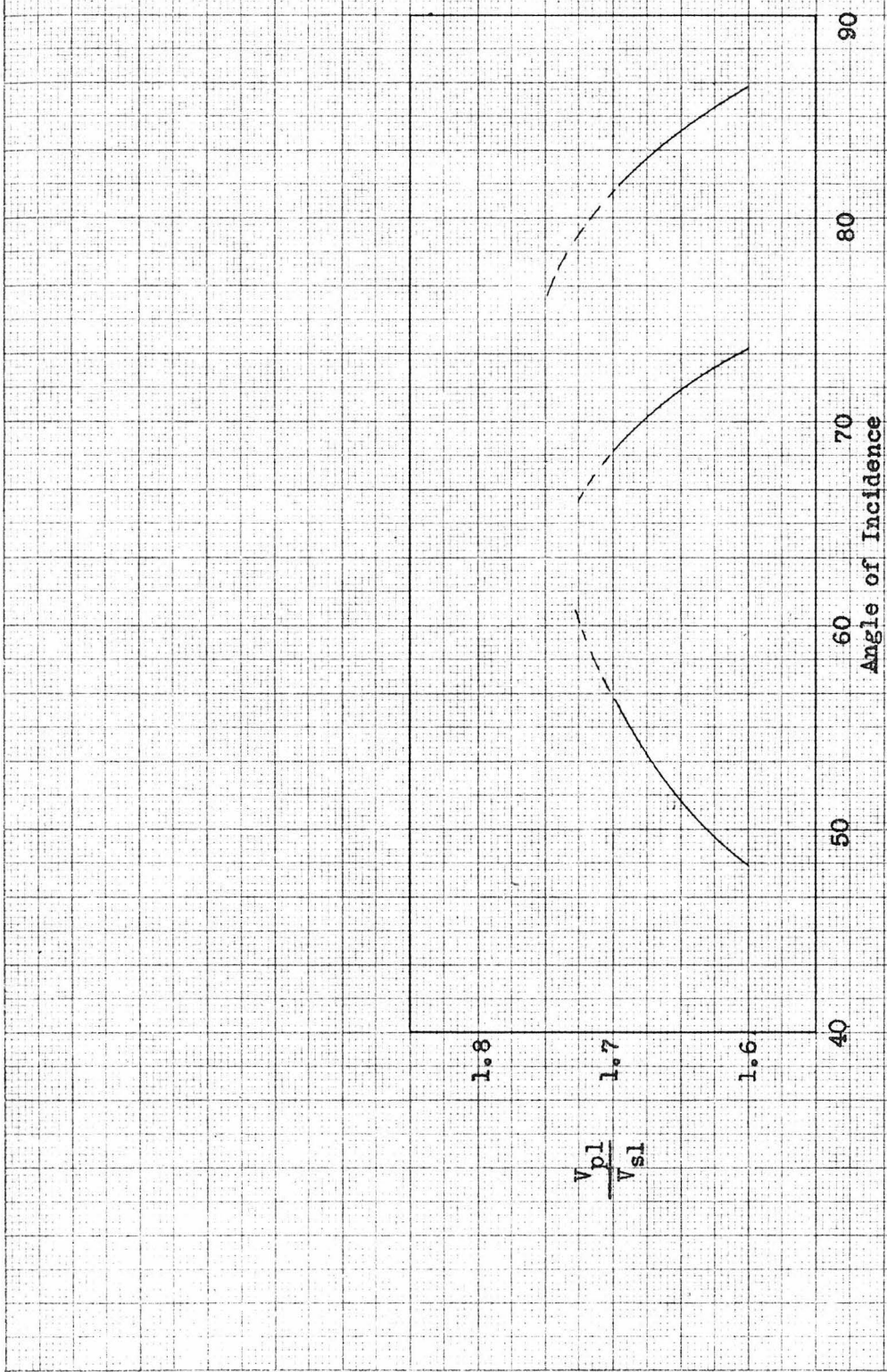


Fig. 8.— Incident P wave in the solid against the water
Extreme points of the energy ratio of the reflected SV wave

$$\frac{V_{p2}}{V_{p1}} = 0.2 \quad \therefore \quad \frac{\rho_2}{\rho_1} = 0.3$$

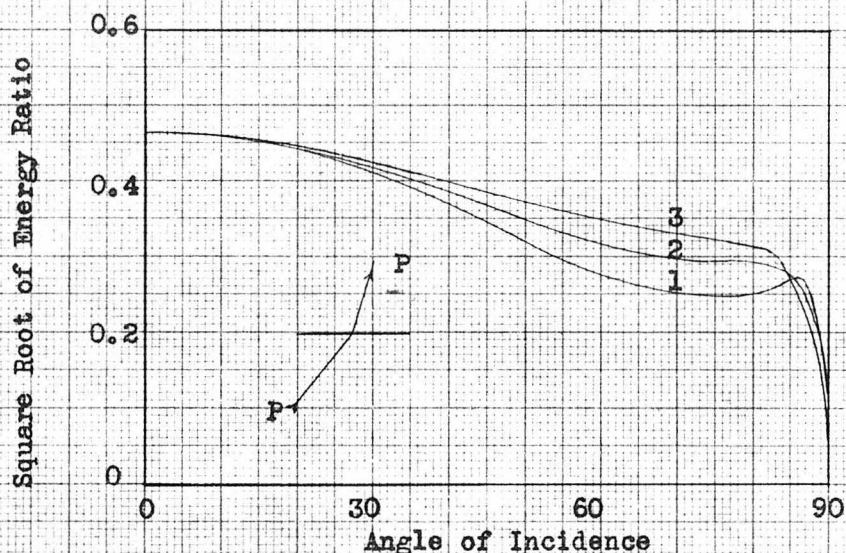


Fig. 9a.- Incident P wave in the solid against the water
Square root of energy ratio of the refracted P wave

Curve	$\frac{V_{pl}}{V_{sl}}$	$\frac{V_{p2}}{V_{pl}}$	$\frac{r^2}{r^1}$
(1)	1.6	0.3	0.3
{2}	1.7	0.3	0.3
(3)	1.8	0.3	0.3

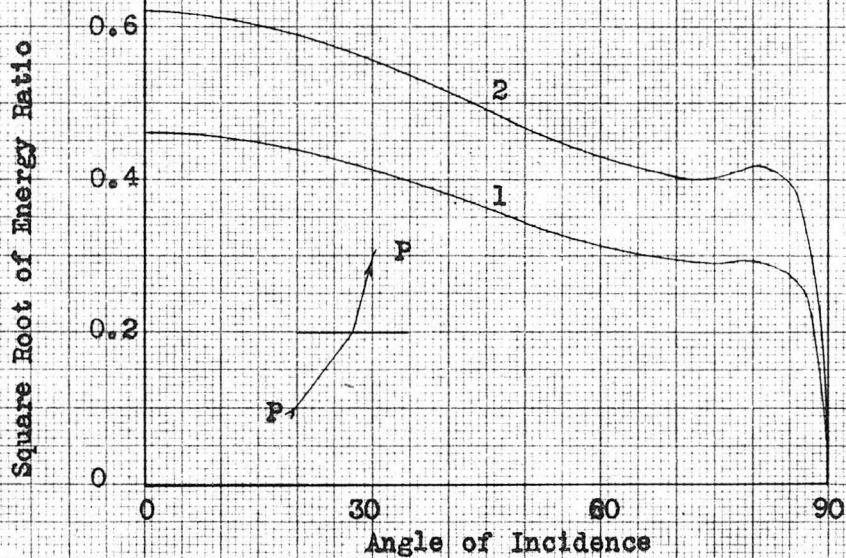


Fig. 9b.- Incident P wave in the solid against the water
Square root of the energy ratio of the refracted P wave

Curve	$\frac{V_{pl}}{V_{sl}}$	$\frac{V_{p2}}{V_{pl}}$	$\frac{r^2}{r^1}$
(1)	1.7	0.2	0.3
(2)	1.7	0.4	0.3

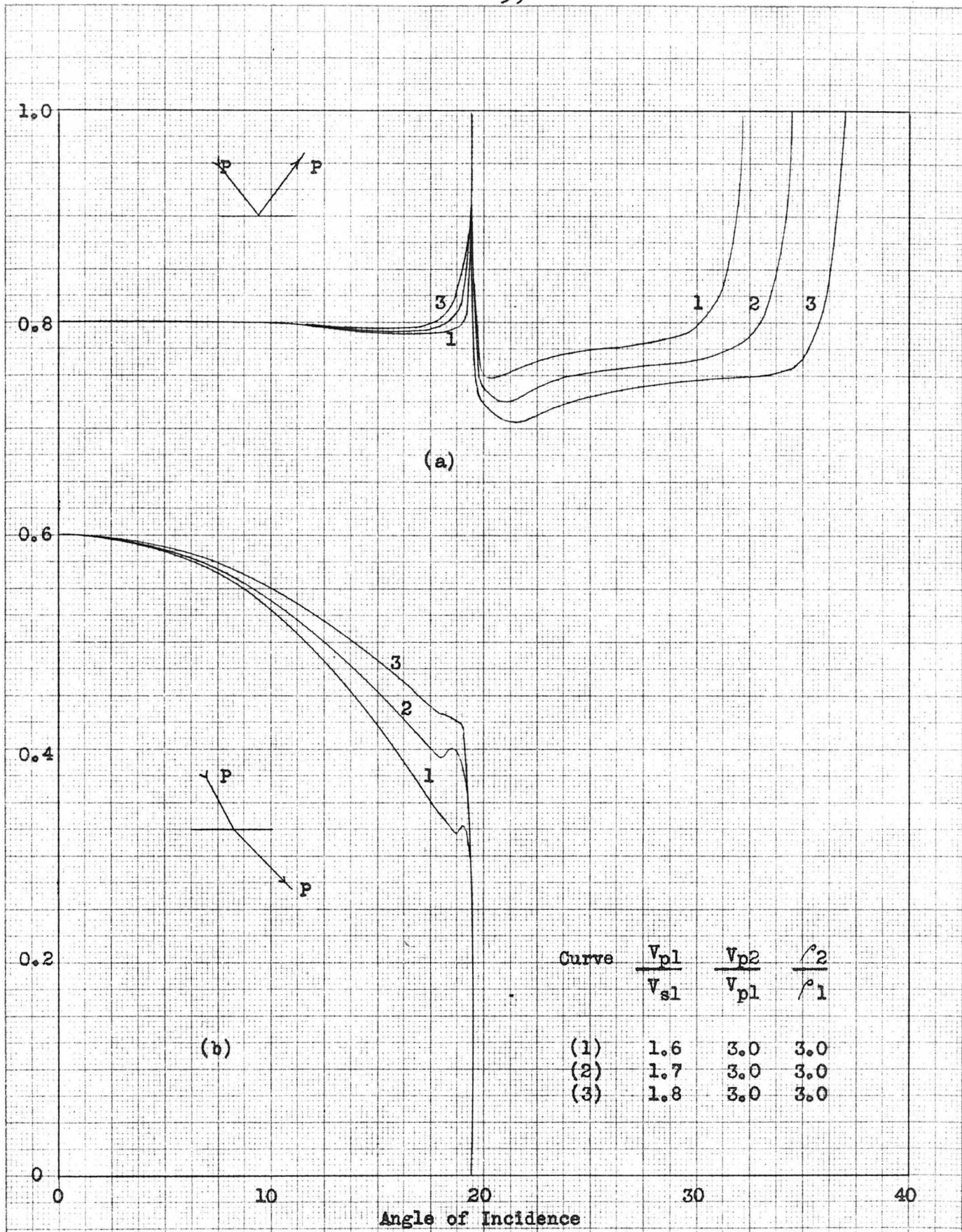


Fig. 10.- Incident P wave in the water against the solid
 (a) Square root of the energy ratio of the reflected P wave
 (b) " " " " " " " " refracted P "

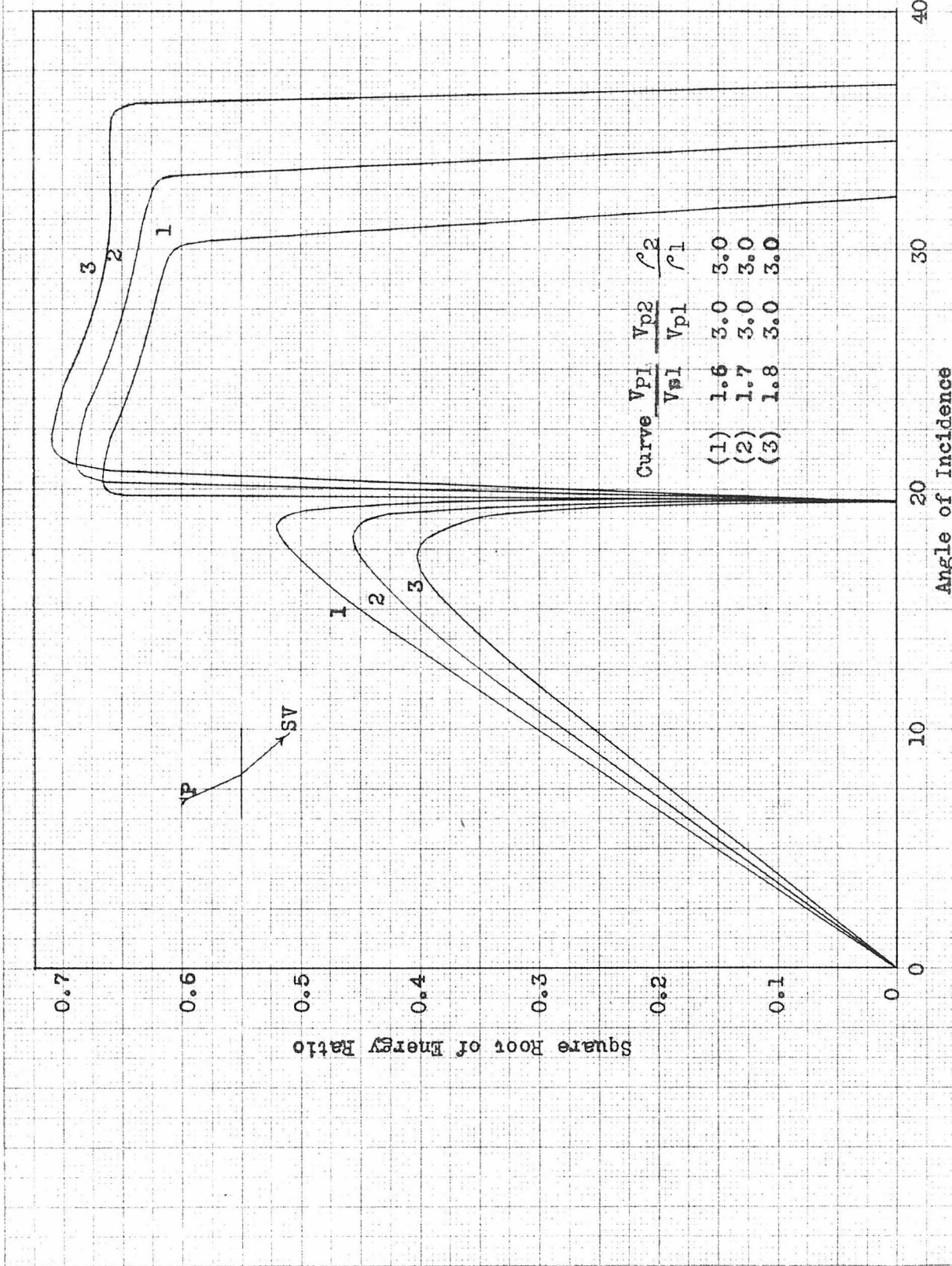
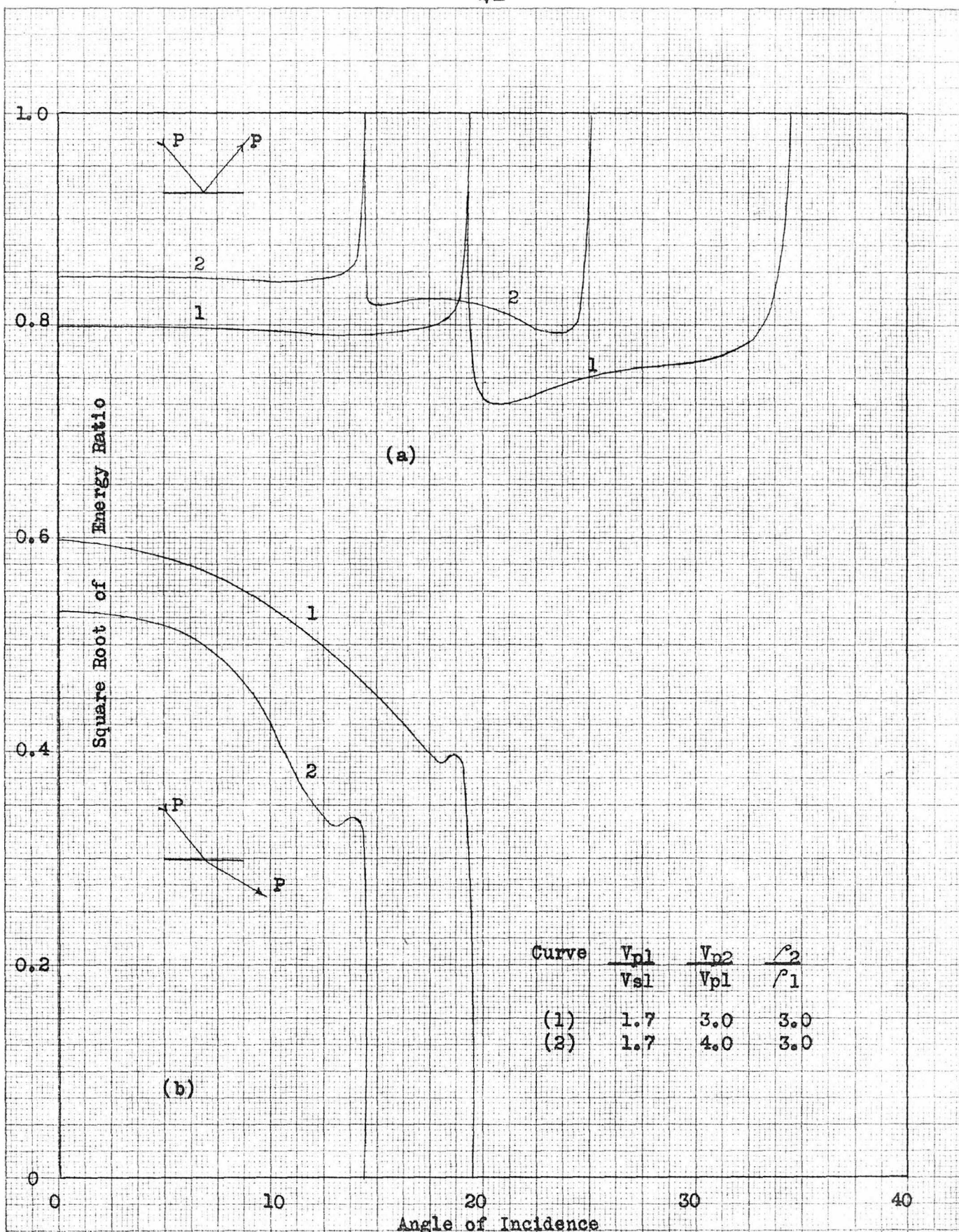


Fig. 11.—Incident P wave in the water against the solid
Square root of the energy ratio of the refracted SV wave



Angle of Incidence
 Fig. 12.- Incident P wave in the water against the solid
 (a) Square root of the energy ratio of the reflected P wave
 (b) " " " " " " " " refracted P "

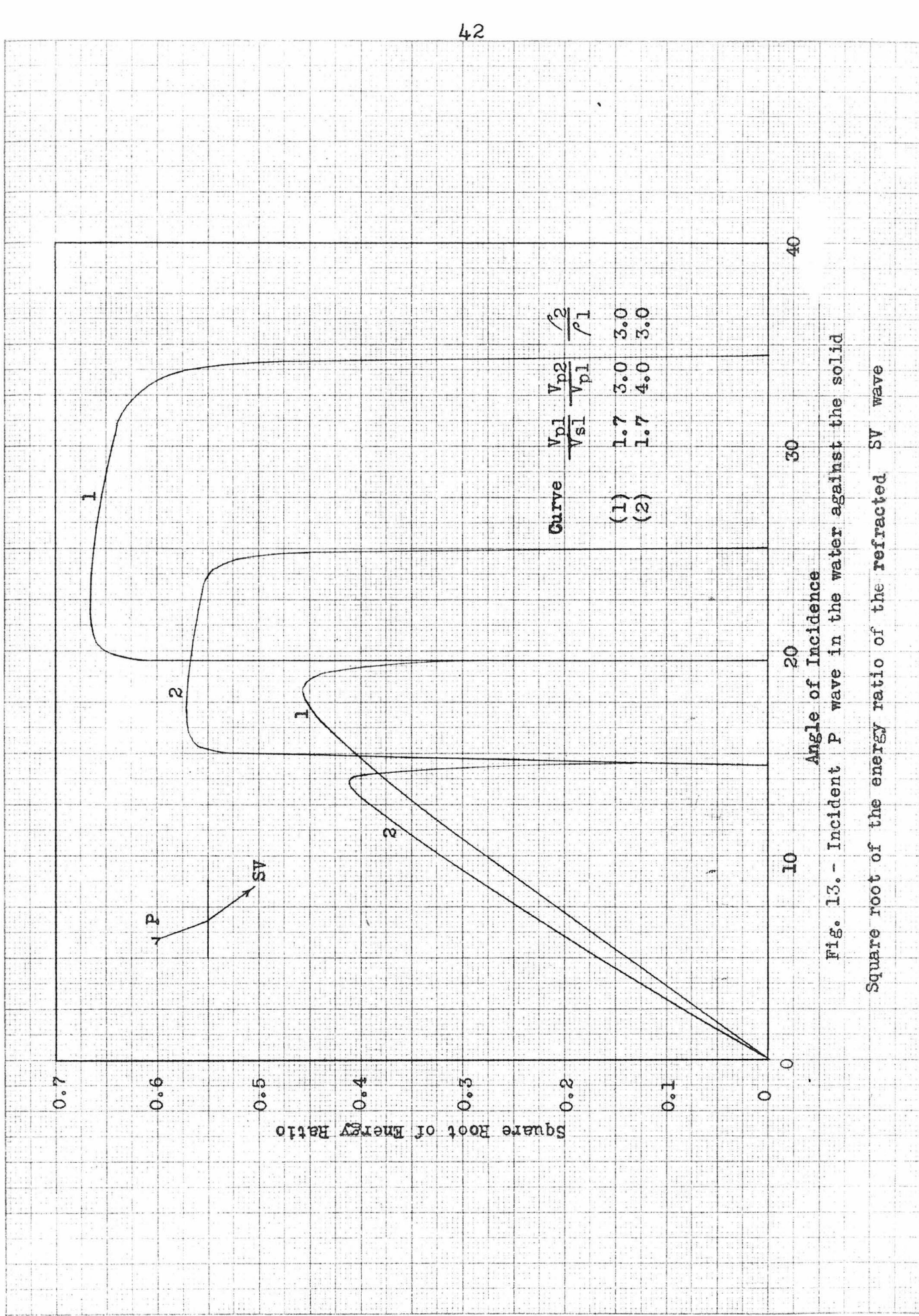


Fig. 13.- Incident P wave in the water against the solid

Square root of the energy ratio of the refracted SV wave

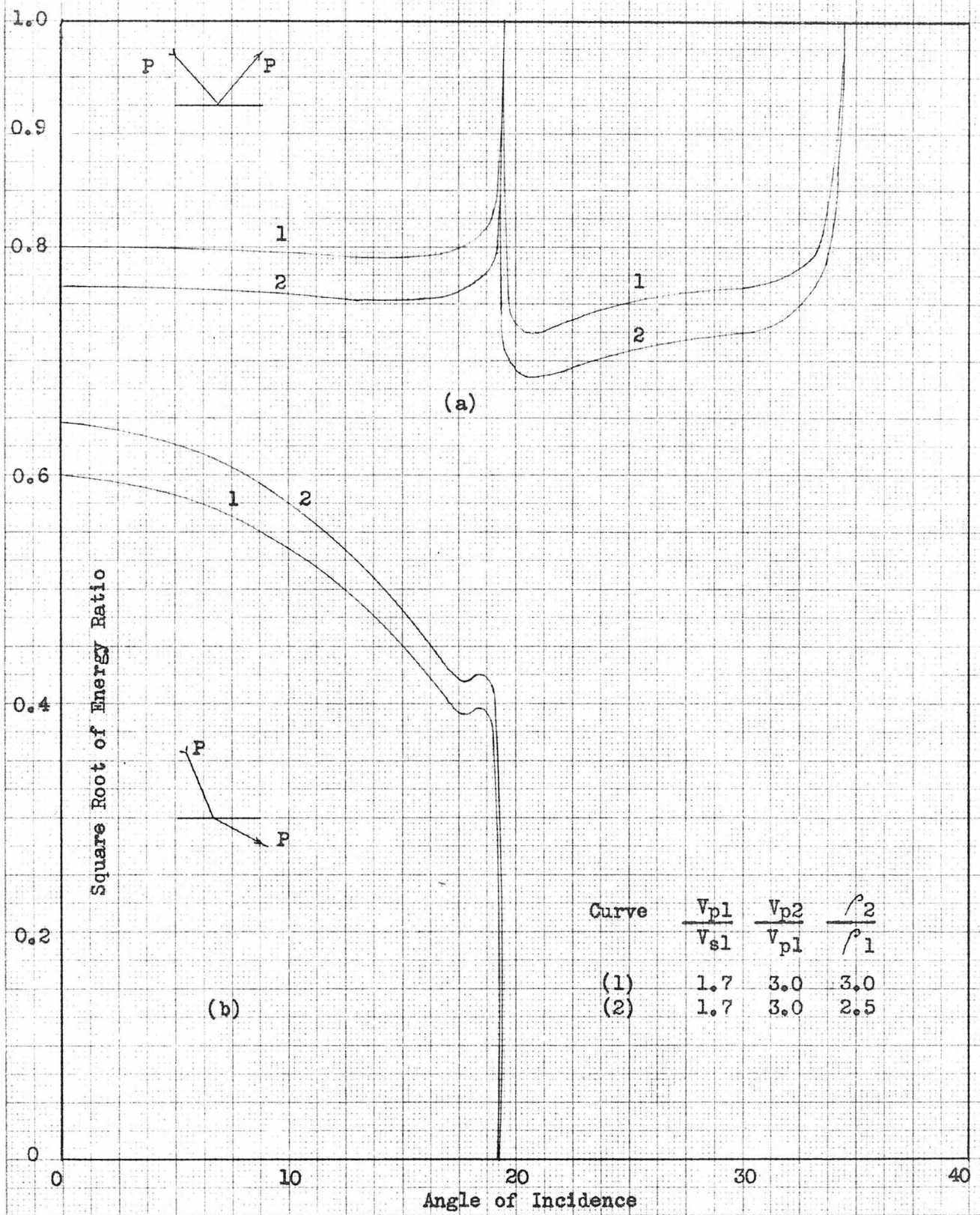


Fig. 14.- Incident P wave in the water against the solid
 (a) Square root of the energy ratio of the reflected P wave
 (b) " " " " " " " " refracted P "

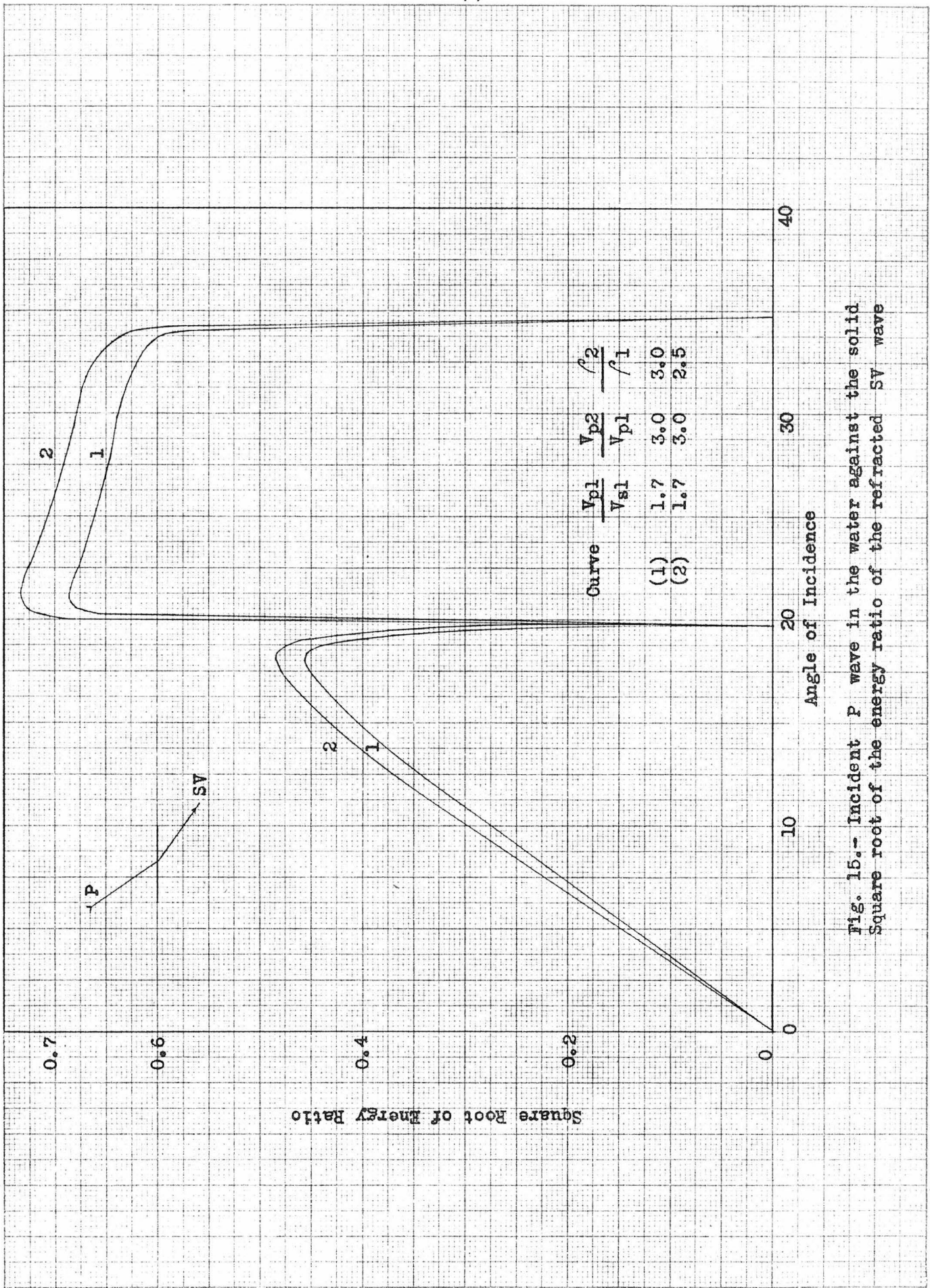
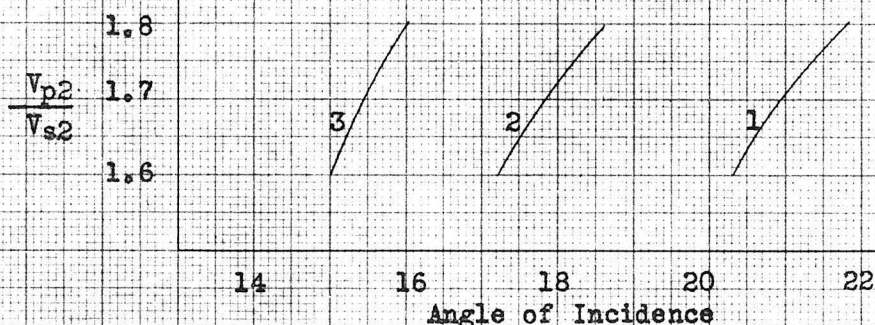
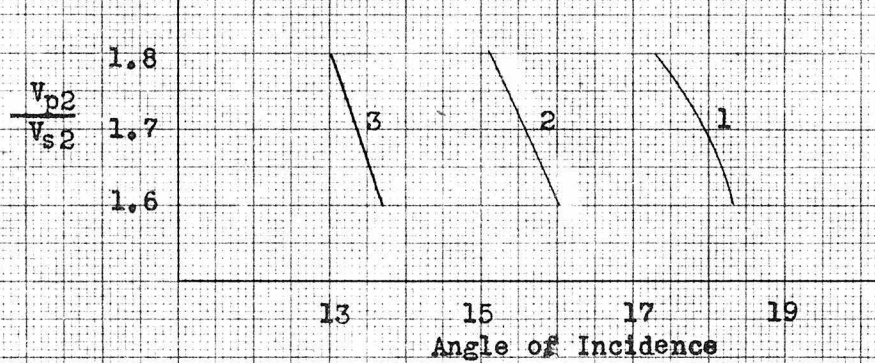


Fig. 15.—Incident P wave in the water against the solid
square root of the energy ratio of the refracted SV wave



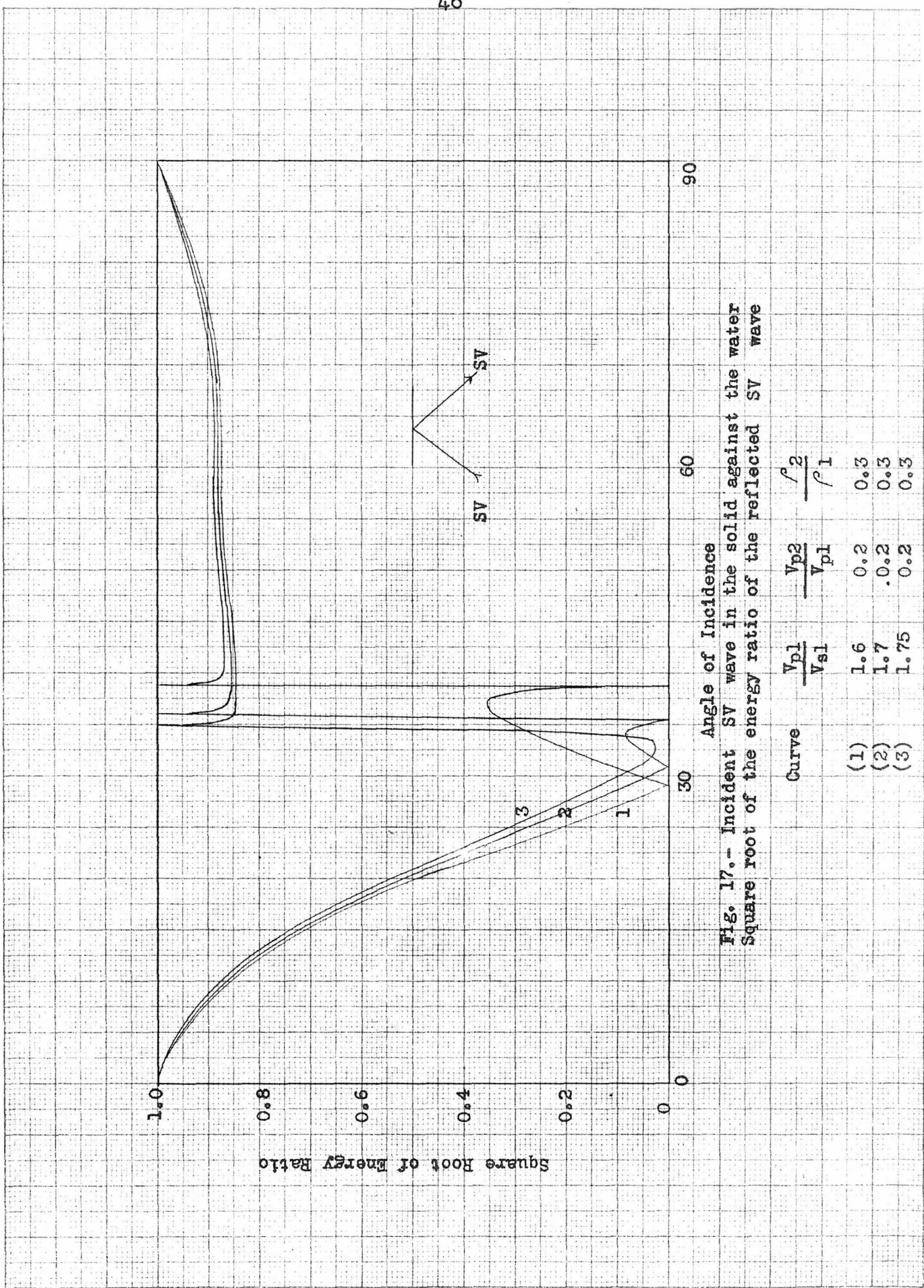
(a) Extreme points of the energy ratio of the reflected P wave and of the refracted SV wave for the angles of incidence greater than the critical angle of incidence

Fig. 16.- Incident P wave in the water against the solid



(b) Extreme points of the energy ratio of the refracted SV wave for the angles of incidence less than the critical angle of incidence

Curve	V_{p2}/V_{p1}	ρ_2/ρ_1
(1)	3.0	3.0
(2)	3.5	3.0
(3)	4.0	3.0



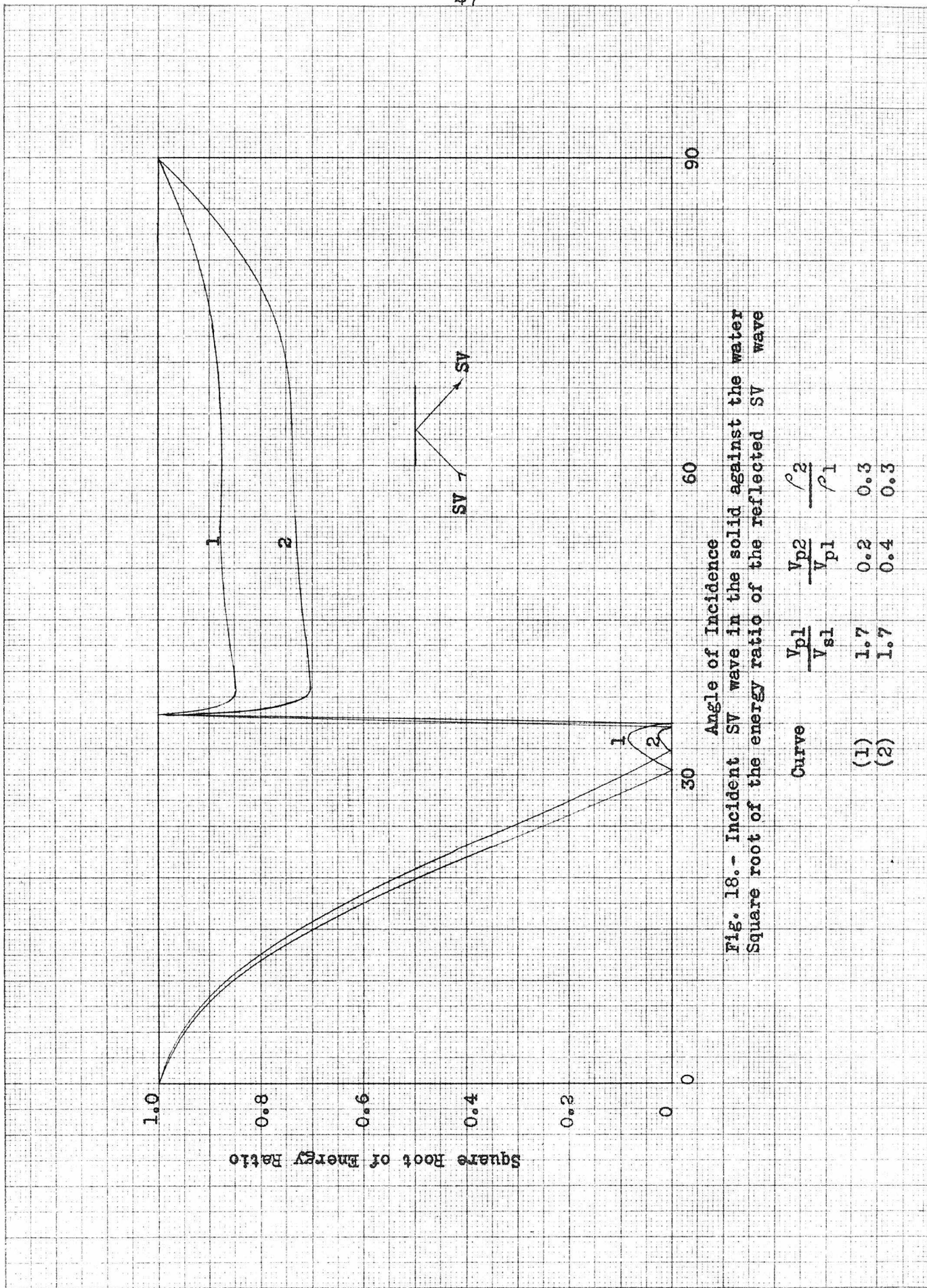
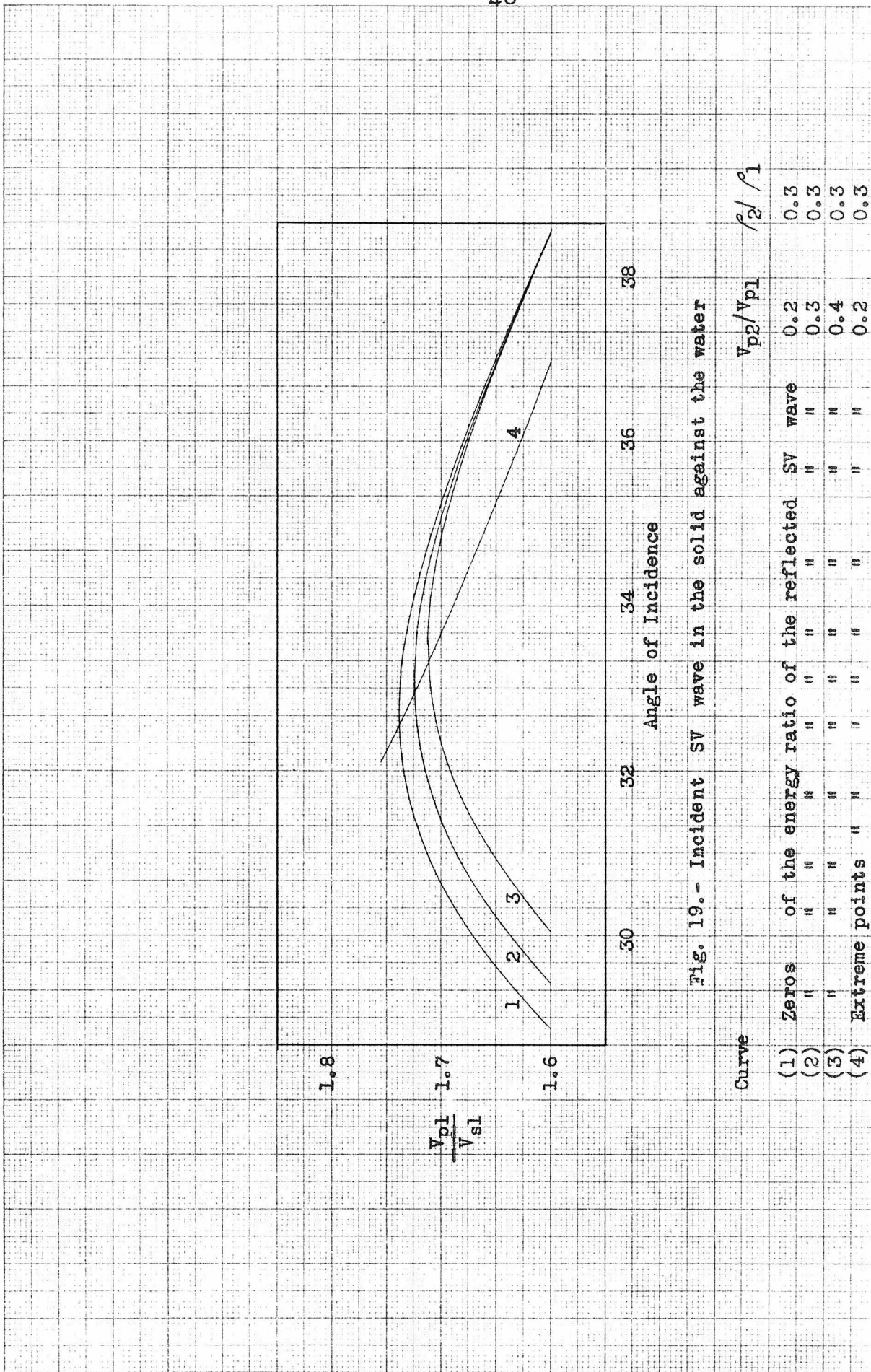


Fig. 18.- Incident SV wave in the solid against the water
Square root of the energy ratio of the reflected SV wave



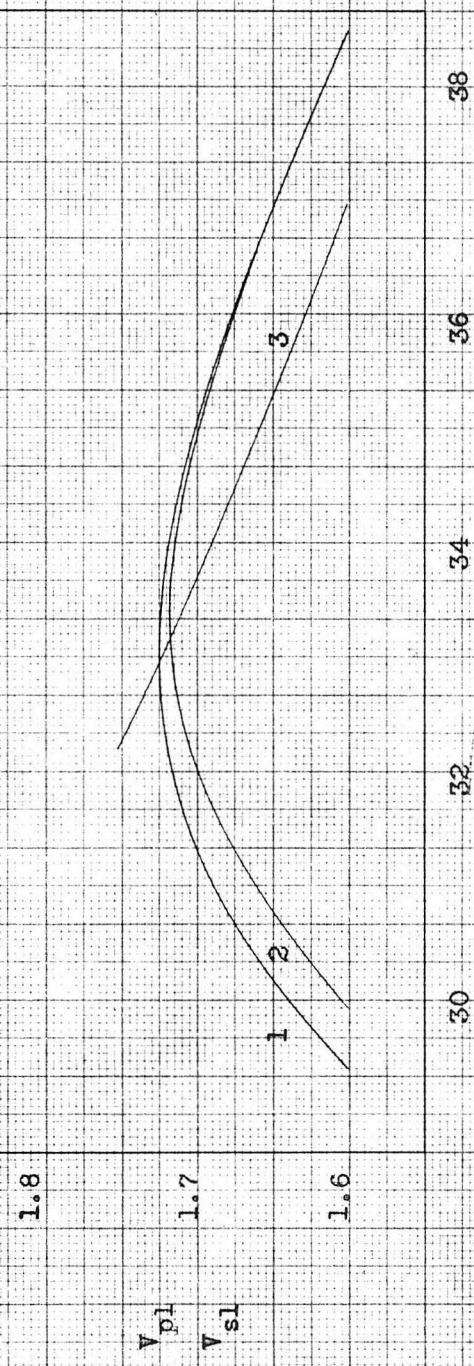


Fig. 20.- Incident SV wave in the solid against the water

Curve	Zeros of the energy ratio of the reflected wave	SV wave	V_{p2}/V_{p1}	γ_2/γ_1
(1)	" "	" "	0.3	0.3
(2)	" "	" "	0.3	0.4
(3)	" "	" "	0.2	0.3

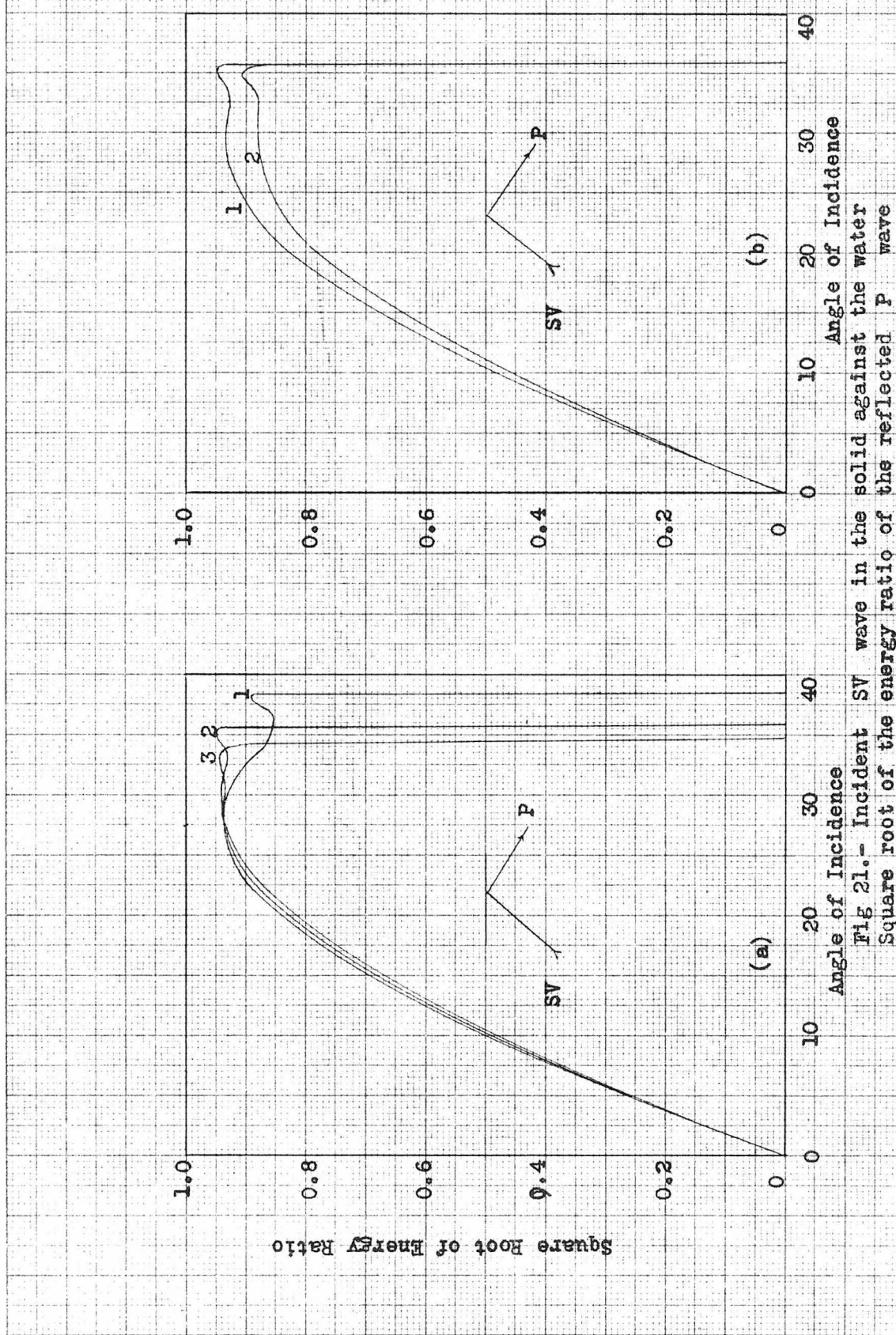


FIG 21.- Incident SV wave in the solid against the water
Square root of the energy ratio of the reflected P wave

(a)	Curve	$\frac{V_{p1}}{V_{s1}}$	$\frac{V_{p2}}{V_{p1}}$	$\frac{2}{1}$	(b)	Curve	$\frac{V_{p1}}{V_{s1}}$	$\frac{V_{p2}}{V_{p1}}$	$\frac{2}{1}$
	(1)	1.6	0.2	0.3		(1)	1.7	0.2	0.3
	(2)	1.7	0.2	0.3		(2)	1.7	0.4	0.3
	(3)	1.75	0.2	0.3					

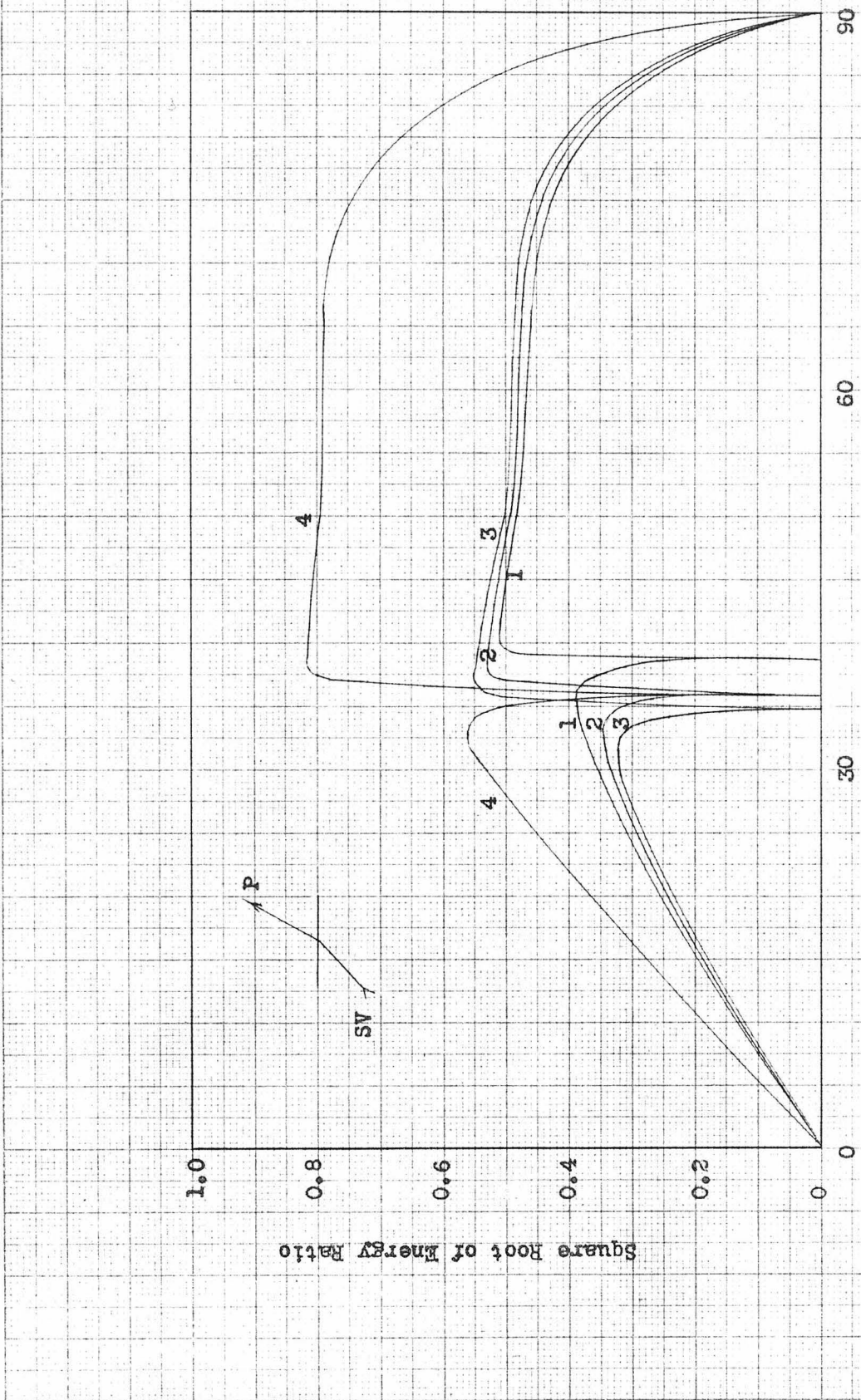


Fig. 22.- Incident SV wave in the solid against the water
Square root of the energy ratio of the refracted P wave

Curve	$\frac{V_{p1}}{V_{s1}}$	$\frac{V_{p2}}{V_{p1}}$	$\frac{\rho_2}{\rho_1}$
(1)	1.6	0.2	0.3
(2)	1.7	0.2	0.3
(3)	1.75	0.2	0.3
(4)	1.7	0.4	0.3

P A R T T W O

pp. 52 - 142

A M P L I T U D E S O F P_oP , P_oS , S_cS , A N D S_cP
I N D E E P - F O C U S E A R T H Q U A K E S

Thesis by

Kazim Ergin

In Partial Fulfillment of the Requirements
For the Degree of
Doctor of Philosophy

California Institute of Technology
Pasadena , California

1950

ACKNOWLEDGMENTS

The writer wishes to thank Dr. B. Gutenberg for his valuable supervision at all stages of the work; Dr. C. F. Richter and Dr. H. Benioff for their generous suggestions.

ABSTRACT

A systematic study has been made of the ratios of the displacements of the core reflections to the direct body waves as well as of the individual displacements, using intermediate and deep focus earthquake seismograms recorded at Pasadena. Theoretical values of the horizontal and the vertical ground displacements have been computed for the direct P and S as well as for P_{cP} , P_{cS} , S_{cS} and S_{cP} waves as a function of the epicentral distance for three focal depths, namely, 100, 400 and 700 km. The results indicate that the observed ratios of the horizontal displacements of the waves that are reflected at the core-mantle boundary as P waves (i.e., P_{cP}/P and S_{cP}/S) and that of the observed vertical displacements of the waves that are reflected as S waves (i.e., P_{cS}/P and S_{cS}/S) are five or more times larger than the theoretical ones. The ratios of the vertical components of the first group and the ratios of the horizontal components of the second group are in fairly good agreement with the theoretical values. It is further found that the behavior of the direct P and SV waves are in accord with the theory, but the vibrations are not in the direction of propagation for the reflected P waves and the vibrations are not perpendicular to the direction of propagation for the reflected S waves. The effect of anisotropic crustal structure on the ground displacements is discussed.

TABLE OF CONTENTS

TITLE	PAGE
Introduction	52
Calculated Values	56
Observed Ground Displacements	60
Methods	64
Results	67
Observed Apparent Angles of Incidence	75
Azimuth Determination from P and P _{cP}	79
Discussion of Results and Conclusions	80
Summary	85
References	88
Tables	
Figures	

INTRODUCTION

The purpose of this work is to compare theoretical and observed ground displacements produced by PcP , PcS , ScS , ScP as well as direct P and S waves, upon their arrival at the surface of the earth, using seismograms of intermediate and deep focus earthquakes that were recorded by standard seismographs at Pasadena. The same problem was treated by Martner (14) using Pasadena seismograms of shallow shocks, ($h = 60$ km.). He has used Dana's (2,4) calculated values, and compared them with his observational results. Dana had previously computed the theoretical ground displacements for P, SV, PcP , PcS , ScS , ScP , etc.... as well as the displacement ratios of the waves reflected at the mantle-core boundary to that of the incident wave. His calculations were based on the formula given by Gutenberg (5,6,7) who has derived it from the original theory of Zeepritz (Zeepritz, Seiger and Gutenberg (19)). The expression for the calculation of the ground displacement during a single body wave as a function of the epicentral distance is

$$KTM\sqrt{E_1} \quad (1)$$

where

$$M = Q \sqrt{(F_1 F_2 \dots F_n)} e^{-kp} \frac{\sin i_h d_i h / d \Delta}{\sin \Delta \cos i_o} \quad (2)$$

In equation (2) :

K is a constant depending on the fraction of the energy E_1 passing into the wave under consideration. It has three distinct values, for waves starting respectively as P, SH and SV.

T is the period of the observed wave.

Q (or u / A_e , w / A_e) is the ratio of the horizontal and the vertical component of the total ground displacement (u and w respectively) to the amplitude of the incident wave.

F is the ratio of transmitted and reflected energy to incident energy at each point where the wave has encountered a discontinuity.

$= kD$

e is the absorption factor, where $k = 0.00012/\text{km}$. as given by Gutenberg (7), and D is the distance measured along the wave path.

i_h is the angle of incidence at the source at a depth h .

i_o is the angle of incidence at the point of arrival at the surface.

\triangle is the epicentral distance.

For shallow shocks we can assume that $h \approx 0$, then if the wave arriving at the recording station is of the same type as it has originally started at the focus, such as P, PP, ..., PSP, ..., Pcp, Scs, PKP, PKKP, SKS, etc., $i_h \approx i_o$, and (2) becomes:

$$N = Q \sqrt{(F_1 F_2 \dots F_n)} e^{-KD} \frac{\tan i_0 d_0}{\sin \Delta d \Delta} \quad (3)$$

But if the wave arriving at the recording station is not of the same type as it has originally started at the source, such as Pcs , Sop , SKP , etc. . . . , even if the focus is assumed to be at the surface, the angle of incidence at the source will be different from that at the recording station. Dana (2,4) has used the formula (3) to calculate the ground displacement of all types of waves. For that reason, his values are correct only for the first group, and the theoretical ground displacements of the waves belonging to the second group (i.e. PeS , SeP , SKP , SKKP) should be recalculated.

Hartner's findings are summarized in his own words as follows:

"The observed horizontal displacement ratios of Pcp/P are definitely larger than that which is expected from the presently accepted theory; the vertical displacement ratios of Pcp/P and the horizontal displacement ratios of Pcs/P are slightly greater, but not unreasonably so; and the horizontal displacement ratios of Sos/S and the vertical displacement ratios of Sos/S and Sop/S are reasonably in accordance with the expected ratios."

Since no theoretical values were computed previously taking the depth of focus into account, we have computed the theoretical values of N using the formula (2) for P , S , Pcp , Pcs , Sos , and Sop , for three different focal depths, namely, 100 , 400 and 700 km.

When a P or S wave is incident at any discontinuity,

the refracted and reflected S waves are of SV type, and when a SH wave is incident, it is reflected as SH wave only and no other type of wave is produced. But the direct S wave and ScS have both SV and SH components. The ratio SH/SV depends mainly on the mechanism of the shock and may have any value. To calculate the values of N for S and ScS , we have assumed that SH/SV is equal to "one", i.e., the energy that passes into the S wave is divided equally between SV and SH . Since SH has no vertical component, any alternate assumption does not affect the value of N of the vertical component.

CALCULATED VALUES

Since in formula (1) K , T , and E_1 are not known, only N which actually is

$$N = \frac{1}{K/E_1} \cdot \frac{U_w}{T} \quad (4)$$

can be calculated numerically. We shall later use the symbols U and W for the horizontal and the vertical N respectively.

The values of Q were taken from Gutenberg (6) table 5c.

For the angles of incidence encountered in this work (0° - 40°) the values of F_n for the waves crossing the discontinuities separating the crustal layers are very close to unity. For this reason we have neglected the effects of these discontinuities on all types of waves under consideration, and used only F due to the reflection at the mantle-core boundary. These values were taken from Dana (2,3).

For the absorption factor $k = 0.00012/\text{km.}$ was used and the distance was read approximately from an actual plot of the ray path.

For the direct P and SV waves, i_o was computed as a function of the epicentral distance, from Benndorf's theorem:

$$\sin i_o = \frac{V_o}{\bar{v}_\Delta} \quad (5)$$

where V_o is the wave velocity at the surface of the earth. We have used Gutenberg's recent figures for V_o , namely,

v_o (SV) = 3.6 km./sec., $v_o(P)$ = 6.5 km./sec., and \bar{v}_Δ is the apparent velocity at the epicentral distance Δ .

Again for the direct P and SV waves i_h was computed from the formula

$$\frac{r \sin i}{V} = \text{Const.} \quad (6)$$

(along the same ray)

assuming the following velocities at different depths:

h	$v_h(P)$	$v_h(SV)$
0 km.	6.5 km./sec.	3.6 km./sec.
100 "	8.0 "	4.5 "
4000 "	9.2 "	5.1 "
700 "	10.6 "	5.9 "

For PcP , PoS , ScS , ScP waves i_o and i_h and Δ were calculated as a function of the angle of incidence at the mantle side of the mantle-core boundary (i_c). i_o and Δ were taken from Dana (2) corresponding to a given i_c . Δ 's were then corrected for the depth of focus. These corrections are given in tables (1a) and (3a) for P and SV waves respectively in Gutenberg and Richter (11, first paper). i_h was computed from formula (6), making the following assumptions:

r_c = the radius of the core = 3466 km.

v_c = the velocity in the mantle just outside the core

$v_c(P) = 13.7$ km./sec., $v_c(SV) = 7.25$ km./sec.

The forms of formula (6) as used for each wave are listed below:

For Pcp , i_o and i_h are calculated from

$$\frac{r_o \sin i_{op}}{v_{op}} = \frac{r_h \sin i_{hp}}{v_{hp}} = \frac{r_c \sin i_{cp}}{v_{cp}}$$

For Pcs , i_o is calculated from

$$\frac{r}{v} \frac{r_o \sin i_{os}}{v_{os}} = \frac{r_c \sin i_{c, refl, s}}{v_{cs}}$$

and i_h is calculated from

$$\frac{r_h \sin i_{hp}}{v_{hp}} = \frac{r_c \sin i_{cp}}{v_{cp}}$$

For SCS , i_o and i_h are calculated from

$$\frac{r_o \sin i_{os}}{v_{os}} = \frac{r_h \sin i_{hs}}{v_{hs}} = \frac{r_c \sin i_{cs}}{v_{cs}}$$

And finally for ScP , i_o is calculated from

$$\frac{r_o \sin i_{op}}{v_{op}} = \frac{r_c \sin i_{c, refl, p}}{v_{cp}}$$

and i_h is calculated from

$$\frac{r_h \sin i_{hs}}{v_{hs}} = \frac{r_c \sin i_{cs}}{v_{cs}}$$

After i_o and i_h are determined as described above, $\cos i_h$ is plotted against Δ . By measuring the slope of this curve , $d \cos i_h / d\Delta$ can be obtained. This is the only

quantity involved in the calculation that does not vary smoothly, if \tilde{v}_Δ values are used to calculate i_o and i_h . For the direct P and SV waves \tilde{v}_Δ were determined for every five degrees of the epicentral distance using Pasadena travel time tables, then $\cos i_h = f(\Delta)$ curves were plotted and smoothed and the slopes were measured. For PcP, Pcs, ScS, and Scp waves i_o , i_h , and Δ were calculated as a function of i_c so that $\cos i_h = f(\Delta)$ curves are rather smooth.

The calculated values are given in tables 1-6 and are plotted in figures 1-12 as $A = 6.3 - \log U$ (or $6.3 - \log W$) against the epicentral distance Δ . (see p. 65 for explanation of "A" values)

OBSERVED GROUND DISPLACEMENTS

Materials used for this research were obtained from the seismograms recorded at Pasadena. Most of the intermediate and deep focus shocks studied were recorded from 1940 to 1945. Some well-recorded shocks from 1937 to 1940 and a few shocks later than 1945 were also included. Since the dynamic magnification of wood - Anderson torsion seismographs changes very little, the seismograms of long period torsion instruments were used whenever the records were good. Unfortunately they only provide the horizontal components. In addition, the seismograms of long and short period Benioff electromagnetic instruments were used. For many shocks which were well recorded by Benioff electromagnetic seismographs, it was impossible to measure the amplitude on the seismograms of the long period torsion instruments. After combining N-S and E-W components into one horizontal component vectorially, the percentage of readings for each instrument is as follows:

Long per. torsion, horiz.	36%	of the total horiz. readings
" " Benioff "	43%	" " " " "
Short " " "	16%	" " " " "
Long " " vertical	50%	" " " " "
Short " " "	50%	" " " " "

Instrumental constants of the seismographs, records of which have been used for this work, are given below:

<u>Inst. No.</u>	<u>Comp.</u>	<u>Type of Instrument</u>	<u>Design To</u>	<u>Design Tg</u>	<u>Normal Static Magnif.</u>
IIA	Z	Benioff Electromagnetic	1 sec	90 sec	
IVA	N-S	" "	1	90	
IVB	E-W	" "	1	90	
V	E-W	Wood-Anderson Torsion	6		800
VA	N-S	" " "	6		800
VIA	Z	Benioff Electromagnetic	1	0.23	
VIB N	N-S	" "	1	0.23	
VIBAE	E-W	" "	1	0.23	

The magnification curves were taken from Martner (14). He discusses the determination of the dynamic magnification of the electromagnetic seismographs in detail. We only like to repeat here that the relative amplifications (the response characteristics) of these seismographs are more accurately known than their absolute magnifications, so that the ratios of the amplitudes of two different waves (e.g., PcP/P) read on the same seismogram are more accurate than the individual ones.

In order to compare the observed values with the calculated ones, on a given seismogram, for each wave the largest amplitude recorded is measured to the tenth of a mm. and expressed in mm., and the period associated with this largest amplitude is read in seconds. Then the amplitude is multiplied by the factor $\frac{A_e}{T_g}$, where A_e is the amplitude of the

ground motion in microns, A_e is the trace amplitude in millimeters, and T_e is the period of the ground motion, to get the A_e/T_e ratio which is another symbol for $\frac{A_e}{T_e}$. In table 8., $\log \left(\frac{A_e}{T_e} \right)_{\text{obs.}}$ are given for six waves under consideration. The abbreviations used in table (8) to indicate the type of the seismograph have the following meanings:

LBV	Long period Benioff seismograph, vert. component					
LBH	"	"	"	"	horiz.	"
LTH	"	"	Tension	"	"	"
SBV	Short	"	Benioff	"	vert.	"
SBH	"	"	"	"	horiz.	"

The periods of P_{cP} are in general less than that of P , but the periods of P_{cS} are larger than that of P . The periods of S_{cS} and S_{cP} are less than the periods of S . The average ratios of periods of the reflected waves to that of incident wave are shown below:

	T_{PcP}/T_P	T_{PcS}/T_P	T_{ScS}/T_S	T_{ScP}/T_S
Long period instr.	0.92(121)	1.46(29)	0.85(122)	0.80(51)
Short	"	0.93(75)	1.15(9)	1.0(4)

(Number of readings are shown in parentheses)

The accurate recognition of the various waves is the most important part of the problem. The P wave is always the first arrival in the range of the epicentral distances we are interested in, so that there is no uncertainty involved in regard to its correct identification. But all the other phases namely, S , P_{cP} , P_{cS} , S_{cP} and S_{cS} , arrive together with

or very close to some other waves at some epicentral distances which differ slightly with the depth of focus. In these instances, separate identification of the two waves is difficult if not impossible, especially when their periods are nearly the same. In order to avoid any uncertainties of this kind, no readings were taken whenever such a circumstance was noticed.

The smallest distances encountered are those of Mexican intermediate shocks which start at $\Delta \approx 21\frac{1}{2}^\circ$, and the largest Δ belong to some Tonga - New Hebrides deep focus earthquakes ranging up to $\Delta \approx 87\frac{1}{2}^\circ$. 631 readings for 69 shocks were used for this report. Their epicentral distance cover the range $21\frac{1}{2}^\circ - 87\frac{1}{2}^\circ$. The focal depth varies from 70 km. to 650 km. There are only twelve real deep focus shocks ($h \geq 300$ km.) included in this work.

METHODS OF COMPARING THE CALCULATED AND THE OBSERVED
GROUND DISPLACEMENTS

One method of comparison is to take the observed ratio of $\frac{U_2}{U_1}$ of the reflected wave to that of the incident wave and compare these with the ratio of N (formula 4) of the reflected wave to N of the incident wave. Since it is assumed that $K \sqrt{E_1}$ has the same value for all waves leaving the source as the same type, by taking the ratio of calculated N 's (or U 's and W 's) for P_{CP}/P , P_{CS}/P , S_{CS}/SV , S_{CP}/S , the value of $K \sqrt{E_1}$ cancel in each case, and the calculated ratios can be compared directly with the observed ratios. To avoid the use of large graph paper sheets and also wide scattering of the observed ratios, logarithms of these ratios are plotted in figures 13-16 which represent respectively,

$$\log \frac{(-\frac{U}{P})_{P_{CP}} / (-\frac{U}{P})_p}{(-\frac{U}{P})_{P_{CS}} / (-\frac{U}{P})_p} \quad (\text{upper part}) \quad \log \frac{(\frac{W}{P})_{P_{CP}} / (-\frac{W}{P})_p}{(-\frac{W}{P})_{P_{CS}} / (-\frac{W}{P})_p} \quad (\text{lower part})$$

$$\log \frac{(-\frac{U}{P})_{P_{CS}} / (-\frac{U}{P})_p}{(-\frac{U}{P})_{S_{CS}}} \quad (\text{upper part}) \quad \log \frac{(-\frac{W}{P})_{P_{CS}} / (-\frac{W}{P})_p}{(-\frac{W}{P})_{S_{CS}}} \quad (\text{lower part})$$

$$\log \frac{(-\frac{U}{P})_{S_{CS}} / (-\frac{U}{P})_S}{(-\frac{U}{P})_{S_{CP}}} \quad (\text{upper part}) \quad \log \frac{(-\frac{W}{P})_{S_{CS}} / (-\frac{W}{P})_S}{(-\frac{W}{P})_{S_{CP}}} \quad (\text{lower part})$$

$$\log \frac{(-\frac{U}{P})_{S_{CP}} / (-\frac{U}{P})_S}{(-\frac{U}{P})_{S_{SV}}} \quad (\text{upper part}) \quad \log \frac{(-\frac{W}{P})_{S_{CP}} / (-\frac{W}{P})_S}{(-\frac{W}{P})_{S_{SV}}} \quad (\text{lower part})$$

The second method for comparing the calculated and the observed values consists of calculating the "A" values.

A values were defined by Gutenberg (7) as follows:

$$\text{Theoretical At: } A_t = C - \log U \text{ (or } C = \log W) \quad (7)$$

$$\text{Observed At: } A_o = M - \log \left(\frac{U_{\text{obs}}}{T} \right)_{\text{obs.}} = 0.1(M - 7) \quad (8)$$

Where C is a constant which for practical purposes was assumed by Gutenberg to have one value in all shocks for P waves and another for all S waves (SV and SH combined). Gutenberg (7) states that, "the value of C for the S waves is so close to that for P that one and same constant C was assumed for all waves. As in general only one decimal is used in the calculations, it was decided to take

$$C = 6.5$$

and take care of the differences, especially those for the vertical components [by using] station corrections." For Pasadena, a station correction -0.2 was used in this work. Thus the formula (8) can be written as

$$A_o = M - \log \left(\frac{U_{\text{obs}}}{T} \right)_{\text{obs.}} = 0.1(M - 7) - 0.2 \quad (8a)$$

In formulae (8) and (8a), M is the magnitude of the earthquake in question as defined originally by Richter (16). The magnitudes are determined (Richter 16, Gutenberg 7 and 8) from observed amplitudes and periods using a variety of stations, instruments, wave types (chiefly P, PP, and S) and distances. For our purpose we use the magnitudes determined in this fashion to compare A_t with A_o , a process which Mooney (15) calls "a vicious circle". We shall comment on this point when we discuss the results in the following section.

A_t 's are tabulated in tables 1-6 and plotted against Δ in figures 1-12, each for three different focal depths: 100,

400 , and 700 km. For each observation $A_t - A_o$ which we shall call "residual" in the following discussion was determined. These residuals are plotted against the focal depth in figures 17-22, and against the epicentral distance in figures 23-28. A positive residual ($A_t - A_o > 0$) means that the observed displacement/period is larger than the theoretical ones, and conversely.

RESULTS

Before making any attempt to seek an explanation for the facts, we like to present these which can be detected from the results.

In fig. 13, $\log \left(\frac{U_{\text{H}}}{T} \right)_{\text{PcP}} / \left(\frac{U_{\text{H}}}{T} \right)_P$ is plotted against the epicentral distance. The solid curves are the corresponding theoretical ratios. The average discrepancy between the observed and the theoretical ratios of the horizontal component is about +0.8* (plus sign meaning the observed ratios larger. when the observed ratios are smaller it will be indicated by a minus sign), except for $\Delta < 30^\circ$ where it is still higher. It is important to note here that no definite appreciable effect of the epicentral distance on the discrepancy can be detected from the results. For the corresponding ratio of the vertical component observed values are on the average higher than the theoretical ones, but not as much as in the case of the horizontal component, the average discrepancy being approximately +0.3 or +0.4. Between 40° and 60° epicentral distances the agreement is fairly good. In any case, when seeking an explanation for the abnormal discrepancies observed, the horizontal component ratios are the ones that should attract more attention; although any explanation that can be proposed should not change the vertical component ratios in the wrong direction.

* These figures are the logarithms of the quantities involved.

The data for SeP / S (Fig. 16) are not abundant and they only cover an epicentral range $25^\circ - 50^\circ$. However, the available data definitely show that the observed horizontal ratios are about five or more than five times larger than the theoretical ones around $30^\circ - 35^\circ$, decreasing somewhat as the epicentral distance becomes larger. The same effect of the epicentral distance can be observed for the vertical component ratios. Here, the average discrepancy is about $+0.4$, indicating that the observed ratios are about two or three times larger than the theoretical ones.

The horizontal components of the observed ratios of PeS/P (Fig. 15) are in good agreement with the theoretical ratios. There are only a limited number of data available, nevertheless all of the points of the observed values fall along the calculated curve. As PeS arrive right after SeP and close to it, in many instances it is difficult to identify them separately. However, the difference in the arrival times of these two waves increases with the focal depth. Although the observed ratios for the horizontal component of PeS/P fit the theory nicely, the observed vertical displacement ratios are on the average five times larger than the calculated ratios.

The observed horizontal SeS/S (Fig. 14) ratios (SH/SV is assumed to be "one") are in fairly good accord with the theoretical results except for $\Delta < 40^\circ$ where they are larger. The observed vertical component ratios of SeS/S are ten or

more times larger than the corresponding theoretical values around $\Delta = 30^\circ$. This difference decreases as Δ increases and for $\Delta = 70^\circ$ the observed results fit the theoretical curve nicely.

The foregoing analysis of data can be summarized as follows:

The observed ratios of the horizontal displacements of the waves that are reflected as P waves at the mantle-core boundary to those of the incident wave are on the average six or seven times larger than the theoretical ratios. The observed ratios of the vertical components of these waves are only two or three times larger than the theoretical ones. (This group includes PcP/P and SeP/S). For the waves that are reflected as S waves at the mantle-core boundary the observed horizontal component ratios are in fairly good agreement with the theoretical ratios, but the observed vertical component ratios of the same waves are considerably larger than the theoretical ratios. (This group includes SeS/S and PcS/P). The vertical component ratios of SeS/S and PcS/P show some effect of the epicentral distance, the discrepancy between the theoretical and the observed ratios decreases for large epicentral distances.

In the set of figures 17-22, the residuals $A_t - A_o$ for different waves as indicated on the figures are plotted against the depth of focus. Each figure consists of two parts, the upper part giving the residuals of the horizontal component, and the lower part giving that of the vertical component.

Looking at these figures one can at once notice that the focal depth has no effect on the residuals. In all cases the residuals scatter a great deal, but for each case a straight line that is parallel to the zero line can be drawn to represent the average value of the residuals.

Analyzing each figure individually, we observe that:

The line representing the mean residuals for both horizontal and vertical ground displacements of the direct P wave and for the horizontal component of the PcS wave are fairly close to the zero line. In the case of both horizontal and vertical component of the direct S wave the line representing the average residual is below the zero line, having an approximate value - 0.1. The residuals of the horizontal ground displacement due to ScS wave are on the average fairly close to the zero line, but that of the vertical component of the same wave have an average value about +0.5. The average horizontal residual of PcP is approximately +0.8, and the average vertical residual of PcP is approximately +0.4, (putting more weight on long period instrument readings). The mean vertical residual for PcS is about +0.6. The mean horizontal and vertical residuals of ScP wave are approximately +0.75 and +0.35 respectively.

To summarize, we can say that the depth of focus does not play any role in the variation of the residuals. The results obtained by a method based on the relationship between the energy and the magnitude of an earthquake (i.e., the residuals $A_t - A_0$), are tabulated below:

	Average residual	
	Horizontal comp.	Vertical comp.
P	$\pm 0.4^*$	$\pm 0.$
PcP	+ 0.8	+ 0.4
PcS	$\pm 0.$	+ 0.6
S	- 0.1	- 0.1
ScS	+ 0.1	+ 0.5
ScP	+ 0.75	+ 0.35

If we remember that the magnitudes used to calculate $A_t - A_0$ values are originally determined from the observed ratios of the displacements of the direct P (and also of PP and S waves), to the observed period, by solving the equation $A_t - A_0 = 0$ for M, the results obtained for the direct P waves (both horizontal and vertical components) should not be surprising. The interesting fact is that if we try to calculate the magnitude from the waves that are reflected from the mantle-core boundary we get larger magnitudes.

The results obtained from $A_t - A_0$ residuals as a function of the focal depth, are in good agreement with those that were obtained from the study of the displacement ratios, which were summarized on page 69.

(*) These figures are the logarithms of the quantities involved.

The residuals $A_t - A_0$ are also plotted against the epicentral distance in figures 23-28. Here again each figure consists of two parts, the upper part represents the horizontal component, and the lower part represents the vertical component. The characteristic features of the residuals as a function of the epicentral distances are listed below:

1. Direct P wave:

(a). Horizontal component: The mean residual curve can be represented by a straight line that has a slight positive slope. The residual is negative for $\Delta < 35^\circ$, and positive for $\Delta > 35^\circ$, thus increasing slightly with the increasing epicentral distance. However, this mean residual line is very close to the zero line at all distances.

(b). Vertical component: these residuals as a whole have a similar picture to that of the horizontal component residuals.

2. PcP:

(a). Horizontal component: For all epicentral distances a line parallel to the zero line can be drawn to represent mean residual which is approximately + 0.8. The residuals for $\Delta < 30^\circ$ are somewhat higher than this overall mean.

(b). Vertical component: The line representing the mean residual has a very slight positive slope. The overall mean residual is about + 0.5 (putting more weight on the readings from the long period seismograph seismogram readings).

3. Pcs:

(a). Horizontal component: There are only a few

readings for this wave all of which line up around the zero line so that the overall average residual is $\pm 0.$.

(b). Vertical component: The overall mean residual is approximately $+ 0.7$.

4. ScS:

(a). Horizontal component: The line representing the average residuals has a slight negative slope. Overall mean is very close to zero.

(b). Vertical component: Here again we observe a very very slight negative slope. The overall mean residual is about $+ 0.3$. The residuals for $\Delta < 40^\circ$ are considerably larger than this overall mean.

5. ScP:

(a). Horizontal component: Here too a slight negative slope is present. The overall mean residual is approximately $+ 0.75$.

(b). Vertical component: The mean residual line is parallel to the zero line and the overall mean is about $+ 0.3$.

6. S:

Both horizontal and vertical components have an average residual line with a slight positive slope, overall mean value is slightly negative for both cases.

The foregoing analysis of the characteristic features of the residuals as a function of the epicentral distance shows that the results are again in good agreement with those that were obtained by considering the displacement ratios which were summarized on page 69.

The advantage of the residual ($A_t - A_o$) method is that it brings up the individual features of the displacements for each wave separately. Furthermore, these results indicate that, whereas the individual residuals from the short period instrument readings are larger than those which are read from the long period instrument seismograms (see vertical components for $A_t - A_o$ curves for P and P_cP), the average curves representing the displacement ratios (vertical) for short and long period instrument data coincide. This result is in accord with the fact that the relative dynamic magnification of the electromagnetic instruments are more accurately known than their absolute dynamic magnification.

OBSERVED APPARENT ANGLES OF INCIDENCE:

The large observed horizontal component ratios of PcP/P and other anomalous large observed results have lead us to investigate the observed apparent angles of incidence for P, PcP , S, and SsS waves. The apparent angle of incidence \tilde{i} is calculated by

$$\tilde{i} = \tan^{-1} \left(\frac{u}{w} \right)_{\text{obs.}} \text{ (for longitudinal waves)}$$

To calculate \tilde{i} by this formula we used u , and w as obtained from the same type of horizontal and vertical instruments. For this purpose only long period Benioff instruments supplied sufficient data. The results are shown on figures 29 and 30 for P and PcP waves respectively. The observed apparent angles of incidence of PcP has an average value $35^\circ - 40^\circ$. The actual angle of incidence corresponding to this average apparent angle of incidence would be approximately two degrees less than these values, i.e., about $33^\circ - 38^\circ$ (see Gutenberg (5)). There is a tendency for the observed \tilde{i} to decrease slightly as Δ increases. The actual angle of incidence of PcP as calculated from the apparent velocity of the same by Benndorf's theorem, starts from zero at $\Delta = 0^\circ$, and increases slowly as the epicentral distance increases and reaches a value little more than 15° at the largest epicentral distances. The observed apparent angles of incidence of P wave are somewhat smaller than the theoretical ones at small epicentral

distances and larger for large epicentral distances. But, in general they fit the theoretical angles of incidence which are obtained from the calculated values of the actual angle of incidence, nicely. The equation, a table and a curve relating these two angles can be found in Gutenberg (5).

From the consideration of the apparent angles of incidence of the direct P wave and P_cP wave, it can be concluded that the anomalous character of the observed P_cP/P displacement ratios are due to the behavior of the P_cP wave and not due to the behavior of the direct P wave. This fact is further evidenced by the results of $A_t - A_o$ residuals. Thus we are lead to seek the cause of the discrepancies at the reflection phenomenon that takes place at the mantle-core boundary.

The apparent angles of incidence of SV type waves can be obtained from the formula

$$I = \tan^{-1} \left(\frac{V}{U} \right) \text{ observed}$$

The equation and a table relating \hat{I} to the actual angle of incidence of SV type waves are given in Gutenberg (5). Using displacement values that were obtained from the records of the long period horizontal and vertical component Benioff electromagnetic instruments, \hat{I} 's for S and ScS were determined and they are plotted against the epicentral distance in figures 31 and 32 respectively. On the average observed apparent angle of incidence for ScS is about 32° at all epicentral distances which is considerably larger than the

calculated ones as shown on in figure 32 by the solid line. On the other hand, the observed angle of incidence for the direct S wave is somewhat smaller than the expected ones for small epicentral distances and larger for large epicentral distances. But in general they are fairly close to the calculated angles of incidence. This result is in accord, as should be expected, with the result that was mentioned previously that the observed and calculated displacement ratios S_{cS}/S are in better agreement for large epicentral distances.

It may be noted here that the observed apparent angle of incidence represents the angle of vibration at the recording station whereas the angle of incidence is the angle that a ray makes with the radius vector of the earth at the recording station upon the arrival of the ray. According to the present theory these two angles should differ from one another for the range of values considered here by only about $2^\circ - 3^\circ$ at the most, assuming, of course, in case of longitudinal wave that the vibration is in the direction of the propagation. The observational results strongly indicate that (e.g., for Pcp) the vibration is not in the direction of propagation.

To check the angles of arrival of Pcp waves, an easy and quick method was suggested by Dr. Benioff. By observing the difference of arrival times of Pcp at two local stations for some shocks, epicenters of which are approximately along the line connecting the two recording stations. If these

differences are equal or close to the ones that would be expected from the travel time curves, it would mean that the angles of arrival check the present theory of propagation. For this purpose nine Mexican and Central American shocks were selected which were recorded at all three stations, namely, Pasadena, Palomar and Tinemaha. The differences of arrival times (d) that were obtained from the Bulletins of the Seismological Laboratory at Pasadena are listed below:

Out of nine cases (Pasadena - Palomar)

For	2	shocks	$d = 2$	seconds
"	4	"	3	"
"	2	"	4	"
"	1	"	7 (?)	"

Out of eight cases (Tinemaha - Palomar)

For	4	shocks	$d = 8$	seconds
"	3	"	9	"
"	1	"	14 (?)	"

In both cases except only for one shock, these differences are in close agreement with the ones given by the travel time curves for the corresponding focal depth and the epicentral distance range ($31^\circ - 35^\circ$).

AZIMUTH DETERMINATION FROM P AND Pcp

Using the seismograms of the long period electromagnetic instruments the azimuths of the epicenters were determined from P and Pcp separately for 22 shocks. The results are given below and plotted in figure 33. δ is the difference between two azimuths determined from P and Pcp.

Out of 22 earthquakes

for 13 shocks	$ \delta < 10^\circ$
" 3 "	$10^\circ \leq \delta < 15^\circ$
" 5 "	$15^\circ \leq \delta < 20^\circ$
" 1 "	$ \delta \geq 20^\circ$ ($ \delta = 23^\circ$)

The azimuths obtained using the ground displacements in N-S and E-W directions of the P waves as well as those of Pcp wave scatter. However, the curve representing the average values as a function of the epicentral distance indicate no appreciable departure from one another to be considered as the cause of the observed discrepancies regarding the ground displacement of Pcp.

DISCUSSION OF THE RESULTS AND CONCLUSION

In the last chapter, we tried to write down all the facts that could be detected from the data, without attempting to give any explanation. Now we are in a position to discuss them in a little more detail and to seek possible sources that can explain (if any such source can be found) the observed results.

The fact that the same results were obtained by another investigator minimizes if not eliminates the cause to be due to a systematic error of measurements. As it was mentioned earlier the instrumental constants are fairly accurate and if the displacement ratios instead of individual displacements are considered the accuracy is higher. Therefore, the sources of error must be sought in the assumptions involved in the derivation of the theoretical formulae (1) and (2). Martner (14) has carefully reconsidered each factor involved in the formula (2), making alternate possible assumptions regarding the velocities of P wave near the surface of the earth, in the mantle just outside the core, and in the core near the mantle-core boundary. He has also tried alternate possible density ratios at the mantle-core boundary. The effects of these alternate assumptions as calculated by Martner can be summarized as follows:

To calculate the energy ratios of the reflected and the refracted waves at the mantle-core boundary, Dana (3) had

used the following velocities and densities: $V(P, \text{mantle}) = 13.7 \text{ km./sec.}$, $V(P, \text{core}) = 8.0 \text{ km./sec.}$, $\rho(\text{core}) / \rho(\text{mantle}) = 10.1/5.4$. Leaving $V(P, \text{mantle})$ as 13.7 km./sec. and assuming for $V(P, \text{core}) = 7 \text{ km./sec.}$ and 9 km./sec. , and for $\rho_2 / \rho_1 = 2.0, 1.5,$ and 1.0 , Martner calculated different curves for $\sqrt{E_{\text{reflected } P} / E_{\text{incident } P}}$ for six possible combinations of these parameters. He finds that only when $V(P, \text{core}) = 9 \text{ km./sec.}$ and $\rho_2 / \rho_1 = 2.0$ the energy ratio curve is above the curve given by Dana, and in that case it only increases by 16 per cent. Assuming the longitudinal wave velocity near the surface of the earth to be 8.0 km./sec. , Martner has calculated the theoretical angles of incidence for PeP. This higher velocity gives an angle of incidence at the largest epicentral distance about $18\frac{1}{2}^\circ$ which is only three degrees larger than the one we have obtained on the assumption that the longitudinal velocity near the surface is 6.5 km./sec. and still far smaller than the observed apparent angle of incidence.

The observed large ground displacements due to PeP and others may seem to suggest that the energy released at the focus does not propagate equally in all directions. This would mean that a larger fraction of energy is propagated vertically downward (thus going into PeP wave) and decreasing as the angle of incidence at the focus increases. If this was the case, the energy going into P and PeP waves at larger epicentral distances should be nearly the same and the observed

values should fit the theoretical curve at the large epicentral distances. And also the discrepancies for the horizontal and the vertical components should be the same. But the results are far different, the discrepancies for P_{CP}/P ratio are almost the same for all distances.

Thus, we are unable to explain the large observed ground displacements due to the waves that are reflected at the mantle-core boundary by any alternate possible assumptions in regard to the velocity and the density distribution in the neighborhood of the discontinuity, and the velocity near the surface of the earth. The azimuths as calculated from P_{CP} show no appreciable departure from those that are calculated from P , and the angle of arrival as calculated from the arrival-time differences of P_{CP} between two nearby stations which line up with the epicenter, show no departure from the present theory of propagation of the seismic waves. But we have strong evidence that the ground vibration due to P_{CP} wave is not in the direction of propagation at the recording station whereas the vibration due to the direct longitudinal wave is nearly in the direction of propagation. It seems logical that we ask ourselves the question at this point: "is it possible to have a P wave for which the vibration is not in the direction of propagation? could it be a combination of transverse and longitudinal wave traveling together?" The theory shows that in an isotropic medium soon after reflection longitudinal and transverse waves will separate as they travel with different velocities. As early as in 1911 Rudzki (17)

has investigated the propagation of a disturbance in an anisotropic medium. He considered the case of the crustal layers of the earth and assumed the medium to be transversely isotropic and vertically anisotropic. Recently Stoneley (18) published a paper in which he considers the same problem in the same manner. Rudzki's original paper where reflection and refraction under assumed conditions were also considered was not available to the writer. In a review of Rudzki's paper it is indicated that under these conditions there will neither be a purely longitudinal nor a purely transverse wave. Stoneley expresses the same opinion in the following words: "under these assumptions, with body waves the sharp distinction into compressional and distortional waves does not hold." Stoneley does not go into the problem of reflection and refraction, he merely indicates that by setting up the relevant boundary conditions the reflection and refraction can be worked out.

If aeolotropy is assumed for the crustal layers, then the waves recorded and recognized as longitudinal type waves would not be purely compressional and similarly the transverse type waves would not be purely distortional. From the observational results we have been inclined to think that the behavior of the direct P and S waves agree with the present theory fairly well. But Fig. 17 and Fig. 18 show that $A_t - A_0$ of P and S waves increase slightly as the epicentral distance increases (i.e., as the angle of incidence decreases). Also the observed apparent angle of incidence of P and S waves are smaller than the expected ones for small epicentral distances (i.e., for large angle of incidences) and larger than

the expected ones for large epicentral distances (i.e., for small angles of incidences). $A_t - A_0$ of PcS and of ScS increase as the epicentral distance decreases (i.e., as the angle of incidence decreases). This indicates that $A_t - A_0$ shows slight tendency to vary as a function of the angle of incidence. $A_t - A_0$ of PcP and of ScP do not exhibit any tendency to decrease as the angle of incidence increases. Furthermore, the observed apparent angles of incidence of PcP and ScS are much larger than the theoretical ones. If the observed apparent angles of incidence of P and PcP are considered together as a function of the actual angle of incidence, the curve representing the average values of these angles has a sharp jump from P to PcP . Therefore, although an anisotropic crustal structure may be the cause of some fraction of the discrepancies, it does not seem to be the main one. Further theoretical research is needed to solve the problem.

SUMMARY

The observed ground displacements of the direct P and SV waves and the waves that are reflected at the mantle-core discontinuity are compared with the calculated ground displacements of the same waves based on theoretical considerations. The theoretical values of the ground displacements can not be calculated directly but the quantity $N = \frac{1}{K\sqrt{E_1}} \times \left(\frac{U_s w}{T} \right)$ can be computed. N was computed for each of the six waves under consideration as a function of the epicentral distance and for three focal depths: 100, 400, and 700 km. . These theoretical values do not vary very much with the depth of focus.

Largest amplitudes recorded on the seismogram for each wave and the period associated with this amplitude were measured, and after converting the trace amplitude to the ground motion, u/T or w/T were obtained. Only seismograms of intermediate and deep focus earthquakes were used for this investigation. 69 shocks ranging in epicentral distance from $21\frac{1}{2}^\circ$ to $87\frac{1}{2}^\circ$ were read. 84% of the horizontal readings were obtained from the seismograms of the long period instruments (torsion and electromagnetic) and 16% were obtained from the short period electromagnetic instrument seismograms. For the vertical components, the readings from both type of instrument readings are equal in number.

The periods of the reflected waves are on the average less than that of the incident waves, except in the case of

PcS where they are larger.

The focal depths of the shocks studied vary from 70 km. to 650 km. There are only seven shocks with focal depth greater than 300 km.

Two methods were used to compare the observed and the theoretical values. First method consists of taking the ratios of the observed ($\frac{N_{\text{obs}}}{N_{\text{inc}}}$) of the reflected wave to that of the incident wave and of comparing these ratios with the ratios of N of the reflected wave to that of the incident wave. This involves the assumption that the factor $1/K\sqrt{E_1}$ is constant for all waves originating from the source as the same type of wave. Second method consists of comparing the observed "A" values (A_{obs}) with the theoretical "A" values (A_t) for each individual wave. The results obtained by both methods are the same. The results obtained by the first method indicate that the observed horizontal component ratios of PcP/P and ScP/S and the observed vertical component ratios of PcS/P and ScS/S are five or more times larger than the theoretically expected ratios, while the observed horizontal component ratios of PcS/P and ScS/S and the observed vertical component ratios of PcP/P and ScP/S are in fairly good agreement with and sometimes only two-three times larger than the theoretical ratios. Furthermore, the results of the second method indicate that the direct P and S waves obey the theory based on the relation between magnitude and energy so that the observed large values of the above ratios are due to the behavior of the waves that are reflected

at the mantle-core boundary.

For P, S, Pcp and ScS waves observed apparent angles of incidence were computed. While these angles agree with the theoretical ones for the direct body waves (P and S), the observed angles are considerably larger than the theoretically expected ones for Pcp and ScS waves. In this connection differences in Pcp arrival times at the two recording stations were observed. They check the time differences indicated by the travel time curves. These results have lead us to conclude that the angle of vibration (apparent angle of incidence) is not the same as the angle of arrival (actual angle of incidence) which means that for Pcp wave the vibration is not in the direction of propagation. According to Rudzki and Stoneley in an anisotropic medium the distinction of the body waves into a purely longitudinal and a purely transverse waves does not hold.

An aeolotropic crustal structure may account for some fraction of the difference between observed and theoretical results but it does not seem to be the main cause. Further theoretical research must be undertaken to solve the problem.

REFERENCES

1. Bullen, K. E. : An Introduction to the Theory of Seismology, Cambridge University Press, 1947.
2. Dana, S. W. : Amplitudes of Seismic Waves Reflected and Refracted at the Earth's Core, unpublished thesis, Calif. Inst. of Technology, Pasadena, Calif. (1944).
3. " : The Partition of Energy among Seismic waves Reflected and Refracted at the Earth's Core, Bull. Seism. Soc. Am., vol. 34 (1944), pp. 189-197.
4. " : The Amplitudes of Seismic waves Reflected and Refracted at the Earth's Core, Bull. Seism. Soc. Am., vol. 35 (1945), pp. 27-35.
5. Gutenberg, B. : Theorie der Erdbebenwellen, Handbuch der Geophys., vol. 4, (1932), pp. 1-80.
6. " : Energy Ratio of Reflected and Refracted Seismic Waves, Bull. Seism. Soc. Am., vol. 34 (1944), pp. 85-102.
7. " : Amplitudes of P, PP, and S and Magnitude of Shallow Earthquakes, Bull. Seism. Soc. Am., vol. 35 (1945), pp. 57-69.
8. " : Magnitude Determination for Deep Focus Earthquakes, Bull. Seism. Soc. Am., vol. 35 (1945), pp. 117-130

9. Gutenberg, B. : Amplitudes of Surface Waves and Magnitudes of Shallow Earthquakes, Bull. Seism. Soc. Am., vol. 35 (1945), pp. 3-12.
10. Gutenberg, B. and Richter, C. F. : On Seismic Waves, Fourth Paper, Gerl. Beitr. z. Geophys., vol. 54 (1939), pp. 94-136.
11. " " : Materials for the Study of Deep Focus Earthquakes, Bull. Seism. Soc. Am., First Paper, vol. 26 (1936), pp. 341-390. Second " " 27 (1937), pp. 157-183.
12. " " : Earthquake Magnitude, Intensity, Energy and Acceleration, Bull. Seism. Soc. Am., vol. 32 (1942), pp. 163-191.
13. " " : Seismicity of the Earth and Associated Phenomena, Princeton University Press, 1949.
14. Martner, S. T. : Observation on Seismic waves Reflected at the Core Boundary of the Earth, Unpublished thesis, Calif. Inst. of Technology, Pasadena, Calif. (1948).
The same in condensed form, Bull. Seism. Soc. Am. (in press)
15. Richter, C. F. : An Instrumental Earthquake Magnitude Scale, Bull. Seism. Soc. Am., vol. 25 (1935), pp. 1-32.
16. Mooney, R. H. : A Study of the Energy Contained in the Seismic waves P and pP, unpublished thesis, Calif. Inst. of Technology, Pasadena, Calif. (1960).

17. Rudski, M. P.: Parametrische Darstellung der elastischen Wellen in anisotropen Medien, pub. Acad. d. Sciences de Cracovie, Okt. (1911), pp. 503-530. An Abstract of the above paper in German is in Berl. Boit. z. Geophys., Kleine Mitteilungen, vol. 11-12, (1911-13), pp. 75-79.
18. Stoneley, R. : The Seismological Implications of Aeolotropy in Continental Structure, Month. Not., R. Astr. Soc., Geoph. Supplement, vol. 5, No. 8, March (1949), pp. 343-353.
19. Zoepfrits, K., Geiger, L. and Gutenberg, B. : Über Erdbebenwellen, V, Nach. k. Ges. d. Wiss. z. Göttingen, math.-phys. Kl., (1912), pp. 121-206.

Table 1. - Values of $\lambda \approx 6.3 - \log U$ (or $6.3 - \log W$) as a function of Δ (in Degrees), for P

<u>Δ</u>	<u>$h \approx 100$ km</u>		<u>$h \approx 400$ km</u>		<u>$h \approx 700$ km</u>	
	<u>Horiz</u>	<u>Vert</u>	<u>Horiz</u>	<u>Vert</u>	<u>Horiz</u>	<u>Vert</u>
20	5.8	5.6	5.8	5.7		
25	6.1	6.0	6.2	6.0	6.2	6.0
30	6.3	6.2	6.5	6.3	6.4	6.2
35	6.6	6.4	6.6	6.4	6.3	6.1
40	6.6	6.4	6.4	6.3	6.3	6.0
45	6.6	6.4	6.5	6.3	6.6	6.3
50	6.8	6.6	6.7	6.4	6.8	6.6
55	7.0	6.7	6.6	6.4	6.6	6.4
60	6.9	6.6	6.7	6.4	6.6	6.3
65	6.8	6.5	6.8	6.5	6.7	6.4
70	6.8	6.5	6.8	6.5	6.7	6.4
75	7.0	6.6	7.0	6.6	7.0	6.4
80	7.1	6.8	7.1	6.7	6.9	6.5
85	7.2	6.8	7.2	6.8	7.0	6.6
90	7.2	6.7	7.1	6.7	7.2	6.7
95	7.6	7.0	7.2	6.7	7.3	6.8
100	7.4	7.0	7.5	7.0	7.4	6.9

Table 2. - Values of $A = 6.3 - \log U$ (or $6.3 - \log W$) as a function of Δ (in Degrees), for PeP

$h = 100$ km			$h = 400$ km			$h = 700$ km		
Δ	Horiz	Vert	Δ	Horiz	Vert	Δ	Horiz	Vert
8.1	9.0	7.7	8.0	8.9	7.6	7.9	8.9	7.6
16.7	8.5	7.5	16.4	8.4	7.4	16.0	8.3	7.3
25.3	8.1	7.3	24.8	8.0	7.2	24.1	7.9	7.1
34.4	7.9	7.2	33.8	7.8	7.1	32.8	7.7	7.0
44.8	7.8	7.2	44.0	7.7	7.1	42.8	7.6	7.0
56.4	7.8	7.2	55.5	7.7	7.1	54.2	7.6	7.0
71.2	8.0	7.4	70.3	7.9	7.3	68.8	7.8	7.3
91.3	8.4	7.8	90.3	8.3	7.8	89.8	8.2	7.7
97.8	9.5	9.0	96.8	9.5	9.0	95.3	9.5	8.9
102.8	7.9	7.4	101.8	7.8	7.3	100.3	7.8	7.3

Table 3. - Values of $A = 6.3 + \log U$ (or $6.3 + \log W$) as a function of Δ (in Degrees), for FeS

<u>$h = 100$ km</u>			<u>$h = 400$ km</u>			<u>$h = 700$ km</u>		
<u>Δ</u>	<u>Horiz</u>	<u>Vert</u>	<u>Δ</u>	<u>Horiz</u>	<u>Vert</u>	<u>Δ</u>	<u>Horiz</u>	<u>Vert</u>
6.3	7.4	9.0	6.2	7.3	8.9	6.1	7.2	8.8
12.6	7.1	8.4	12.5	7.0	8.5	12.0	6.9	7.9
19.0	7.0	8.1	18.5	6.9	8.0	17.8	6.8	7.9
25.6	6.9	7.9	25.0	6.8	7.8	24.1	6.8	7.7
32.9	7.0	7.9	32.1	6.9	7.8	30.9	6.8	7.7
40.2	7.1	7.9	39.3	7.0	7.8	38.0	6.8	7.7
48.6	7.2	8.0	47.7	7.0	7.8	46.2	7.0	7.8
57.5	7.3	8.0	56.6	7.2	8.0	55.5	7.1	7.9
61.2	7.4	8.2	60.2	7.3	8.1	58.7	7.2	8.2
65	∞	∞	64	∞	∞	62.6	∞	∞

Table 4. - Values of $A = 6.3 - \log U$ (or $6.3 - \log W$) as a function of Δ (in Degrees), for SV

Δ	$h = 100$ km		$h = 400$ km		$h = 700$ km	
	Horiz	Vert	Horiz	Vert	Horiz	Vert
20	6.5	6.7				
25	6.8	6.1	6.8	6.0	6.9	6.1
30	6.2	6.4	6.1	6.3	6.2	6.5
35	6.4	6.6	6.3	6.5	6.3	6.5
40	6.4	6.6	6.3	6.6	6.3	6.5
45	6.5	6.8	6.4	6.8	6.4	6.6
50	6.8	7.0	6.5	6.8	6.4	6.7
55	6.5	6.8	6.5	6.8	6.5	6.6
60	6.5	6.8	6.4	6.7	6.3	6.6
65	6.6	6.9	6.6	6.9	6.5	6.8
70	6.7	7.1	6.8	7.1	6.7	7.1
75	7.0	7.3	6.8	7.1	6.6	6.9
80	6.9	7.2	6.7	7.0	6.5	6.9
85	6.6	7.0	6.6	6.9	6.5	6.8
90	6.6	7.1	6.5	7.0	6.5	7.0
95	6.8	7.3	6.8	7.2	6.8	7.2
100	7.0	7.4	7.0	7.5	6.9	7.4

Table 5. - Values of $A = 6.3 - \log U$ (or $6.3 - \log W$) as a function of Δ (in Degrees), for ScS

$h = 100$ km			$h = 400$ km			$h = 700$ km		
Δ	Horiz	Vert	Δ	Horiz	Vert	Δ	Horiz	Vert
3.2	6.6	7.8	8.0	6.5	7.8	7.7	6.4	7.7
17.2	6.7	7.6	16.8	6.6	7.6	16.3	6.5	7.5
26.1	6.8	7.6	25.5	6.7	7.5	24.8	6.6	7.4
26.9	6.8	7.6	26.3	6.7	7.5	25.6	6.6	7.4
27.9	6.6	7.4	27.3	6.5	7.3	26.5	6.4	7.2
30.5	7.0	7.7	29.8	6.9	7.7	29.0	6.8	7.6
35.5	7.1	7.8	34.8	7.0	7.7	33.8	6.9	7.6
46.1	7.1	7.7	45.3	7.0	7.6	44.2	7.0	7.6
58.1	7.0	7.6	67.1	7.0	7.5	55.9	6.9	7.4
72.4	7.0	7.5	71.4	6.9	7.5	69.9	6.8	7.4
90.8	7.2	7.7	89.7	7.2	7.6	88.1	7.0	7.5
100.8	7.3	7.8	99.7	7.3	7.8	98.0	7.2	7.6

Table 6. - Values of $A = 6.3 - \log S$ (or $6.3 - \log N$) as a function of Δ (in Degrees), for ScF

$h = 100 \text{ km}$			$h = 400 \text{ km}$			$h = 700 \text{ km}$		
Δ	Horiz	Vert	Δ	Horiz	Vert	Δ	Horiz	Vert
0	∞	∞	0	∞	∞	0	∞	∞
12.7	8.4	7.4	12.6	8.3	7.3	12.3	8.2	7.2
28.9	7.9	7.2	28.4	7.8	7.1	27.8	7.7	7.0
48.7	7.9	7.4	48.2	7.9	7.4	47.4	7.8	7.3
54.4	8.0	7.5	53.8	8.0	7.5	53.0	7.9	7.4
65.4	∞	∞	64.7	∞	∞	63.8	∞	∞

Table 7. - Regional List of Shocks Used in this Report

Region 1 (Aleutian Islands, Alaska), Intern. Shocks

No.	Date	Time (GCT)	Depth	Location	Δ	M
80	1940, July 14	05:52:53	80	51 $\frac{1}{2}$ N 177 $\frac{1}{2}$ E	48 $\frac{1}{2}$	7 $\frac{1}{2}$
120	1941, Aug. 4	10:53:09	70	53 $\frac{1}{2}$ N 179 E	47 $\frac{1}{2}$	6 $\frac{1}{2}$
160	1937, Sept. 3	18:56:27	80	52 $\frac{1}{2}$ N 177 $\frac{1}{2}$ W	45 $\frac{1}{2}$	7.3
360	1944, July 27	00:04:23	70	54 N 165 $\frac{1}{2}$ W	38 $\frac{1}{2}$	7.1
420	1942, Sept. 9	01:25:26	80	53 N 164 $\frac{1}{2}$ W	37 $\frac{1}{2}$	7.0
500	1941, Aug. 6	06:16:06	150	55 $\frac{1}{2}$ N 163 W	36	6 $\frac{1}{2}$
780	1944, Aug. 14	11:07:23	100	59 N 155 W	35	6 $\frac{1}{2}$

Region 5 (Mexico), Intermediate Shocks

75	1942, June 20	10:02:07	100	19 N 101 W	21 $\frac{1}{2}$	6 $\frac{1}{2}$
150	1945, April 21	17:14:28	100	19 N 100 $\frac{1}{2}$ W	22	6 $\frac{1}{2}$
200	1938, June 28	19:17:42	110	18 N 100 W	22 $\frac{1}{2}$	6 $\frac{1}{2}$
250	1937, Oct. 6	09:47:18	100	18 $\frac{1}{2}$ N 99 W	23	6.9
475	1937, July 26	03:47:11	100	18.4N 95.8W	25 $\frac{1}{2}$	7.3
600	1941, June 27	17:11:44	220	17 $\frac{1}{2}$ N 92 $\frac{1}{2}$ W	28	6 $\frac{1}{2}$
675	1944, Aug. 24	23:37:54	100	16 N 93 $\frac{1}{2}$ W	28	6
800	1943, Sept. 23	15:00:44	110	15 N 91 $\frac{1}{2}$ W	31 $\frac{1}{2}$	6 $\frac{1}{2}$
825	1942, Apr. 11	01:25:12	140	14 $\frac{1}{2}$ N 91 $\frac{1}{2}$ W	31	6 $\frac{1}{2}$
850	1940, July 27	13:32:30	90	14 $\frac{1}{2}$ N 91 $\frac{1}{2}$ W	31	6 $\frac{1}{2}$
875	1943, Aug. 31	16:10:40	80	14 $\frac{1}{2}$ N 91 $\frac{1}{2}$ W	31	6 $\frac{1}{2}$
935	1945, Oct. 27	11:24:41	200	15 N 91 $\frac{1}{2}$ W	31	6 $\frac{1}{2}$
	1948, July 16	07:19.7	100	14 $\frac{1}{2}$ N 92 W	31	6 $\frac{1}{2}$

Region 6 (Central America), Intermediate Shocks

No.	Date	Time (GCT)	Depth	Location	Δ	M
50	1944, Oct. 2	17:22:00	160	14½ N 89½ W	32½	6.5±
330	1944, April 7	13:32:58	200	12 N 85½ W	36½	6
	1947, Jan. 26	10:06:46	170	12½ N 86½ W	36	7.2

Region 7 (Caribbean), Intermediate Shocks

600	1940, July 6	03:40:18	160	13 N 61½ W	55	6.5
-----	--------------	----------	-----	------------	----	-----

Region 8 (South America), Intermediate Shocks

15	1938, Feb. 5	02:23:34	100	4½ N 76½ W	43½	7.0
30	1945, July 9	16:42:08	160	2½ N 76½ W	49½	6.5
	1943, Jan. 30	05:33:03	100	2 S 80½ W	50	6.9
50	1940, Oct. 23	02:23:15	140	2 S 76 W	53	6.0
110	1942, Nov. 6	13:31:10	130	6 S 77 W	55½	6.4±
155	1945, Aug. 21	16:29:37	120	10½ S 75 W	60	6½
195	1941, Sept. 18	13:14:09	100	13½ S 72½ W	64	7.0
210	1944, Feb. 29	03:41:53	200	14½ S 70½ W	66	7.0
220	1943, Feb. 16	07:28:33	190	15 S 72 W	66	7.0
235	1940, Dec. 22	18:59:46	230	15½ S 68½ W	68	7.1
415	1940, Oct. 3	04:56:08	110	21 S 70 W	71	6½±
475	1941, April 3	14:55:16	260	22½ S 66 W	75	6½
476	1941, April 3	15:21:39	260	22½ S 66 W	75	7.2
545	1940, Sept. 18	15:09:03	110	23 S 68 W	74	6.5
587	1944, July 23	16:13:39	250	24 S 66½ W	76	6.0
610	1942, July 8	06:55:45	140	24 S 70 W	74	7.0
755	1942, June 29	06:26:40	100	32 S 71 W	78½	6.9

**Region 8 (South America), Intermediate Shocks
(continued)**

<u>No.</u>	<u>Date</u>	<u>Time (GCT)</u>	<u>Depth</u>	<u>Location</u>	<u>△</u>	<u>M</u>
765	1945, Sept. 13	11:17:11	100	32½ S 70½ W	79½	7.1

Region 8 (South America), Deep Shocks

201	1940, Sept. 24	09:55:44	600	9½ S 70½ W	62½	6
240	1935, Dec. 14	01:31:13	650	9½ S 70½ W	62½	6.9
300	1944, June 8	02:38:04	600	10 S 71 W	63	6½
480	1940, Sept. 23	07:15:10	550	23 S 64 W	76½	6.5

Region 12 (Kermadec and Tonga Islands), Intermediate Shocks

275	1941, Nov. 24	21:46:23	80	28 S 177½ W 83½	7.3
375	1943, March 26	17:38:14	100	23 S 176½ W 79½	6.9
	1948, Jan. 22	13:55:3	150	22 S 175 W 77½	7.0
625	1944, Aug. 25	12:25:02	240	18 S 175½ W 76	6½
875	1944, Oct. 11	09:45:15	80	15 S 175 W 72	6½
880	1944, July 10	13:24:59	180	14½ S 175½ W 73	6½

Region 12 (Kermadec and Tonga Islands), Deep Shocks

No.	Date	Time(GCT)	Depth	Location	Δ	M
270	1944, April 23	10:57:45	370	22 S 177½W	79½ 6½	
300	1944, May 25	01:06:37	640	21½ S 179½W	80½ 7.2	
320	1940, Oct. 30	11:48:28	610	21½ S 179 W	80½ 6½	
360	1945, Nov. 26	05:13:10	600	21 S 180	80½ 7.0	
430	1942, July 7	02:53:52	430	21 S 178 W	79 6½	
690	1941, May 8	10:21:48	530	17 S 179 W	77 6.9	

Region 13 (Fiji), Deep Shocks

200	1941, Jan. 25	23:35:15	370	16 S 176½W	75	6.5
800	1943, March 15	22:59:15	300	14½ S 177 W	74	6½

Region 14 (New Hebrides), Intermediate Shocks

113	1944, Oct. 5	17:28:27	120	22½ S 172 E	87½	7½
380	1944, Nov. 24	04:49:03	170	19 S 169 E	87½	7½
680	1942, Feb. 16	18:08:15	110	11½S 166 E	85½	6.9

Region 19 (Japan to Kamchatka), Intermediate Shocks

190	1944, Aug. 18	10:33:17	150	38 N 140 E	78	6.9
340	1944, Oct. 2	20:29:51	75	42½ N 142½E	74	7.0
420	1945, Oct. 9	14:36:35	80	43½ N 147½E	71	7.0
520	1943, Nov. 9	11:46:32	90	44 N 147½E	70½	6½
550	1942, March 5	19:48:16	260	44½ N 142½E	73	6.9
640	1942, Nov. 26	14:27:28	110	45½ N 150 E	68	7.4

Table 8. - Observed log (- U_{AII} -)

<u>Shock No.</u>	<u>Instr.</u>	<u>P</u>	<u>PeP</u>	<u>PeS</u>	<u>S</u>	<u>SeS</u>	<u>SeP</u>
1- 80	LBV	0.85	0.09	0.13	0.55	0.30	0.41
	LBH	0.50	0.17		1.00	0.46	0.14
	LTH	0.34	0.24		0.83	0.32	0.10
1-120	LBV	9.85	9.42	9.37	9.62	9.04	9.04
	LBH				9.93	9.47	9.05
	SBV	0.47	0.22	9.38			
1-160	SBH	0.27	9.89				
	LTH	0.32	0.20	9.80	0.69	0.08	0.10
	LBV	0.27	0.08	9.32			9.56
1-360	LBH				0.10	9.89	
	LTH	0.11	9.91	9.74	0.17	0.02	9.92
	SBV	0.11	0.08	9.15	9.70		9.72
	SBH	0.60				0.22	
1-420	LBH				9.93	9.15	
	LTH				9.92		
	SBV				0.27	9.15	
	SBH				0.61	0.11	
1-500	LBV	0.23	9.48				
	LBH	9.91	9.48				9.46
	LTH	0.09	9.68			9.64	9.59
1-780	SBV	0.92	0.31	9.53	0.44	9.25	9.76
	LBV	9.30	9.08	9.10		9.10	9.04
	SBV	9.60	8.90				
	SBH	9.16					

<u>Shock No.</u>	<u>Instr.</u>	<u>P</u>	<u>PcP</u>	<u>PcS</u>	<u>S</u>	<u>SeS</u>	<u>SeP</u>
5- 75	LBV	9.88	9.53				
	SBV	0.35	9.79				
5-150	LBV	9.56	9.40				
	LBH	9.59	9.38				9.23
5-200	LTH	0.17	9.54		9.92		
	LTH	0.54	0.00		0.30		9.92
5-250	LBH	0.55	9.92		0.36		
	LTH	0.85	0.35		0.57		0.05
5-475	SBV	1.16	0.78				
	LBV	9.26	9.00		9.38		9.34
5-600	LTH	9.65	9.29		9.40		
	SBV	.00	9.38				
5-675	LBH				9.54	9.75	9.40
	LTH				9.83	0.02	9.45
	SBV	9.80	9.46				
5-800	LBV	9.98	9.69		9.56	9.85	9.76
	LBH				0.17	0.60	9.78
	LTH				0.00	0.03	9.70
5-825	SBV	0.54	0.35	0.45			
	SBH	0.15	9.81				
5-850	LBV	9.65	9.61	9.40	9.45	9.67	9.58
	LBH				9.80	9.87	9.47
	SBV	0.48	0.50				
5-850	LBH	9.84	9.51		0.44	0.32	9.69
	SBV	0.20	9.90				

<u>Shock No.</u>	<u>Instr.</u>	<u>P</u>	<u>PcP</u>	<u>PcS</u>	<u>S</u>	<u>SsS</u>	<u>ScP</u>
5-875	LBV	0.11	0.46	9.53	9.65	9.60	9.85
	LBH	9.98	9.21	9.26	9.86	9.97	9.54
	LTH	0.05	9.67	9.45	9.70	9.74	9.30
	SBV	0.24	0.20	9.89			
5-935	LBV	0.16	9.86		9.78	9.78	9.81
	LBH	9.84		9.23	0.07	0.11	9.67
	LTH	0.27		9.65	0.25	0.26	9.83
	SBV	0.27	0.17			0.71	0.18
	SBH	0.14	9.07		0.60	0.03	9.15
1948, July 16 07:19.7	LBV	9.81	9.51	9.34			
	LBH				9.70	9.92	9.32
	LTH	9.70			9.70	9.66	
	SBV	0.26	9.45	9.58			
6-50	LBV	9.97	9.43	9.11	9.28	9.20	9.20
	LBH	0.34					9.00
	LTH	9.88			9.65	9.53	
	SBV	0.24	9.42				
1947, Jan. 26 10:06:46	LBV	0.34	0.23				
	LBH	0.11	9.62	9.76	0.63	0.71	9.85
	LTH	0.37	9.92	0.10	0.68	0.84	0.02
	SBV	0.80	0.56	0.04			0.24
	SBH	0.16	9.82	9.71	0.11		9.70

<u>Shock No.</u>	<u>Instr.</u>	<u>P</u>	<u>Pep</u>	<u>PcS</u>	<u>S</u>	<u>ScS</u>	<u>SeP</u>
6-330	LBV	9.54	9.00				
	SBV	9.53	9.25				
7-600	LBV	0.18	9.71	9.28	9.37	9.37	9.41
	LBH	9.97	9.23		9.64	9.49	
	LTH	9.87			9.32	9.32	
8- 15	LBH	0.24	9.95	9.87	0.17	0.31	9.99
	LTH	0.56	0.29	9.99	0.17	0.35	9.97
8- 30	LBV	9.76	0.45				
	SBV	0.58	9.76				
1943, Jan 30 05:33:03	LBV	0.18	9.72	9.15	9.45	9.38	9.38
	LBH	9.95	9.58	9.49	0.07	9.73	9.40
	LTH	9.96	9.56		9.60	9.40	
	SBV	0.74	0.36	9.26			
8- 50	LBH				0.27	9.00	
	SBV	0.00	9.51				
8-110	LBV	9.68	9.42	9.23	9.46	9.00	9.32
	LBH	9.61	9.46		9.71	9.42	
	LTH	9.75	9.50		9.48	9.28	
8-155	LBV	9.78	9.76				
	LBH	9.38	9.32				
	LTH	9.50	9.57				
	SBV	0.38	0.80				
8-195	LBV	0.51			9.68	9.77	
	LBH	9.79			9.89	9.81	
	LTH	9.97			9.92	0.03	
	SBV	0.54			0.16	0.16	

<u>Shock No.</u>	<u>Instr.</u>	<u>P</u>	<u>PcP</u>	<u>PcS</u>	<u>S</u>	<u>ScS</u>	<u>ScP</u>
8-210	LBV	0.77	0.36		0.00	9.87	
	LBH	0.36	9.93		0.45	0.25	
	LTH	0.32	0.13		9.95	9.65	
	SBV	0.67	0.13				
8-220	LBV	0.30	9.72		9.46	9.45	
	LBH	9.98	9.58		9.93	9.59	
	LTH	0.10	9.75				
	SBV	1.11	0.46				
8-235	LBV	0.28	9.54				
	LBH				0.05	9.72	
8-415	SBV	9.83	9.00				
8-475	LBV	0.51	0.18				
	LBH	0.57	0.28		0.61	0.06	
8-476	LBV	9.70	9.08				
	SBV	9.86	9.08				
	SBH	9.37	9.25				
8-545	LBV	0.37	9.60				
	SBH	9.90	9.66				
8-610	LBV	0.12	0.19		0.02	9.67	
	LBH				0.32	9.88	
	SBV	0.56	0.56				
8-755	LBV	0.01	9.46		9.45	9.38	
	LBH	9.75	9.45		9.90	9.59	
	LTH				9.67		
	SBV	0.81	0.00				

<u>Shock No.</u>	<u>Instr.</u>	<u>P</u>	<u>PcP</u>	<u>PcS</u>	<u>S</u>	<u>ScS</u>	<u>ScP</u>
8-765	LBV	0.06	9.66		9.73	9.67	
	LBH	9.53	9.45		9.94	9.69	
8-201	SBV	0.00	9.56				
8-240	LTH	0.41	0.17		0.40	9.70	
	SBV	0.98	0.24			0.50	
8-300	SBV	9.34	8.8			8.3	
8-480	LBH				0.42	9.65	
12-275	LBV	0.34	0.23		9.81	9.75	
	LBH	9.85	9.66		9.98	9.98	
12-375	LBV	9.98	9.49		9.62	9.42	
	LBH	9.51	9.49		9.82	9.72	
	LTH	9.53	9.40		9.45	9.38	
1948, Jan. 22 13:55.3	LBV	9.94	9.81		9.45	9.38	
	LBH	9.82	9.60		0.00	0.02	
	LTH				0.13	9.98	
	SBV	0.30	0.03				
12-625	SBV	9.43	8.78				
12-875	LBV	9.94	9.46				
	SBV	0.06	9.70				
12-980	LBV	9.51	9.25				
	SBV	9.75	9.40				

<u>Shock No.</u>	<u>Instr.</u>	<u>P</u>	<u>PcP</u>	<u>PcS</u>	<u>S</u>	<u>ScS</u>	<u>ScP</u>
12-270	SBV	9.96	9.63				
12-300	LBV	9.72	9.60		9.66		
	SBV	0.75	0.65				
	SBH	0.52	0.50		0.55		
12-320	LBV	9.46	9.00				
	LBH				9.43	9.00	
	SBV	9.91	9.46				
12-360	LBV	0.11	9.89				
	LBH	9.62	9.44				
	LTH	0.05	9.58				
	SBV	0.46	0.41				
12-430	LBV	0.01	9.85		9.67	9.64	
	LBH				9.72	9.65	
	SBV	0.56	0.15				
12-690	LBV	0.17	9.71		9.67	9.38	
	LBH				9.89	9.74	
	LTH				0.02	9.99	
13-200	SBV	9.94	9.66				
13-800	LBV	0.09	9.41		0.01	9.84	
	LBH				0.48	0.00	
	LTH				0.17	9.64	
	SBV	0.52	0.04				
14-113	LBV	9.45	9.51		9.44		
	LBH	9.12	9.45		0.12		
	LTH	9.70	9.74		0.17		
	SBV	0.16	9.65				
	SBH	9.80	9.72				

<u>Shock No.</u>	<u>Instr.</u>	<u>P</u>	<u>PerP</u>	<u>PerS</u>	<u>S</u>	<u>ScS</u>	<u>ScP</u>
14-380	LBV	0.55	9.91		0.45	9.97	
	LBH	9.88	9.72		9.86	9.48	
	LTH	0.00	9.83		9.97	9.62	
	SBV	0.68	9.96		9.51	9.00	
	SBH	0.16	9.97				
14-680	LBV	9.98	9.97				
	LBH	9.44	9.63		9.81		
	LTH	9.70	9.69		9.81		
	SBV	0.51	0.35				
19-190	LBV	0.31	9.86		9.60	9.52	
	LBH	9.77	9.74		9.73		
	LTH	0.09	9.97		9.91	9.43	
	SBV	0.57	9.99				
	SBH	0.19	9.96		0.07		
19-340	LBV	9.41	9.04		9.45	9.08	
	LBH				9.59	9.32	
	LTH				9.95	9.58	
	SBV	9.54	9.34				
19-420	LBV	9.72	9.40				
	LBH				9.89		
	SBV	0.26	9.80				

<u>Shock No.</u>	<u>Instr.</u>	<u>P</u>	<u>Pcp</u>	<u>Pcs</u>	<u>S</u>	<u>ScS</u>	<u>ScP</u>
19-520	LBV	9.96	9.46		9.38		
	LBN	9.56	9.40		9.59		
	SBV	0.68	0.11				
	SBH	0.18	0.83				
19-550	LBV	0.01	0.71		0.05	9.85	
	LBN	9.80	9.63		0.14	0.00	
	LTH				9.88	0.01	
	SBV	0.87	0.38				
19-640	LBV	0.39	0.90				
	LBN	9.97	9.79		0.07	9.65	

Fig. 1. - A_t vs. Δ for P-Horizontal

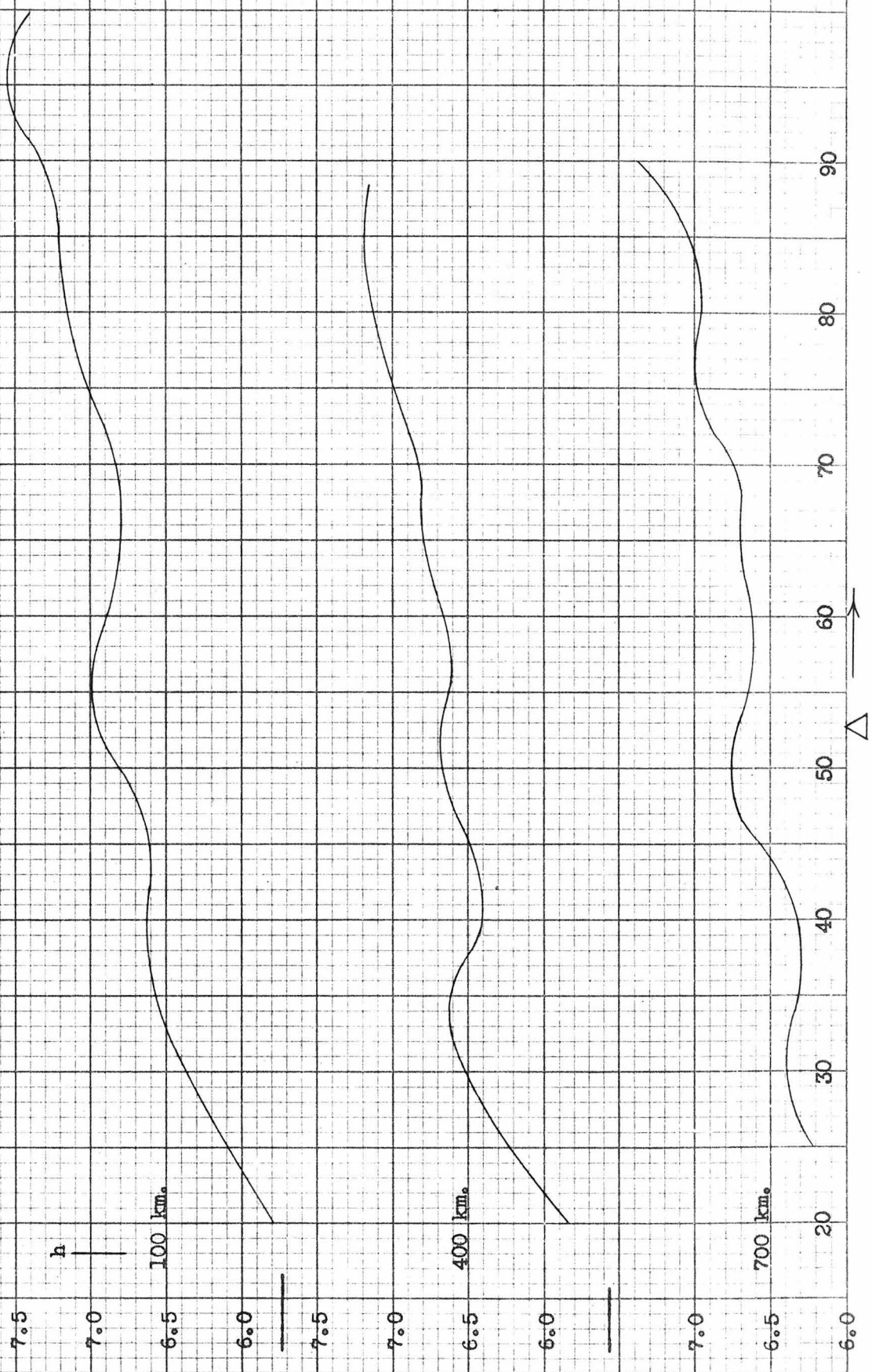
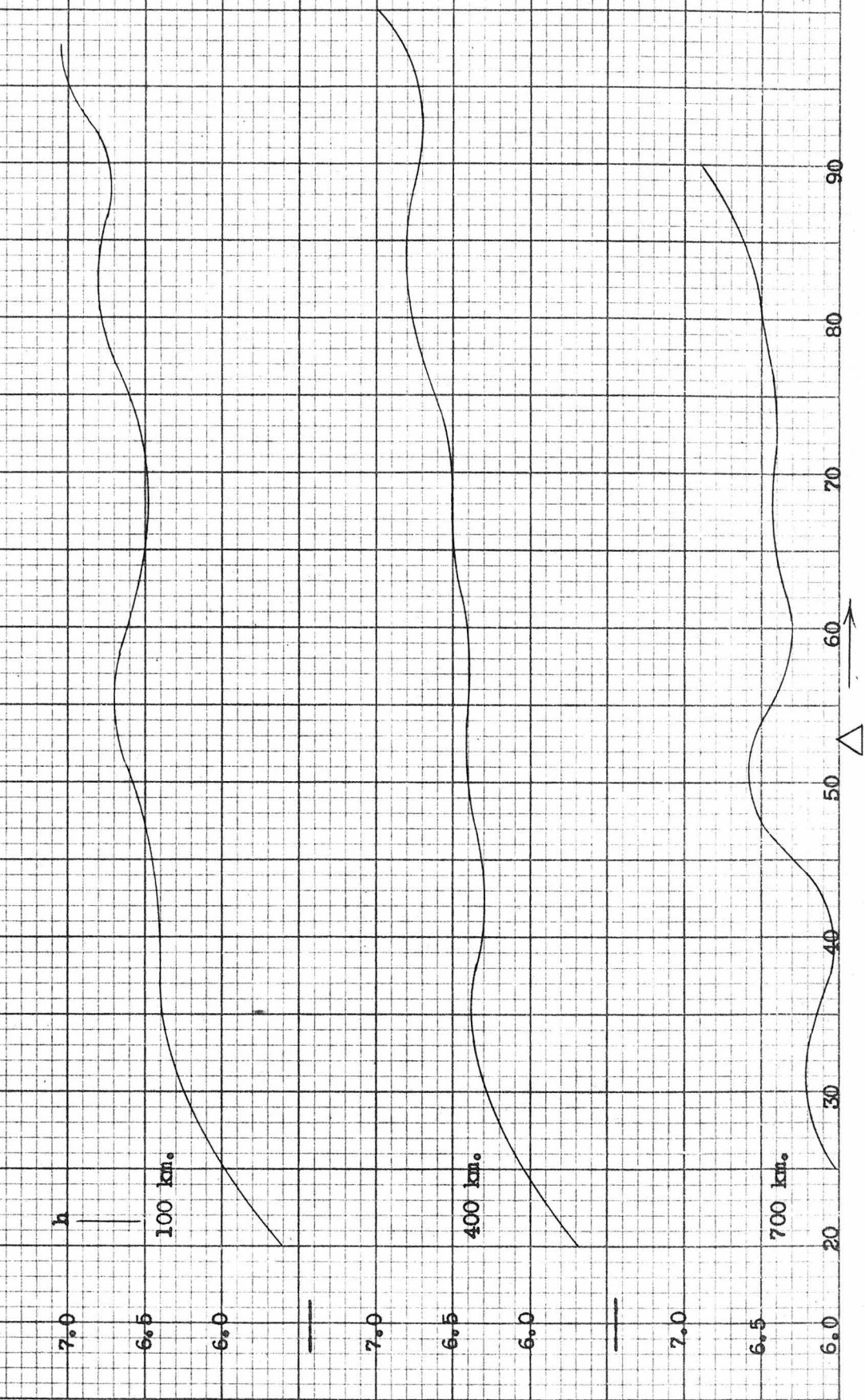


FIG. 2. - A_0 vs. Δ for P Vertical

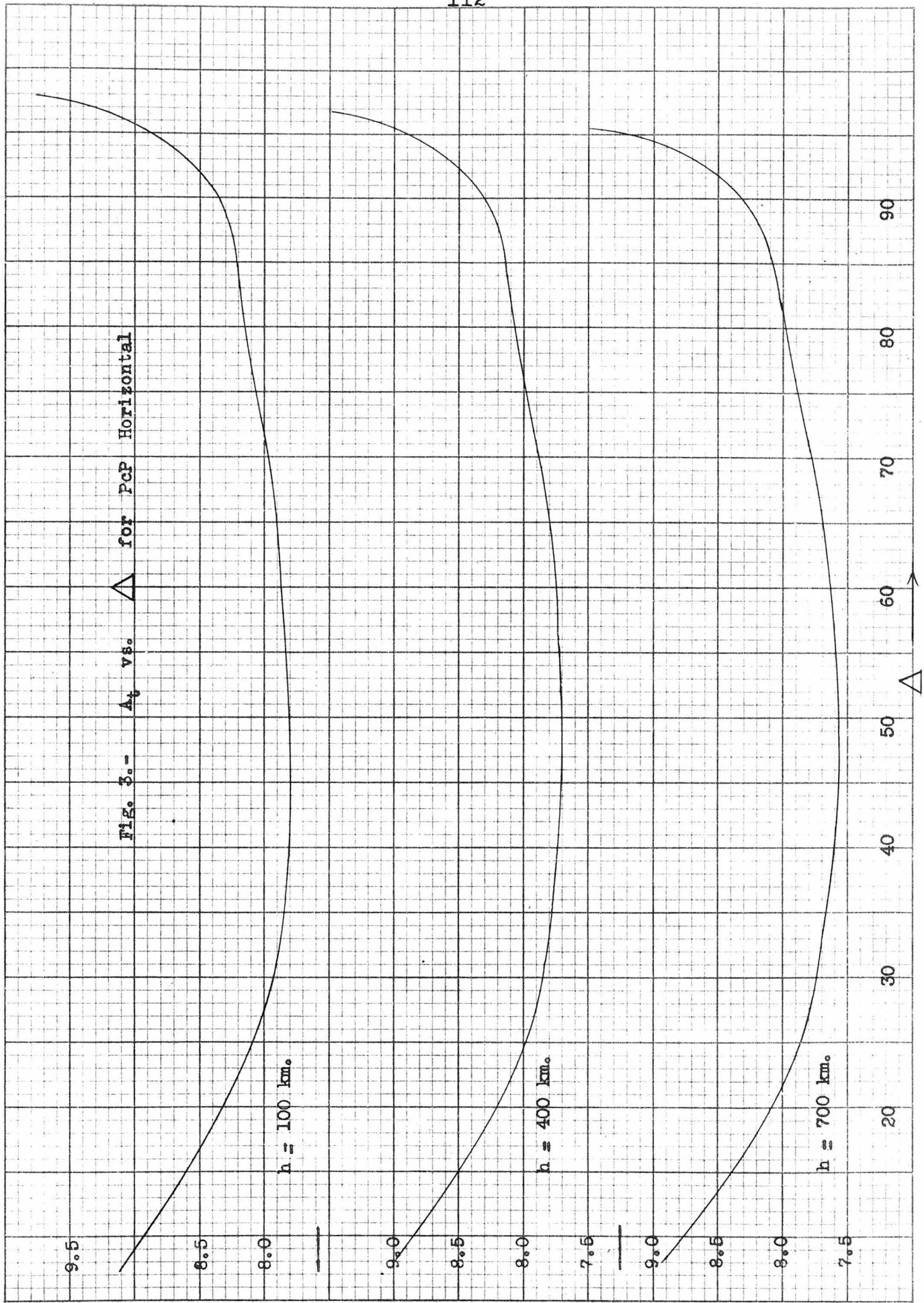


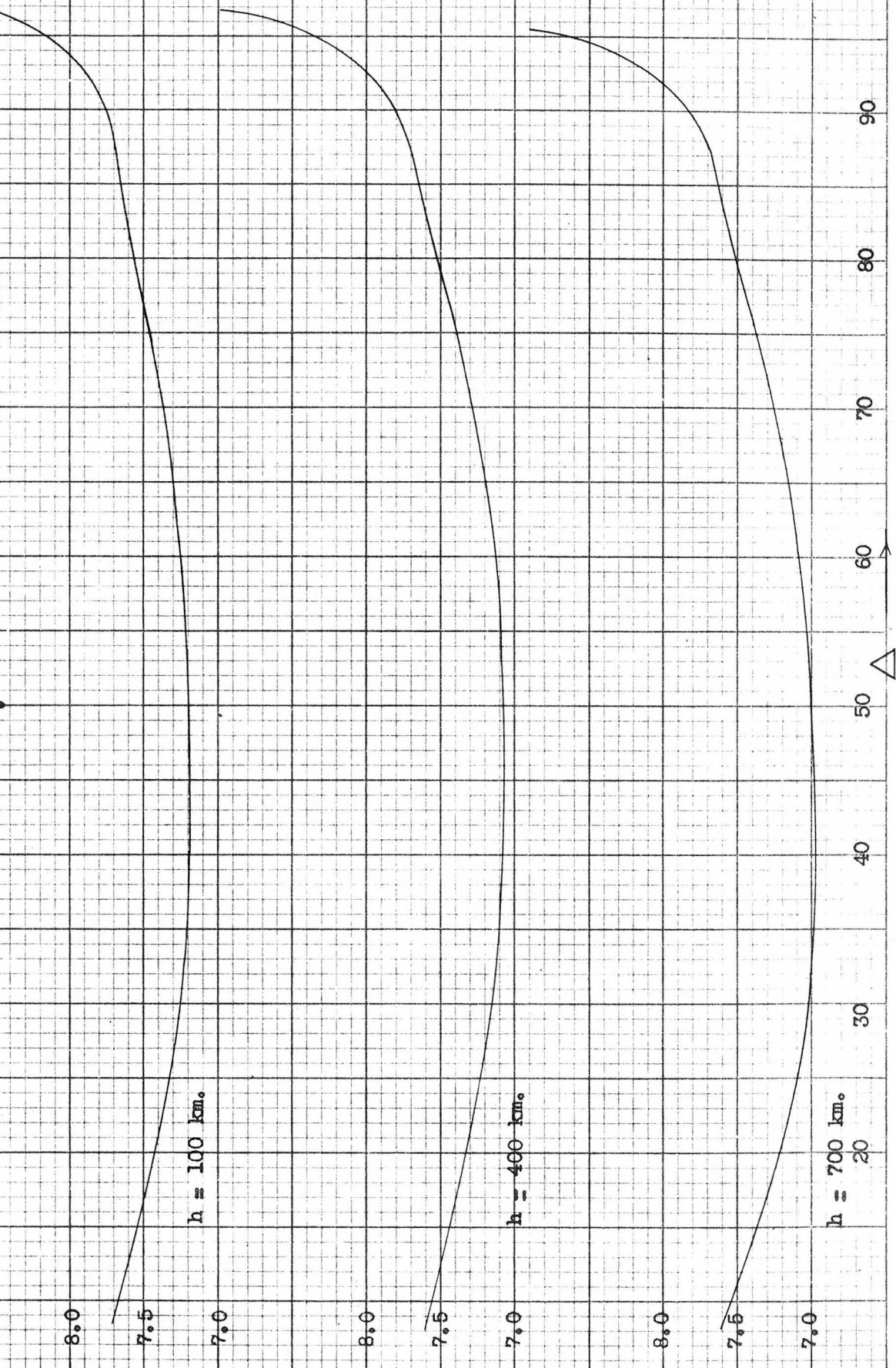
Fig. 4a = A_c vs. Δ for PCP Vertical

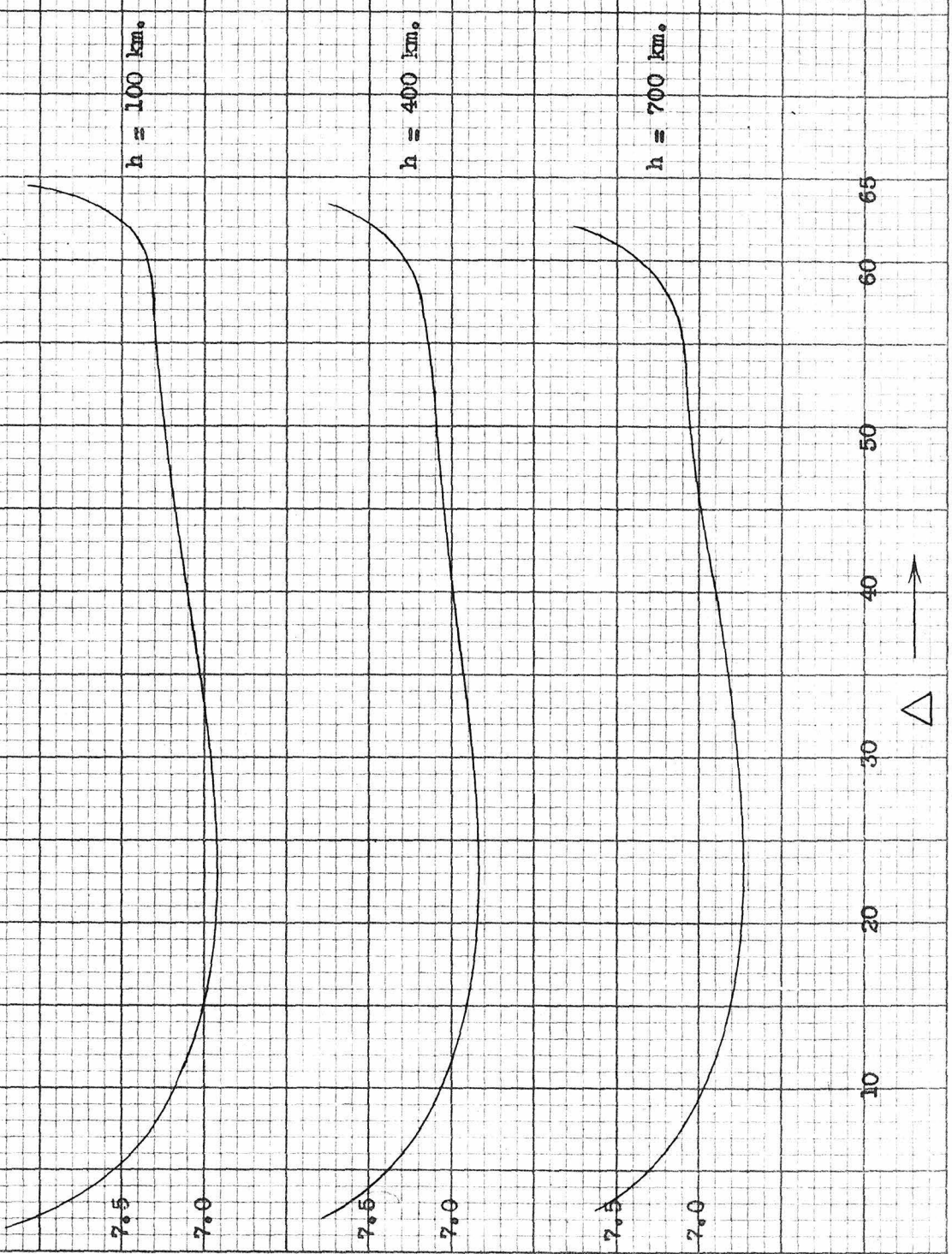
Fig. 5.- Δ_t vs. Δ for PCS Horizontal

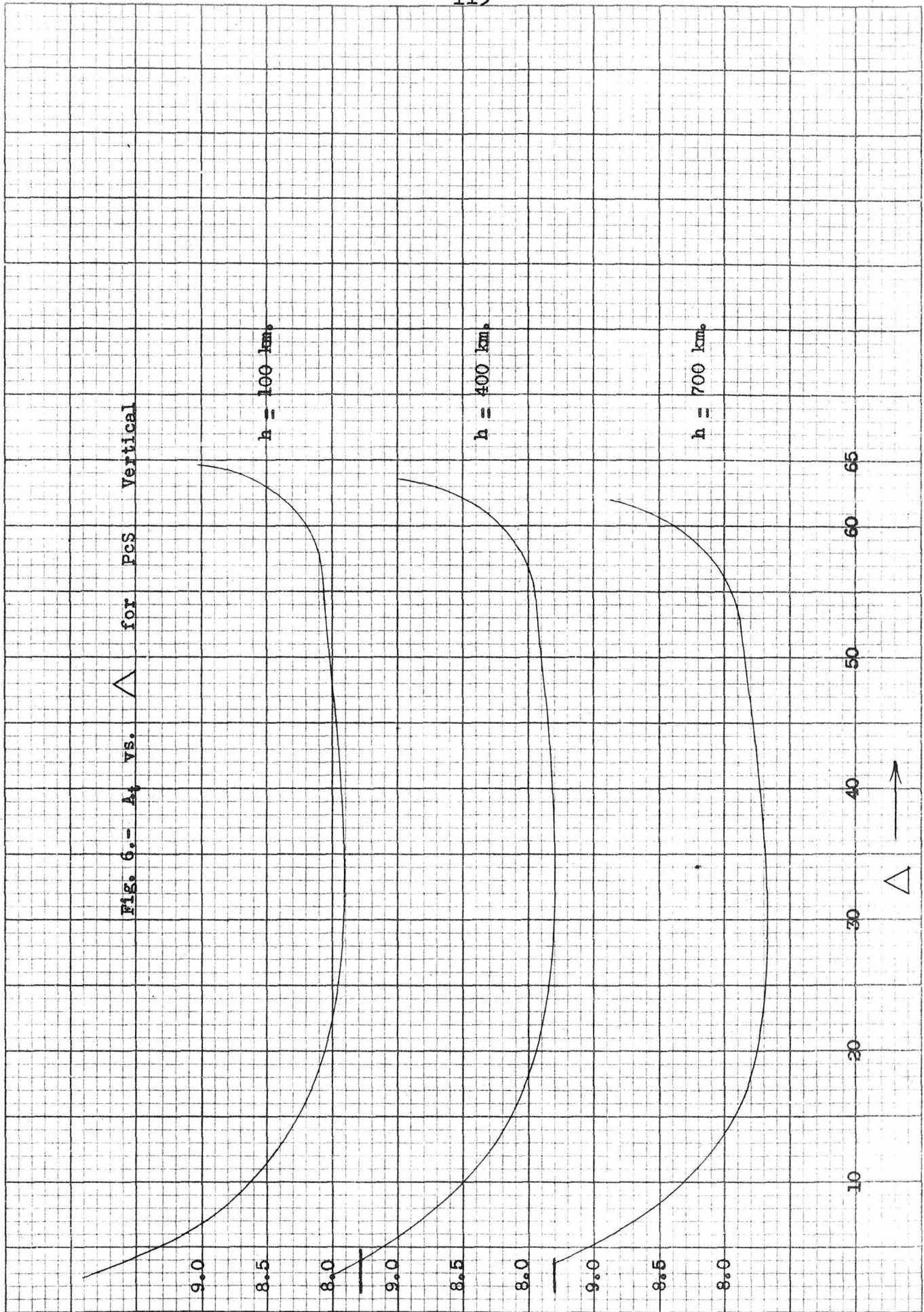
FIG. 6.— A_4 vs. Δ for PCS Vertical

Fig. 7. - At. vs. Δ for S Horizontal

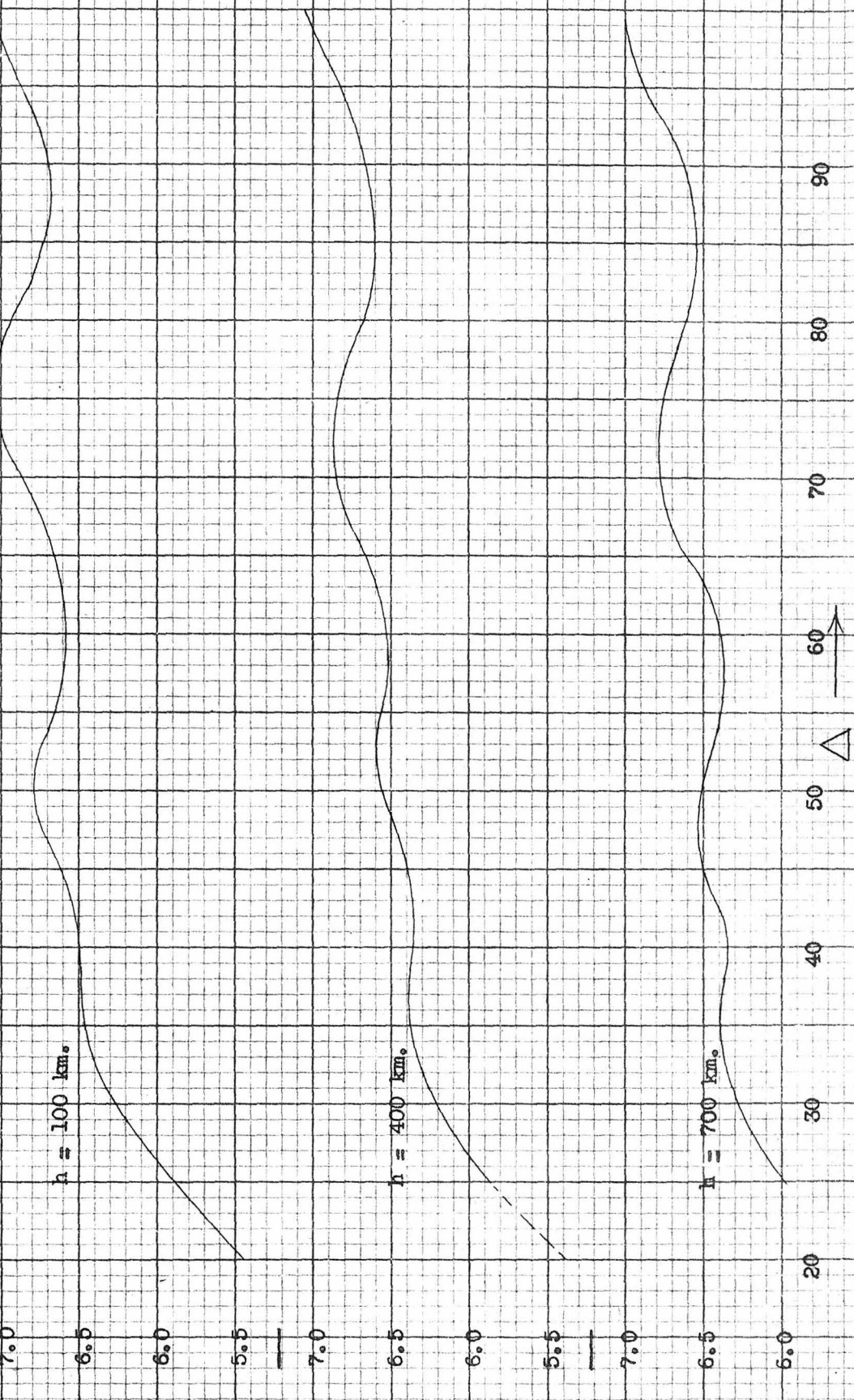


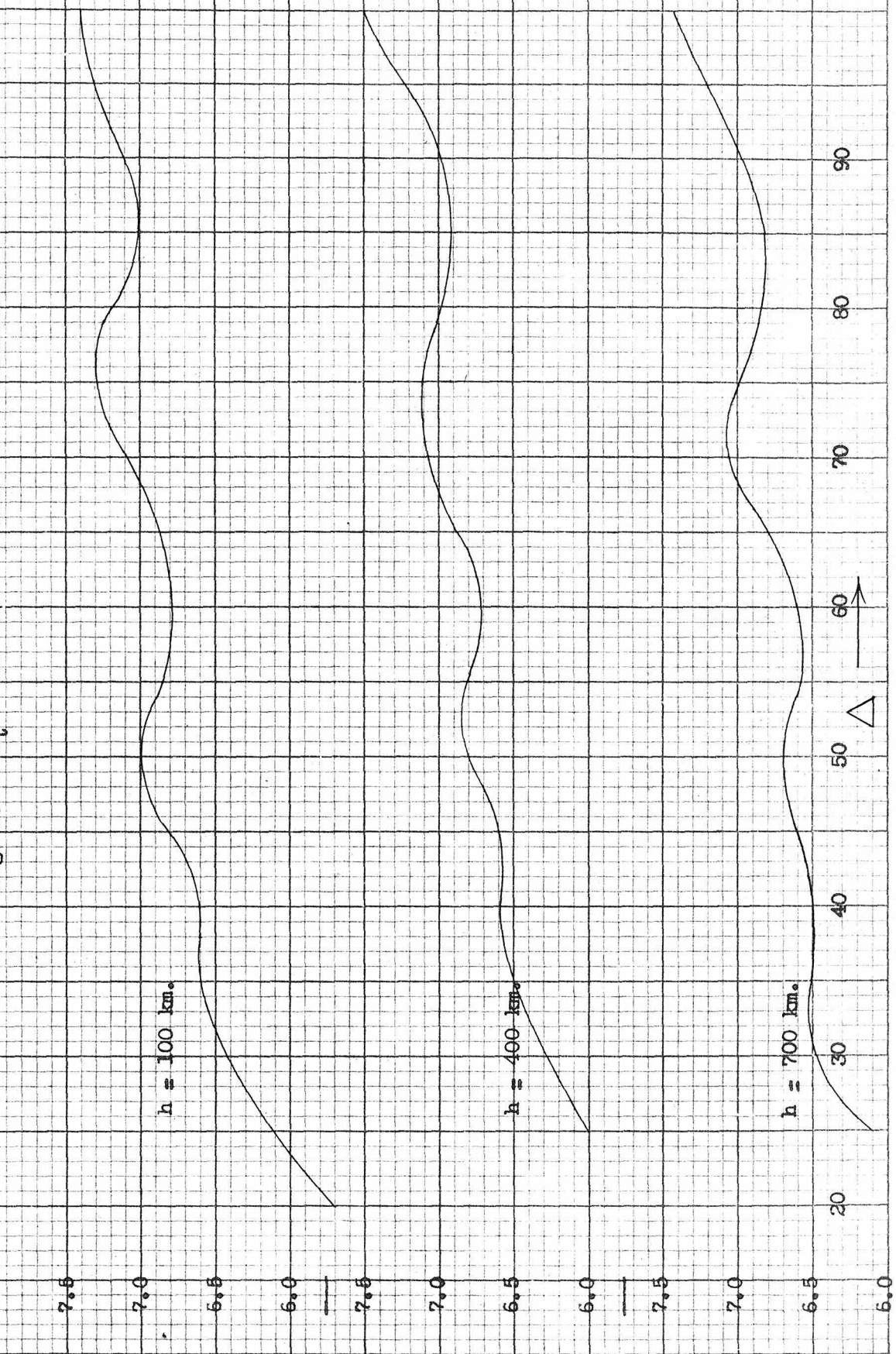
FIG. 8. - At. vs. Δ for S Vertical.

Fig. 9.- A_L vs. Δ for SCS Horizontal

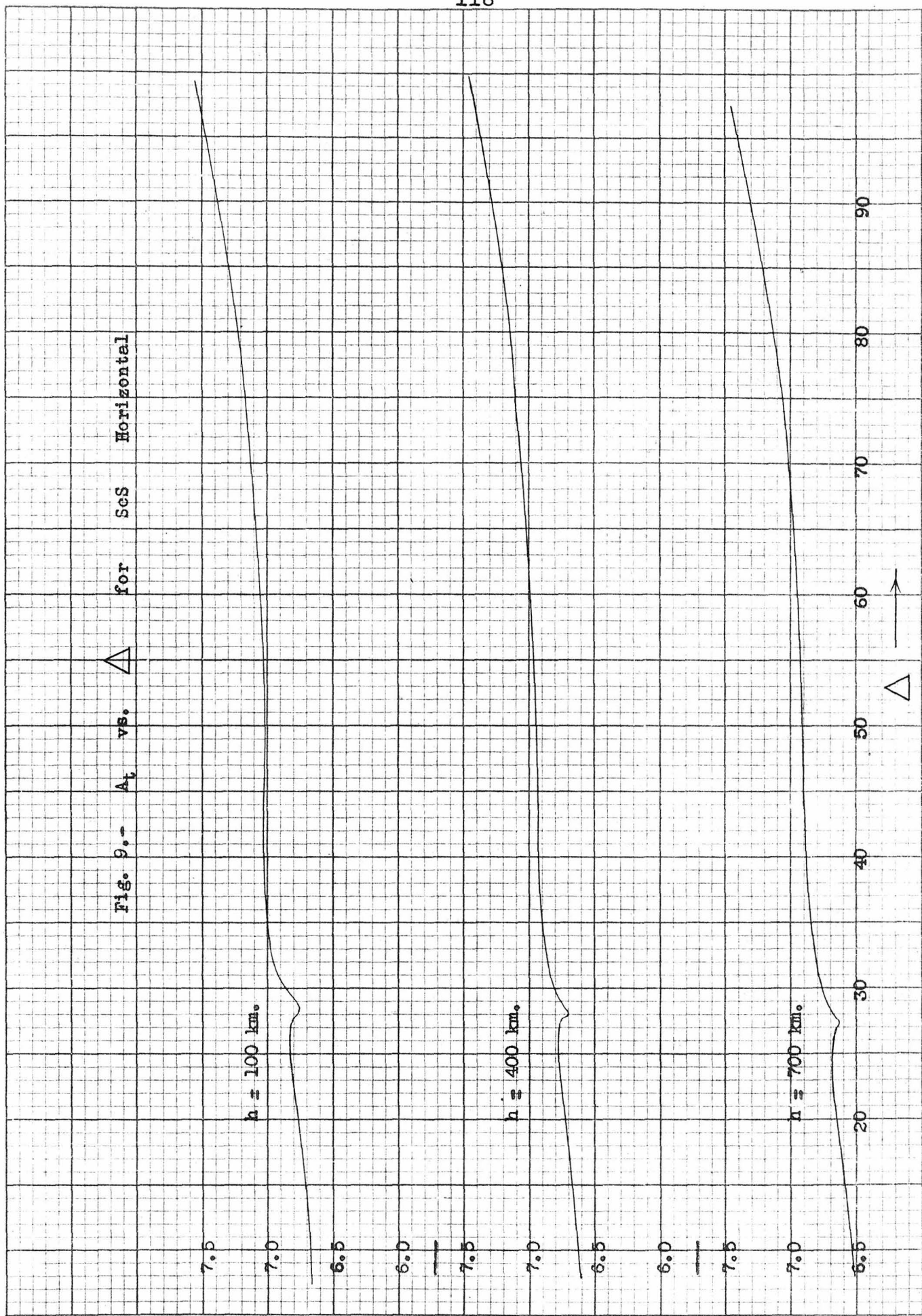


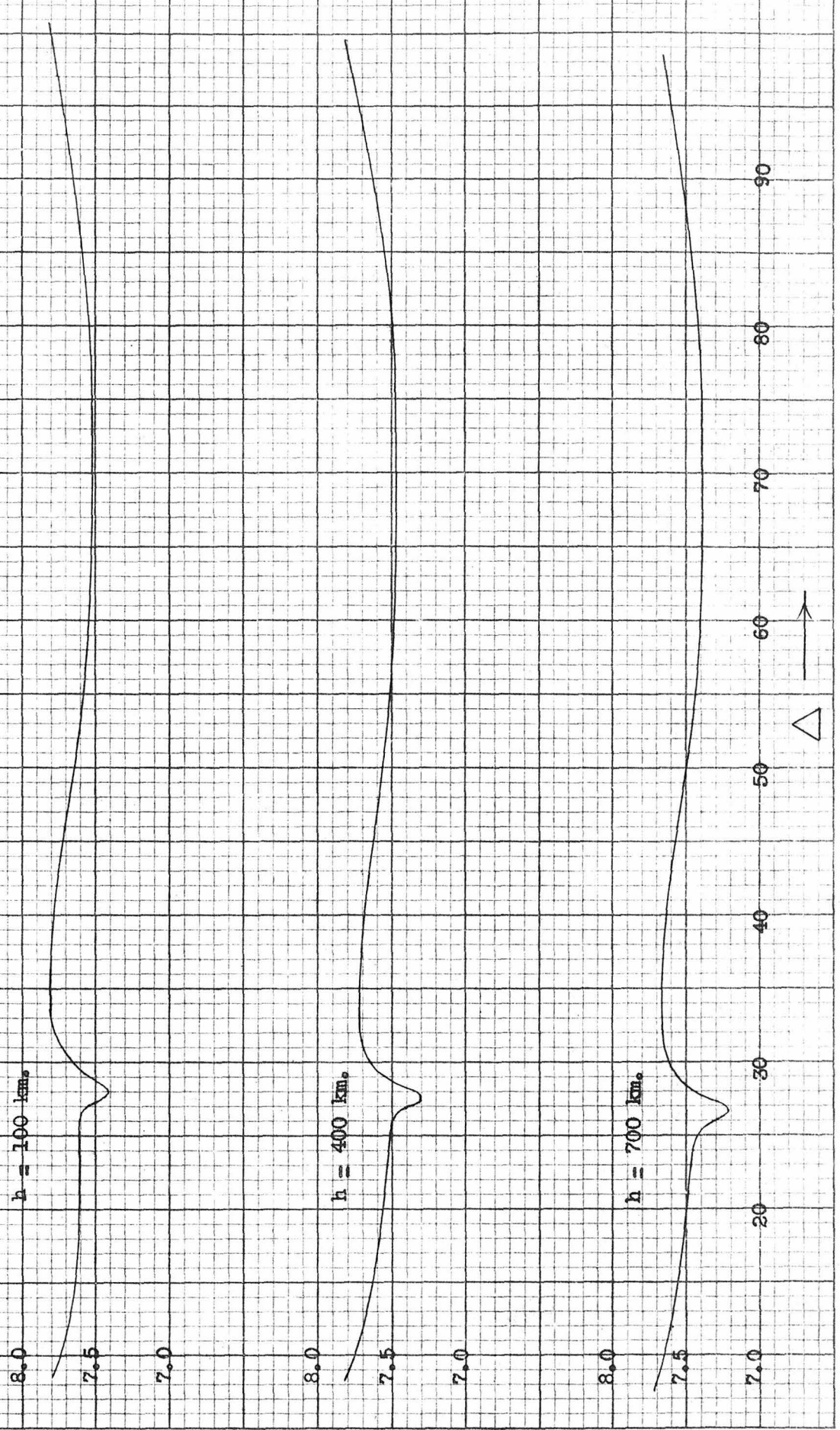
Fig. 10.- At. vs. Δ for SCS Vertical

Fig 11. - A_t vs. Δ for SCP Horizontal

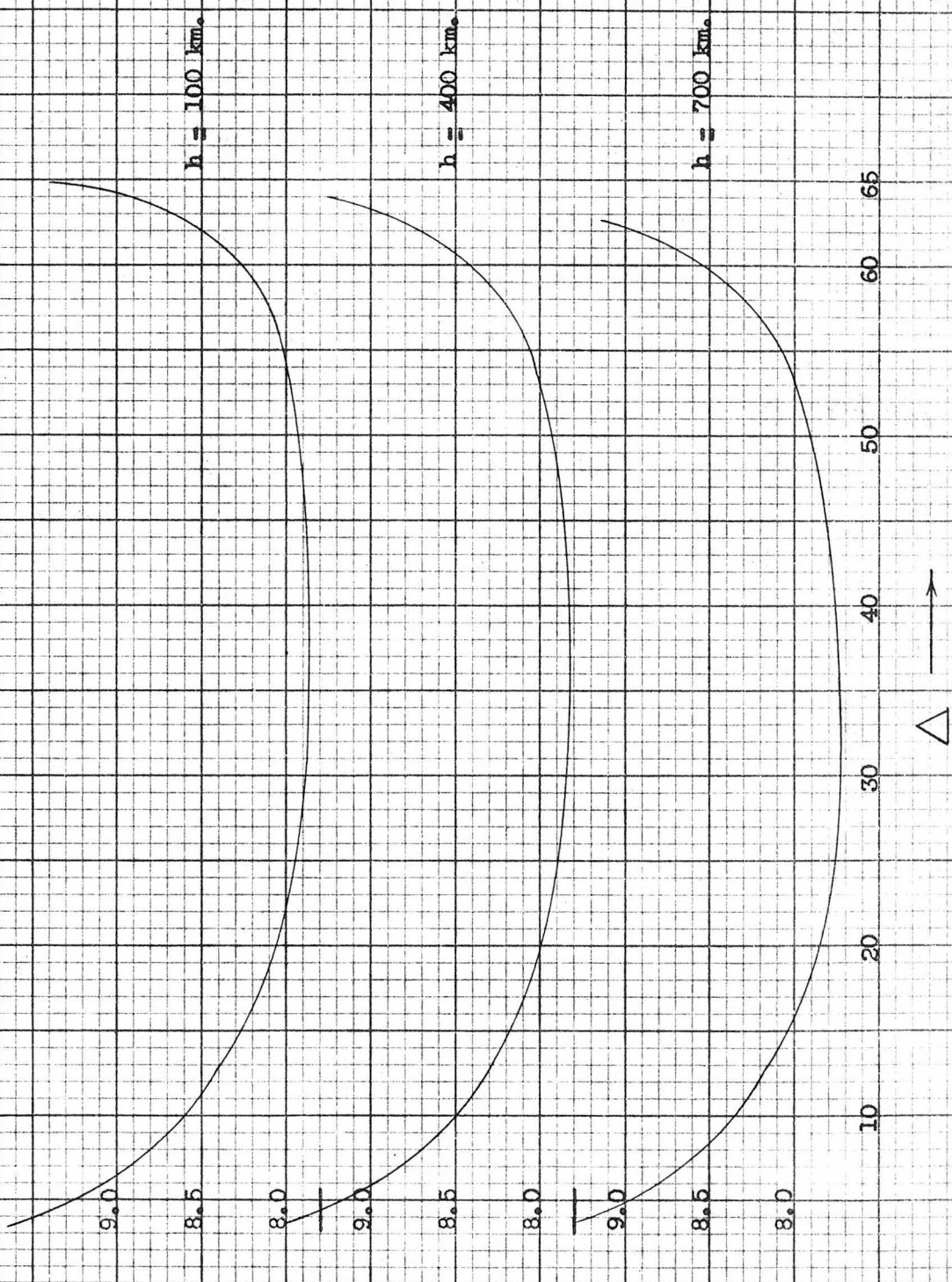
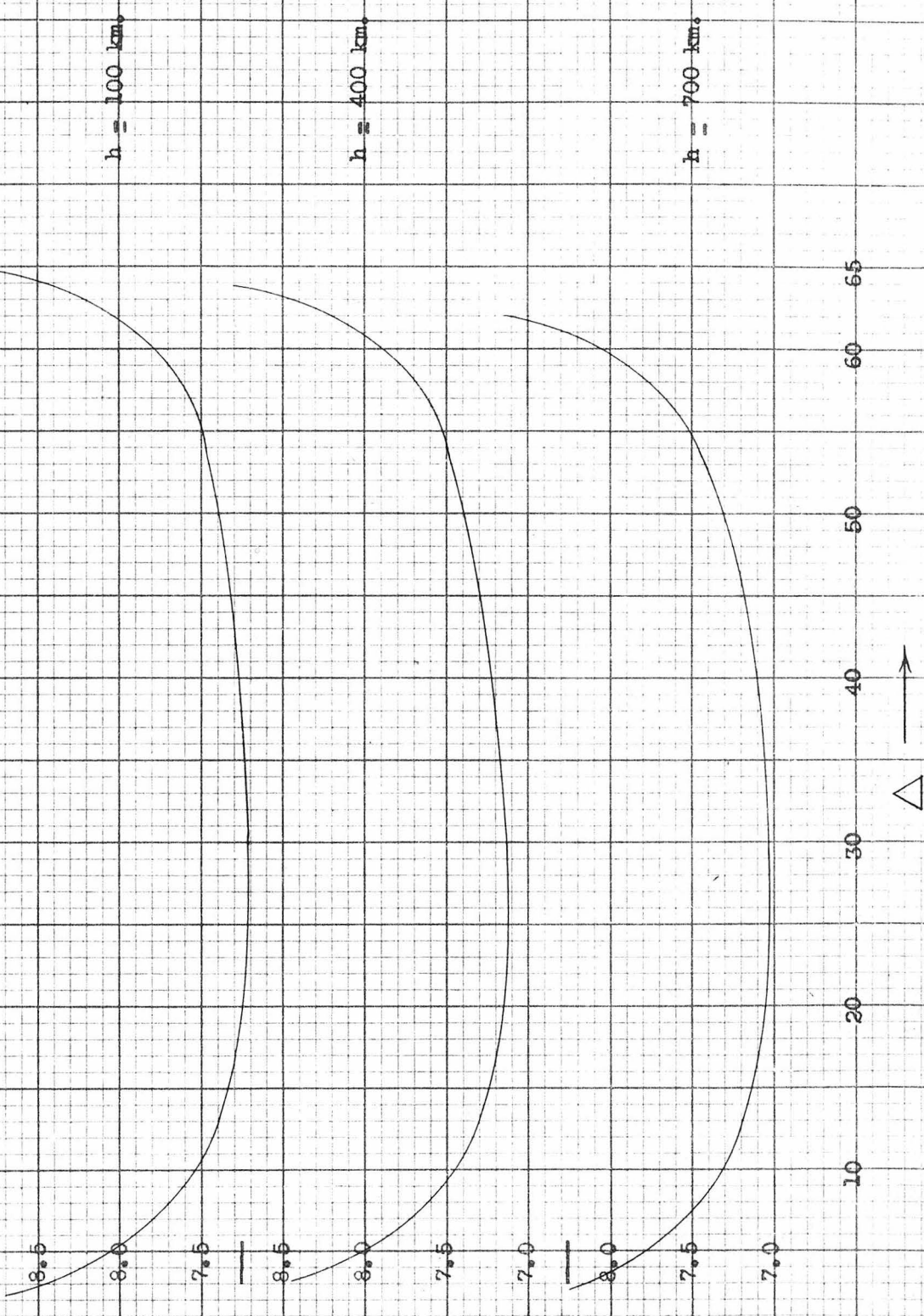
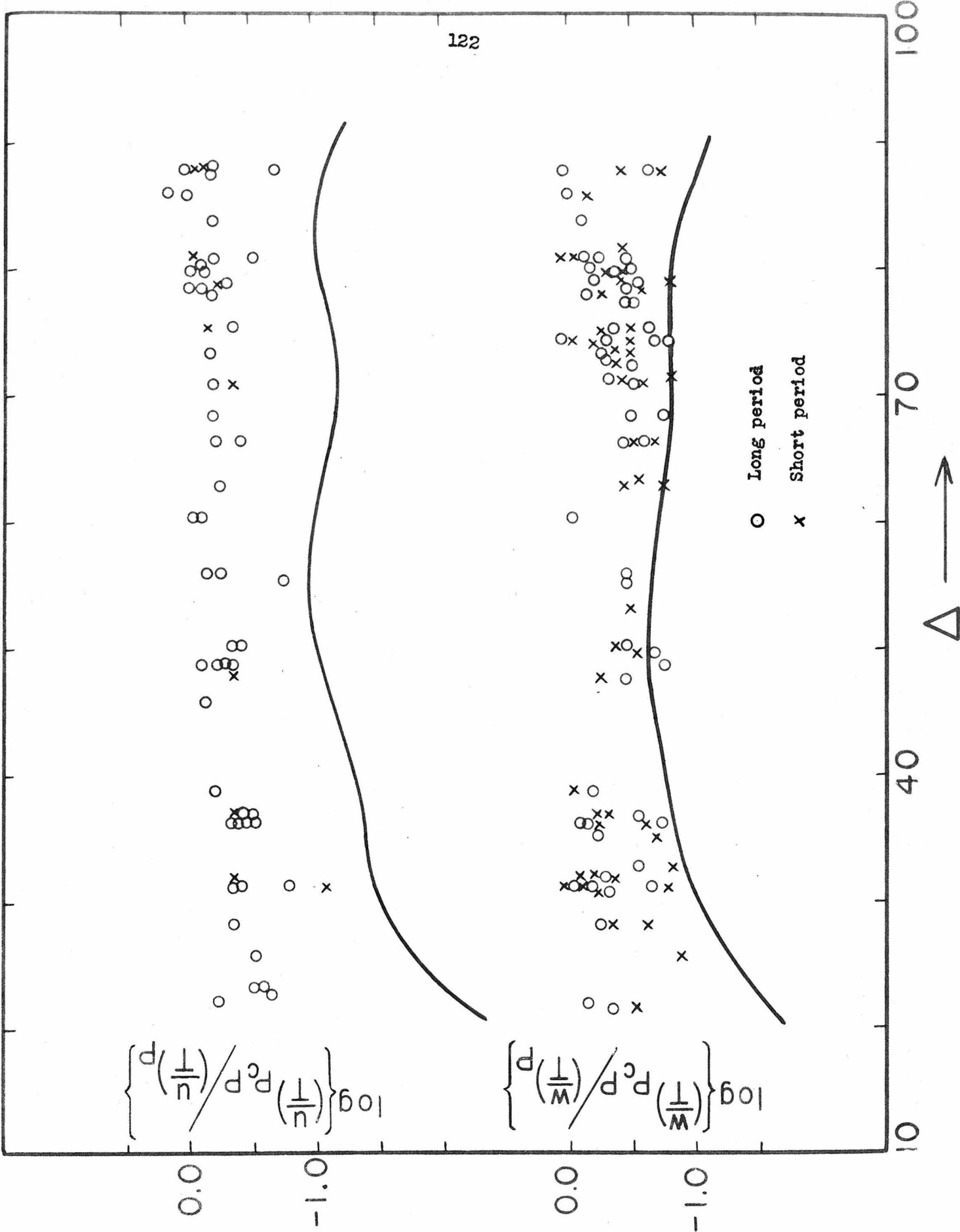
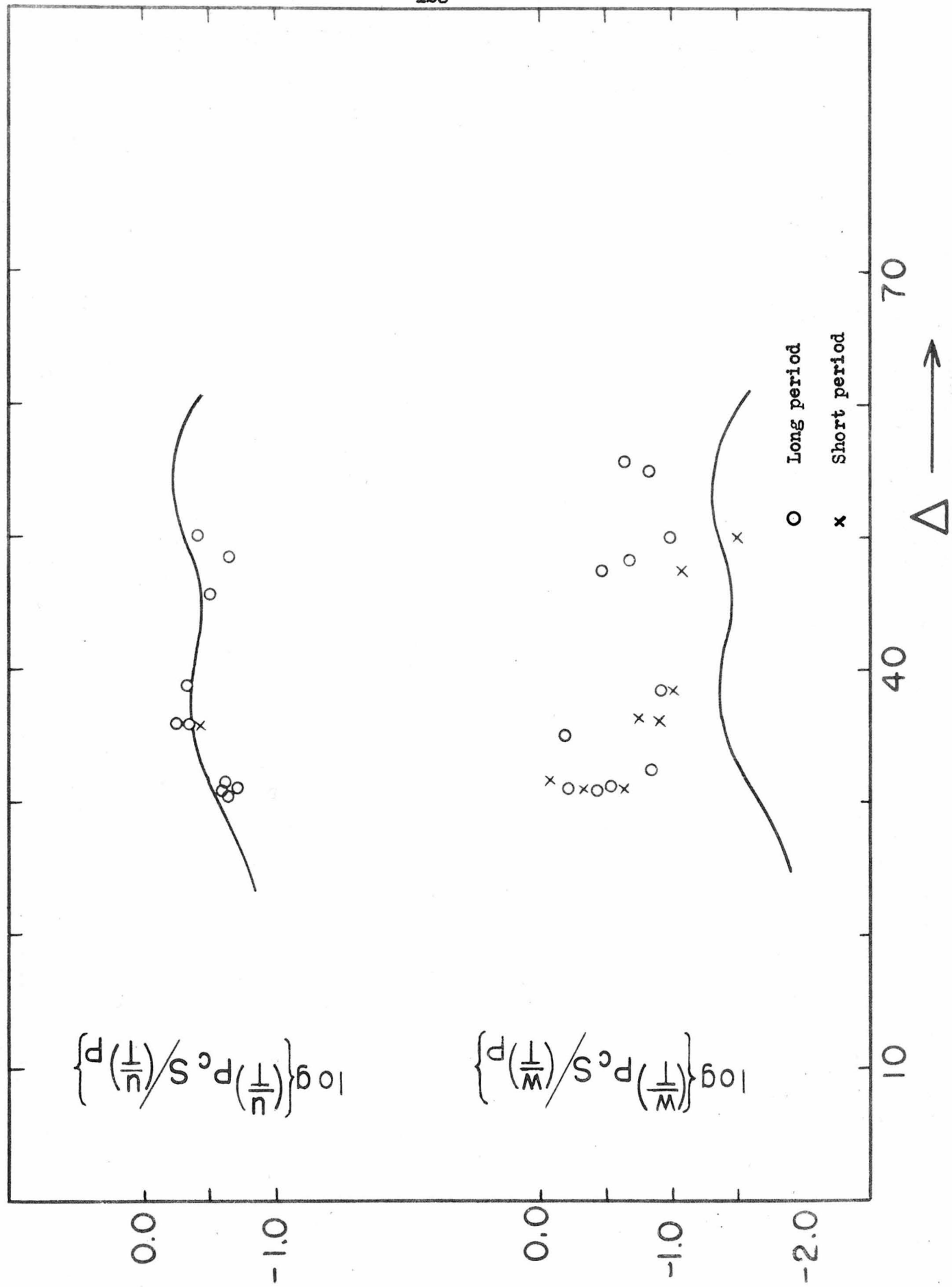
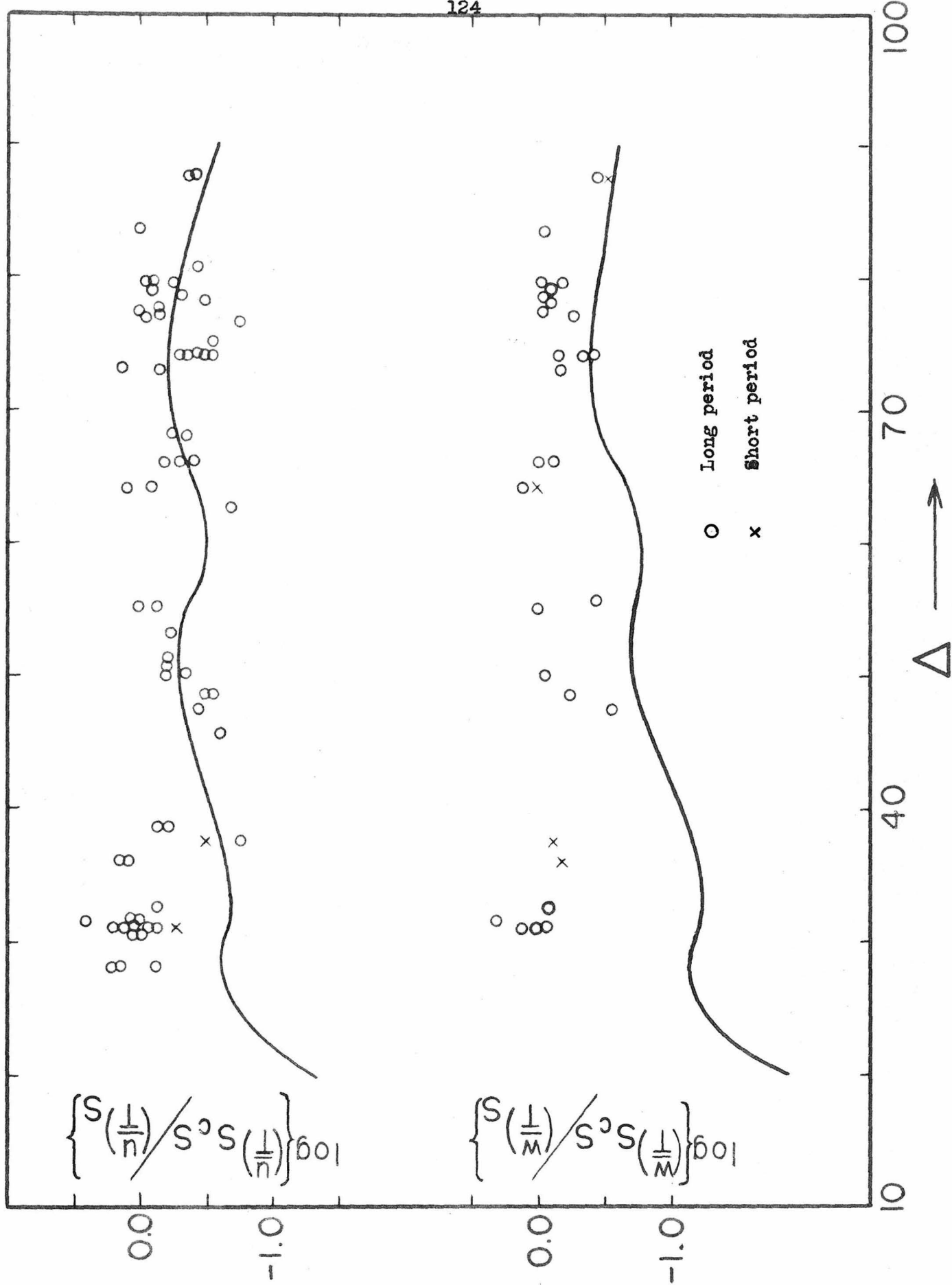


Fig. 12.- At vs. for Sop Vertical









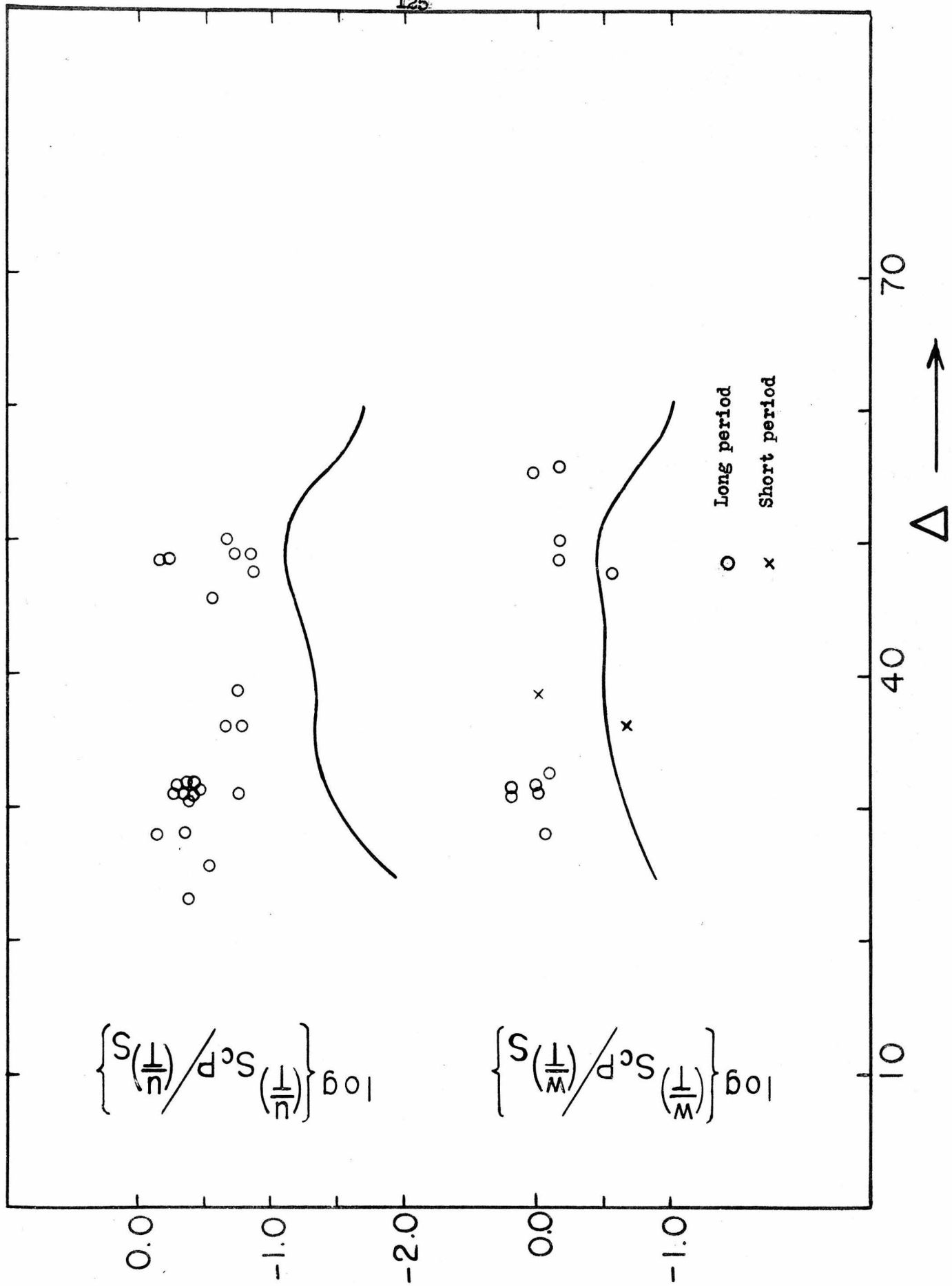


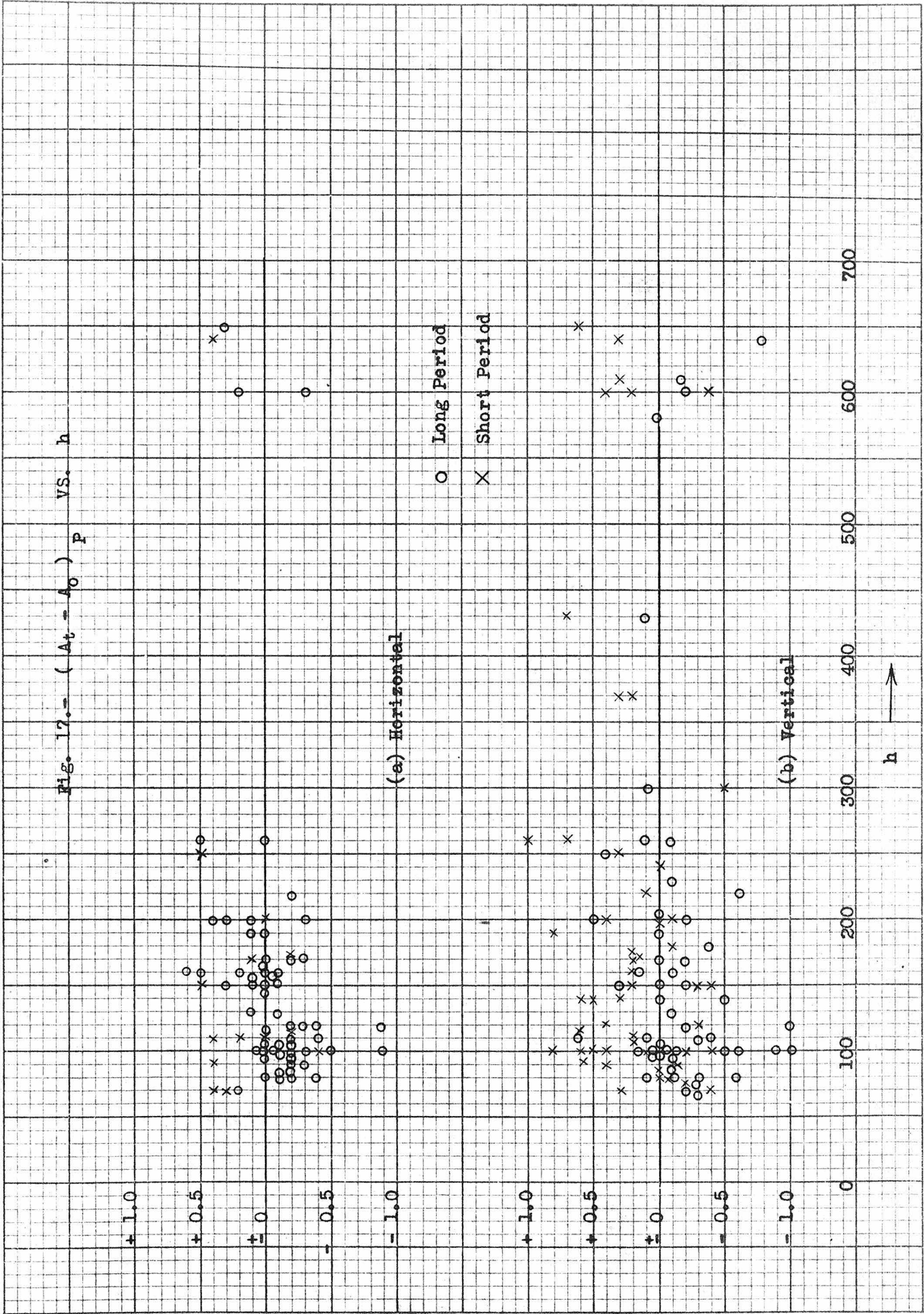
Fig. 12. - ($A_t = A_0$) P vs. h 

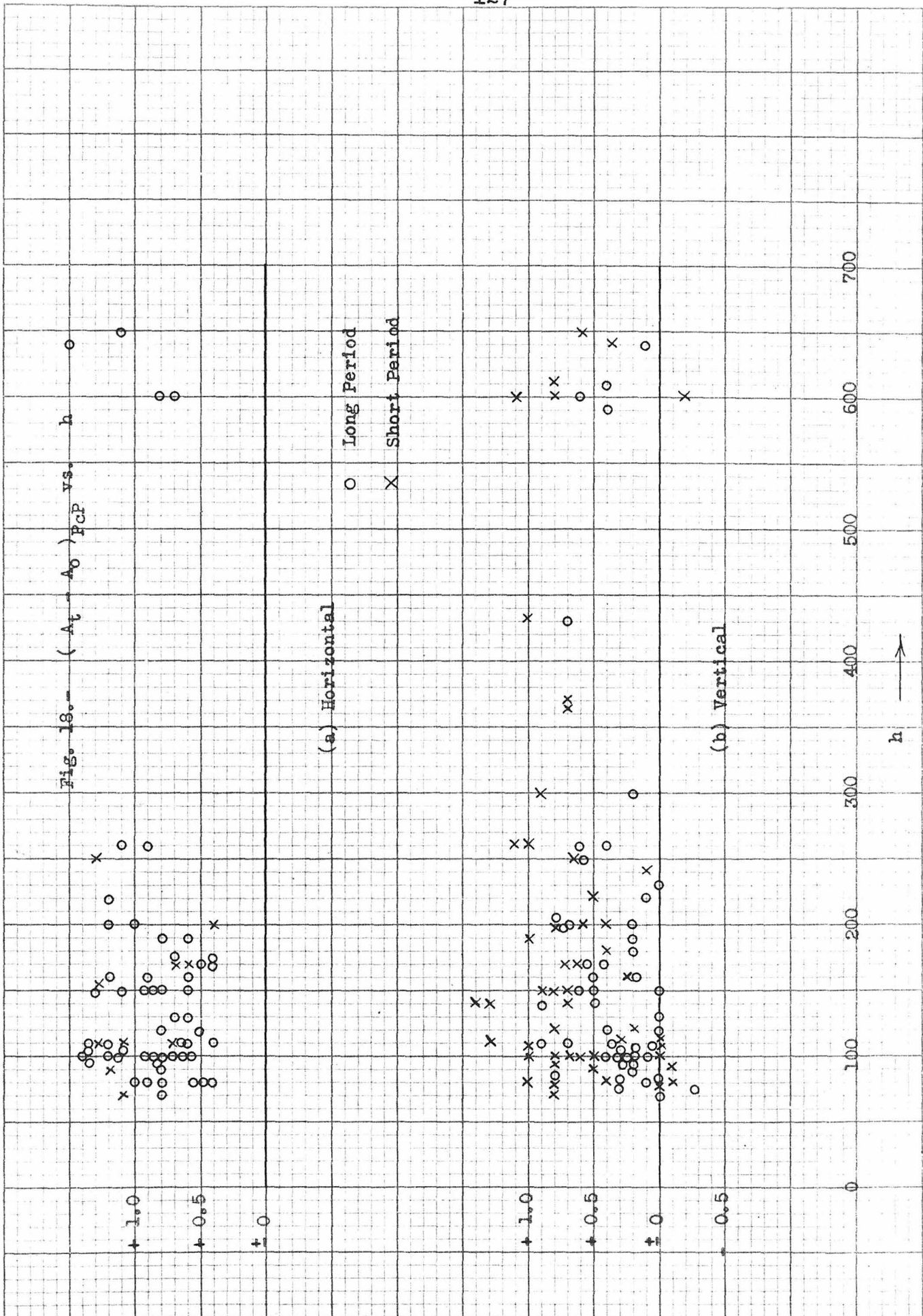
Fig. 18. - $(A_t - A_0)_{PCP}$ v.s. h 

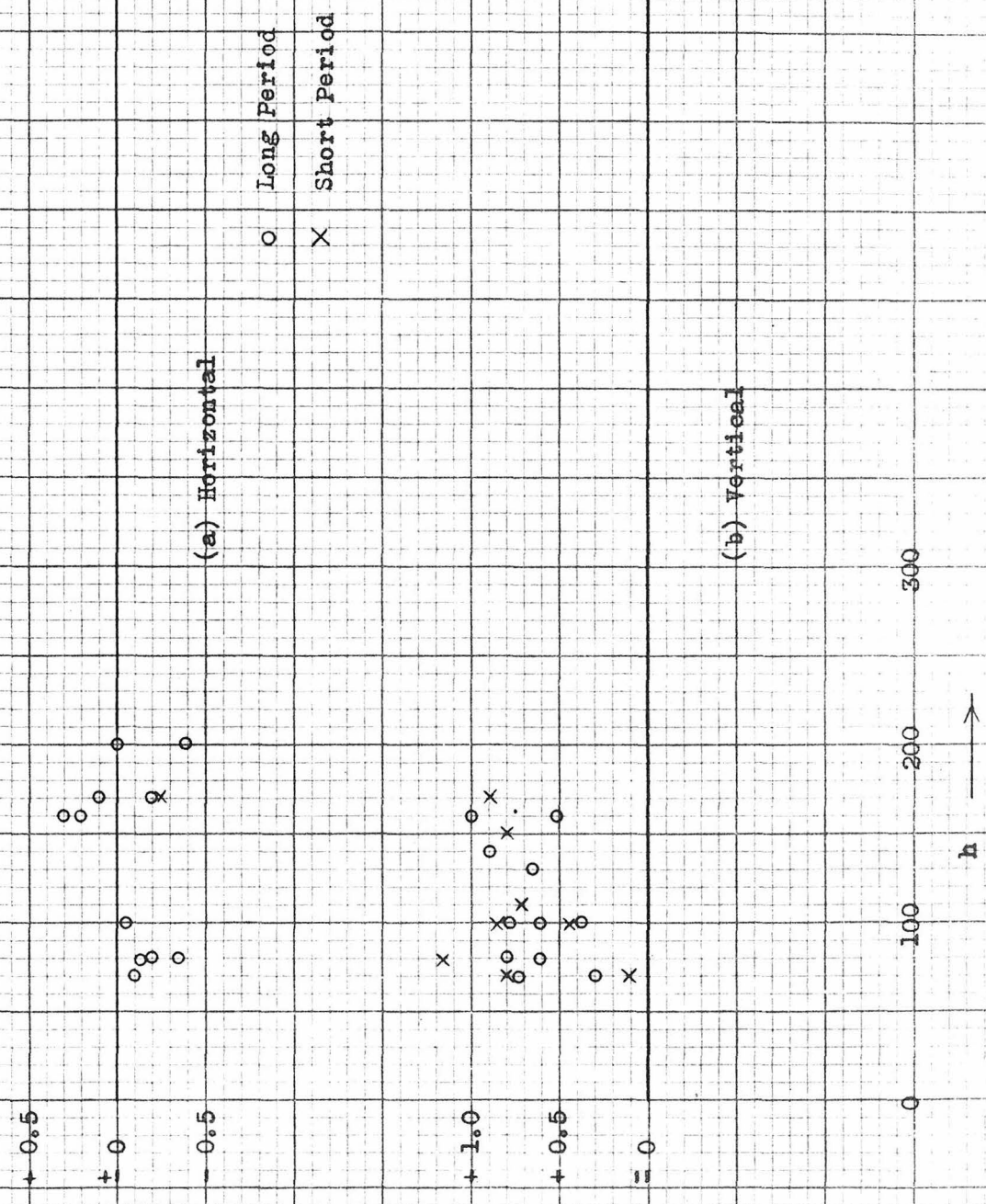
FIG. 19.- $(A_t - A_0)_{Pcs}$ vs. h 

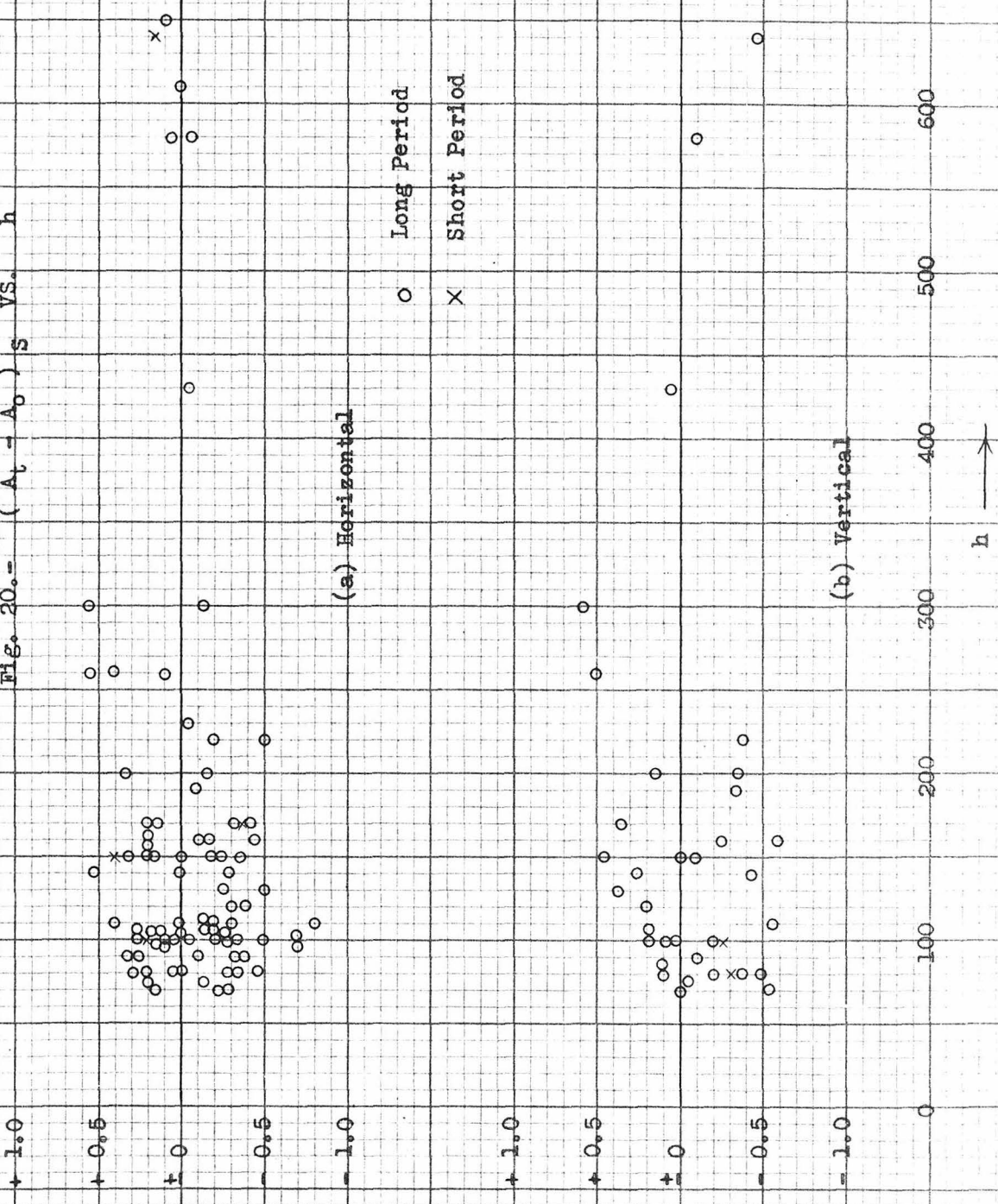
FIG. 20.- $(A_t - A_0)_S$ VS. h 

Fig. 21.0 - $(A_t - A_0)_{SCS}$ vs. h

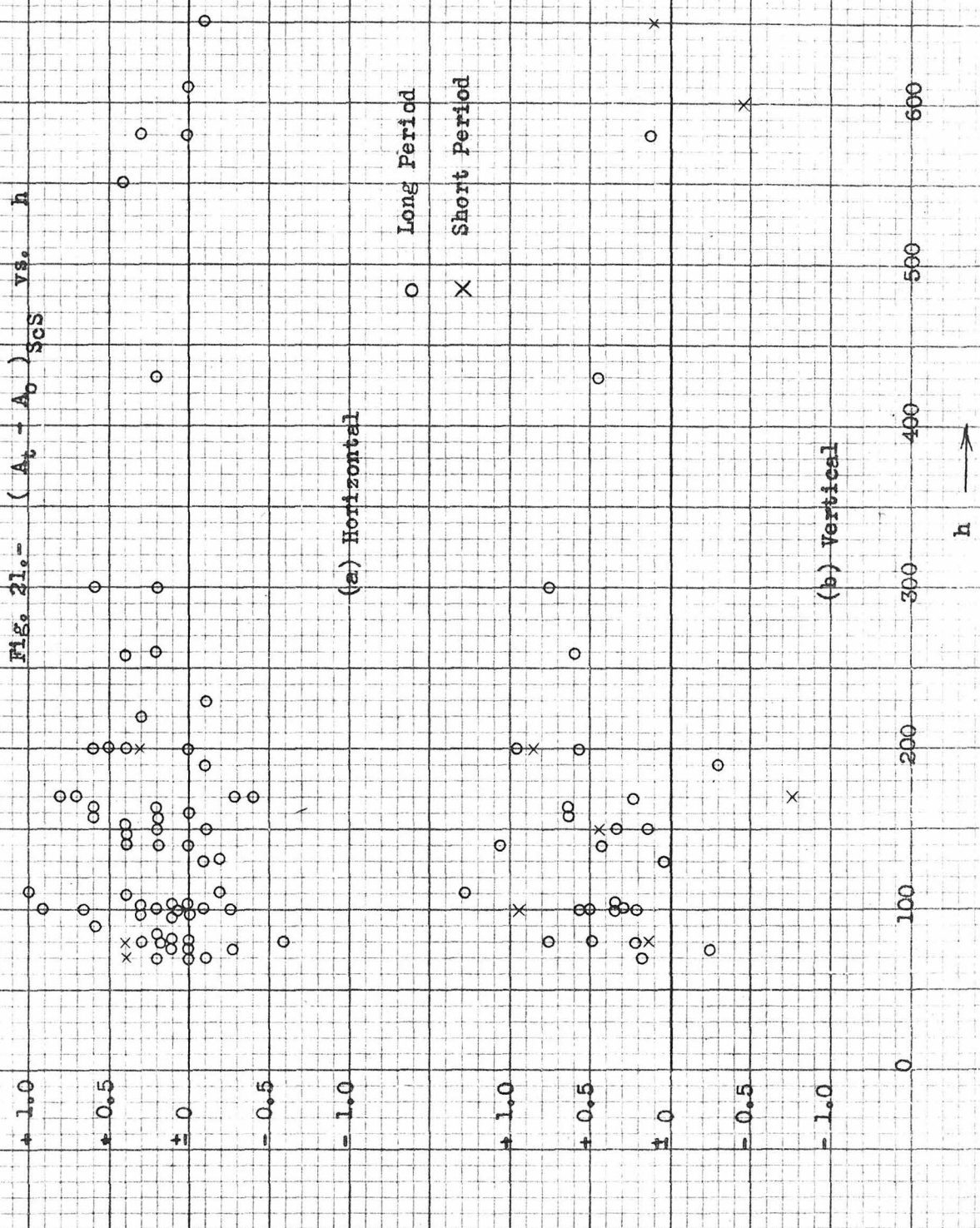
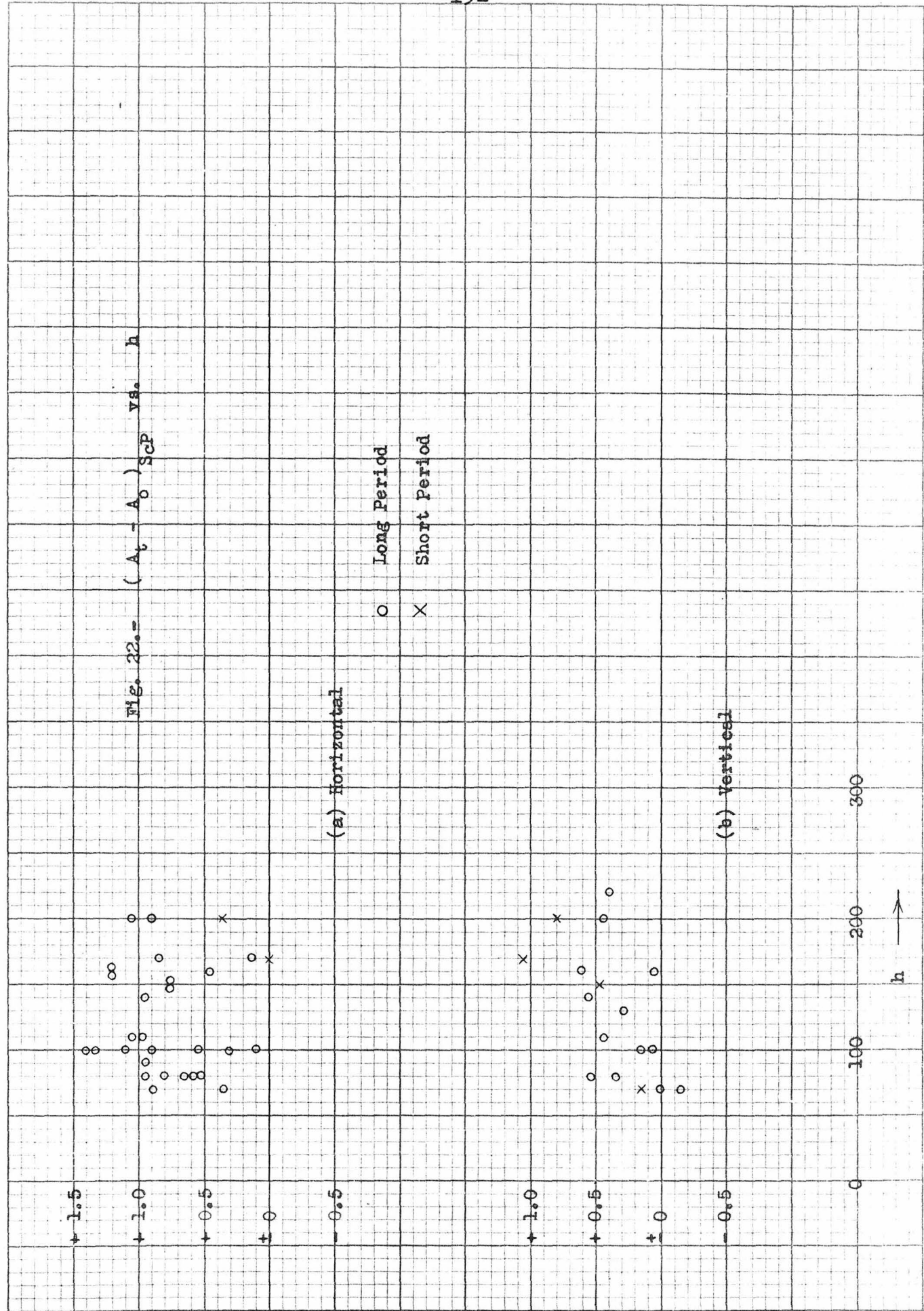
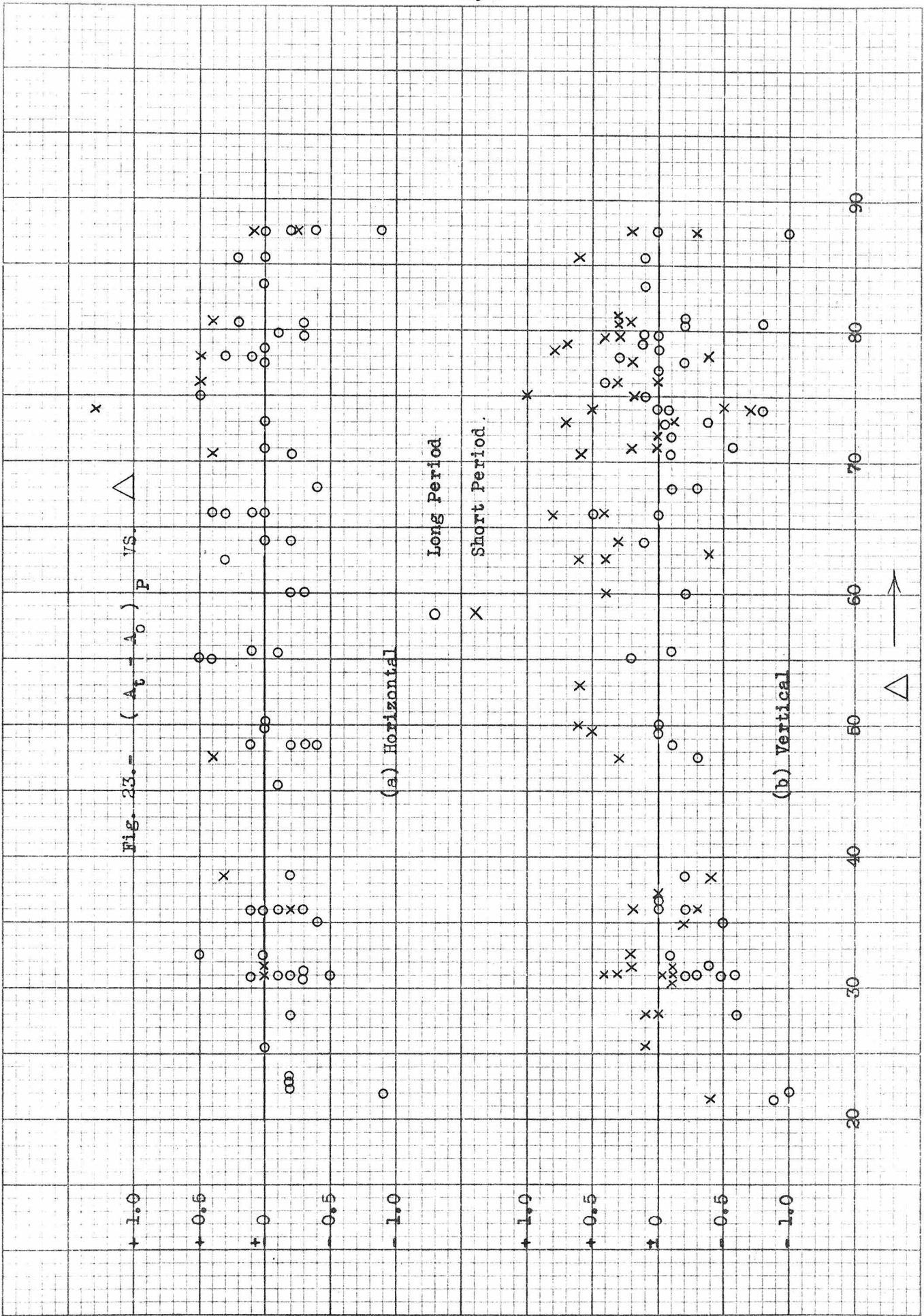
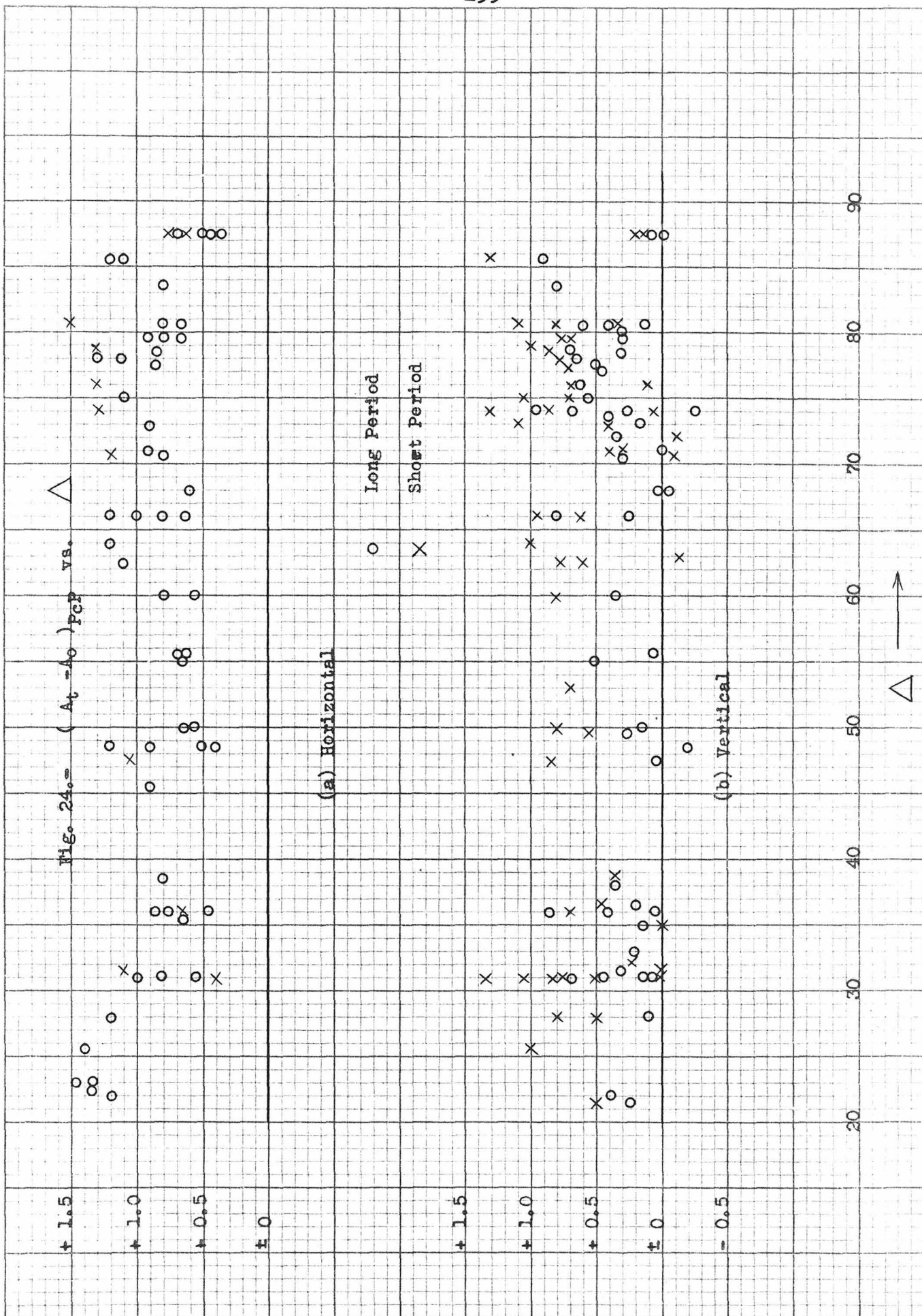


Fig. 22. $(A_t - A_0)_{SCP}$ vs. h 





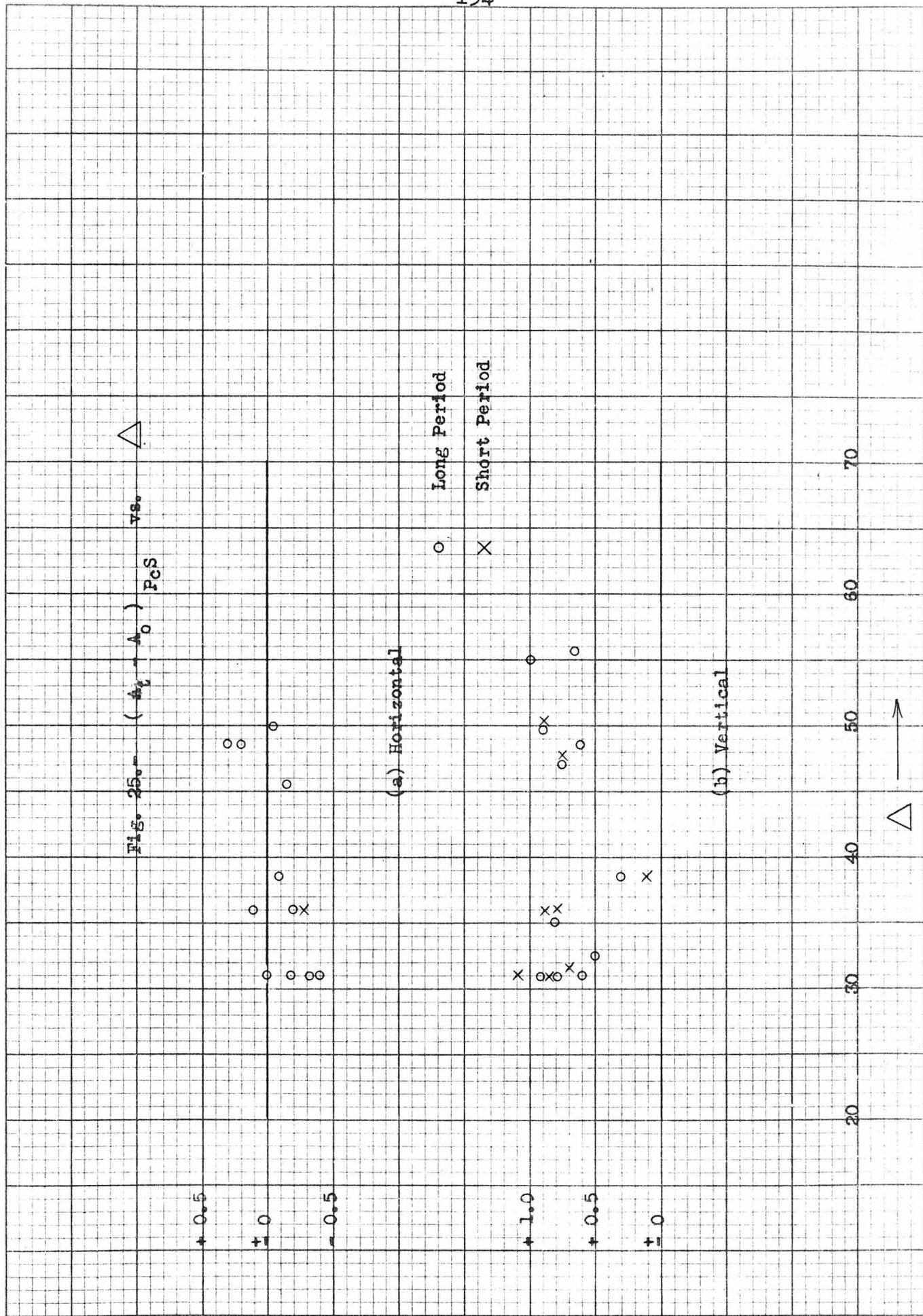


Fig. 26o - $(A_t - A_0)_S \nabla S_o$



1.0

0.5

+ 0.5

- 0.5

- 1.0

1.0

0.5

+ 0.5

- 0.5

- 1.0

(a) Horizontal

1.0

0.5

+ 0.5

- 0.5

- 1.0

○ Long Period

X Short Period

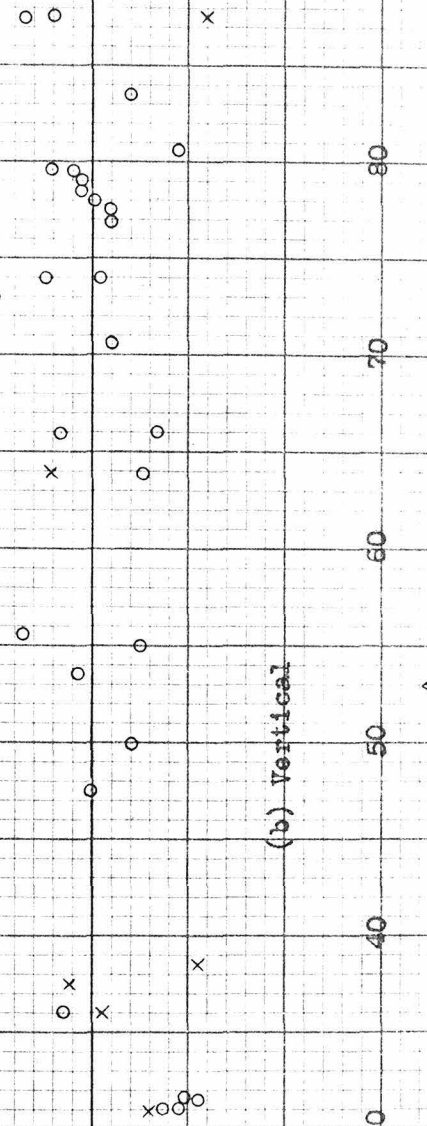
1.0

0.5

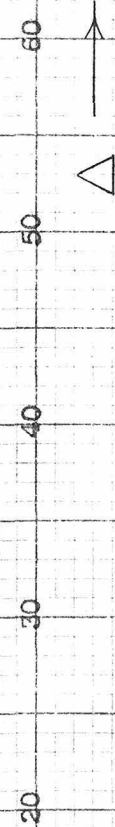
+ 0.5

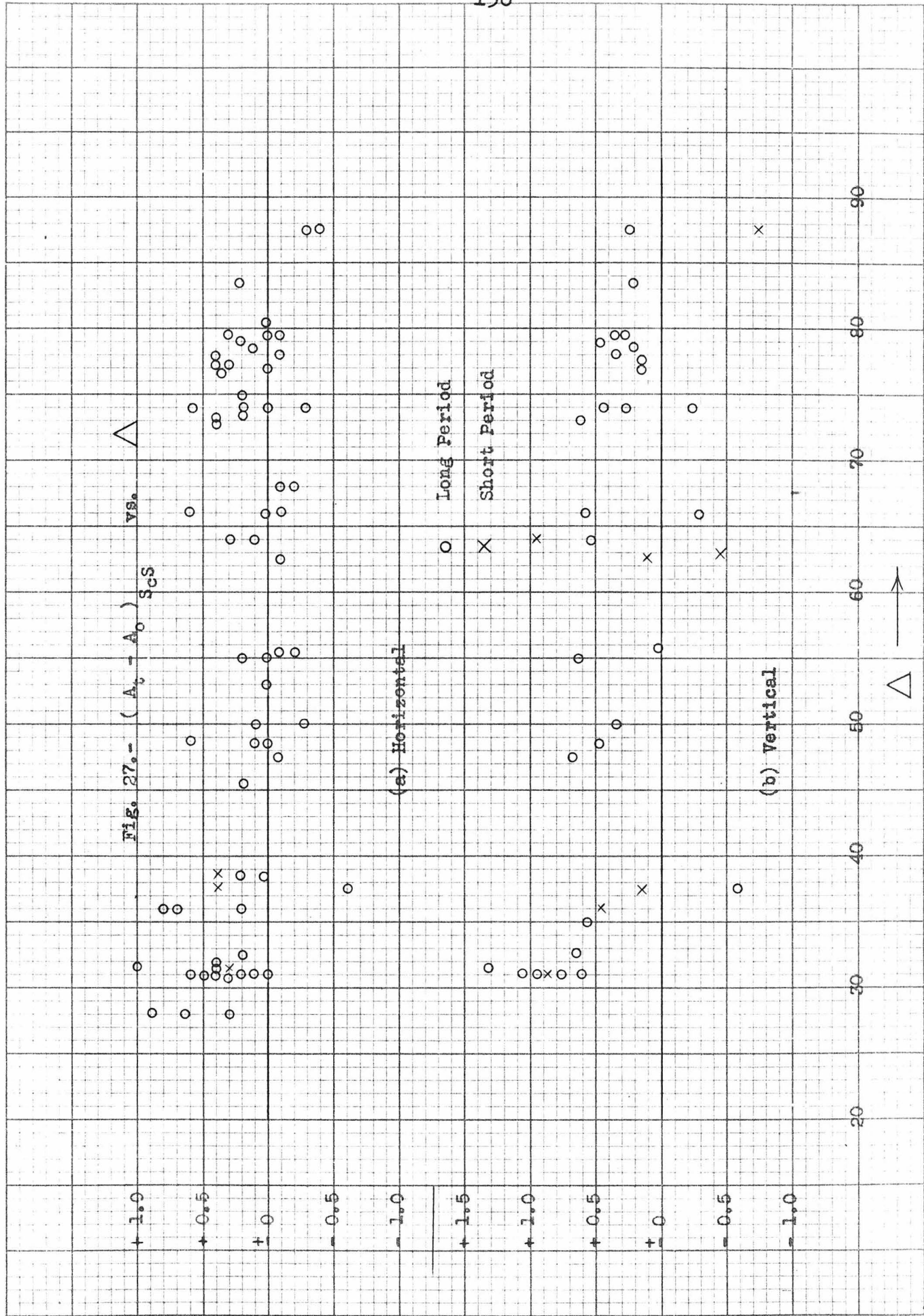
- 0.5

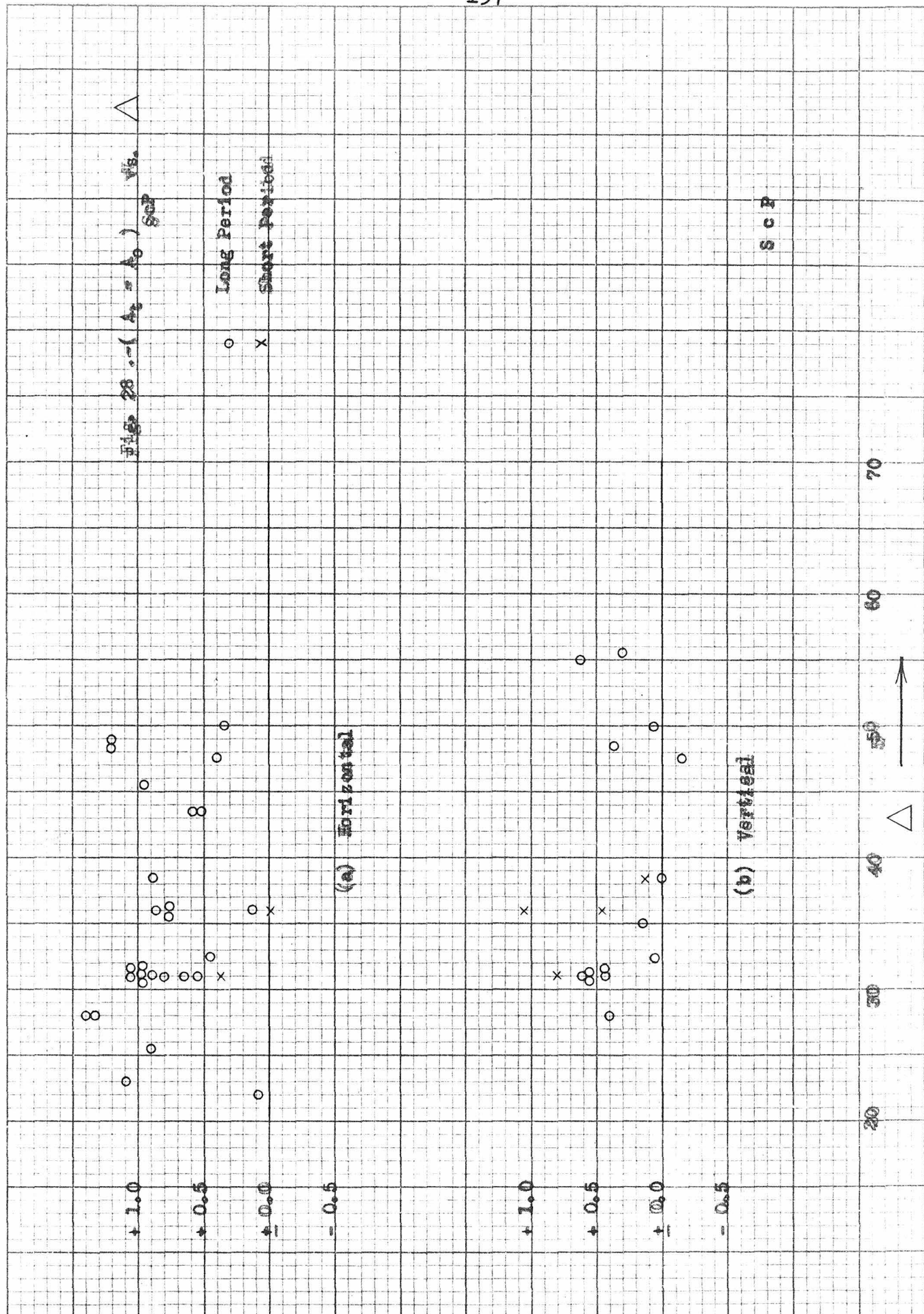
- 1.0



(b) Vertical







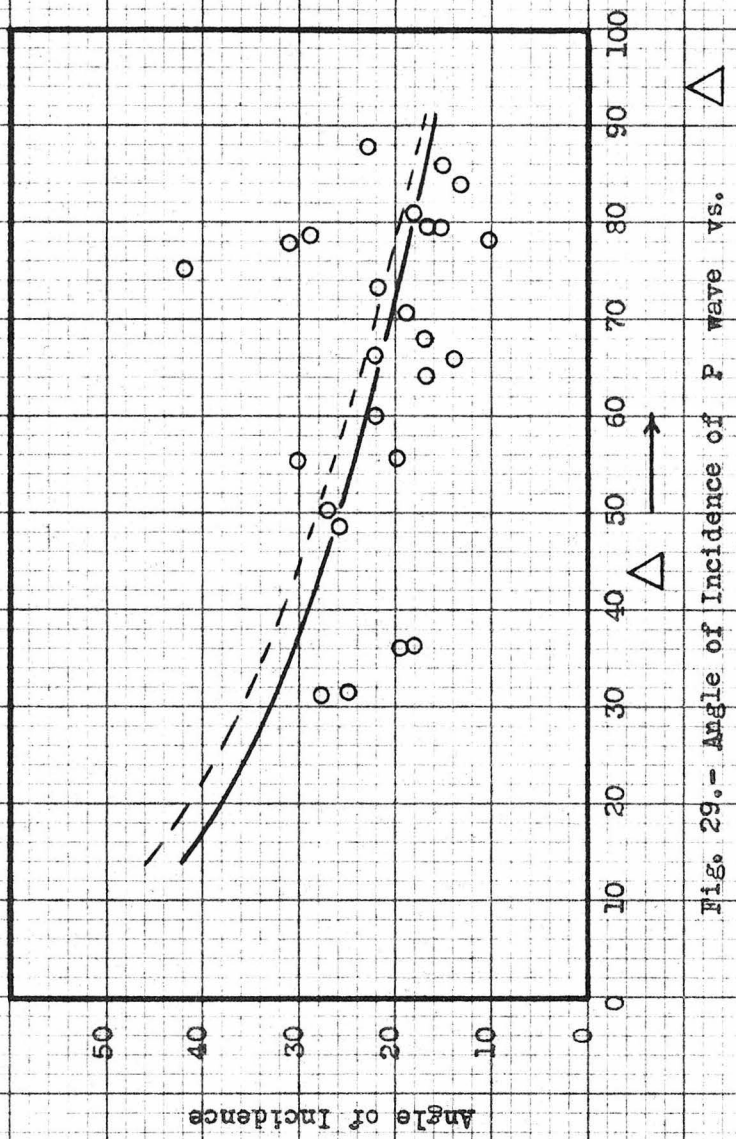
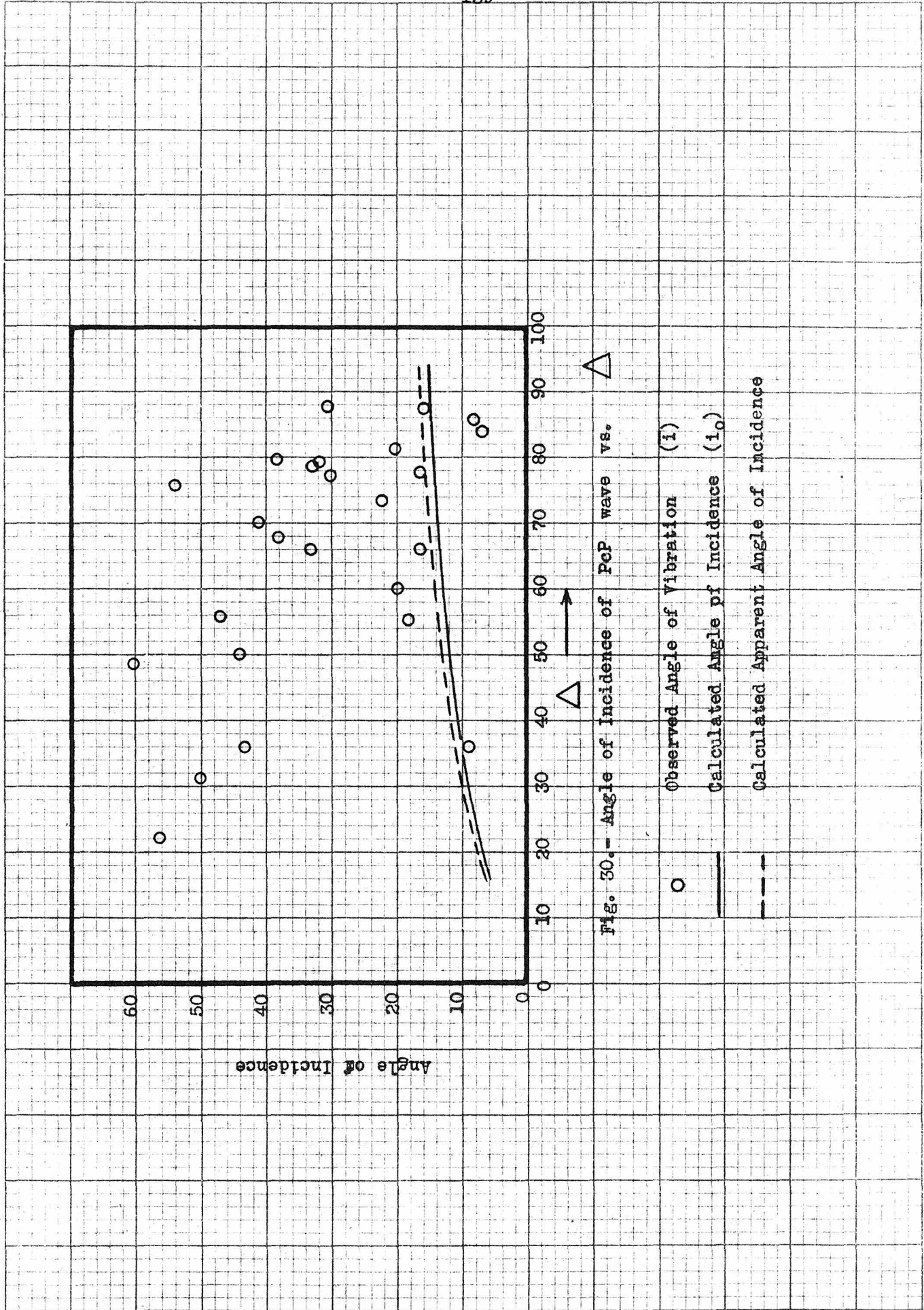


Fig. 29.- Angle of Incidence of P wave vs.

○ Observed Angle of Vibration (\bar{I}_1)
 — Calculated Angle of Incidence (I_{10})
 - - - Calculated Apparent Angle of Incidence



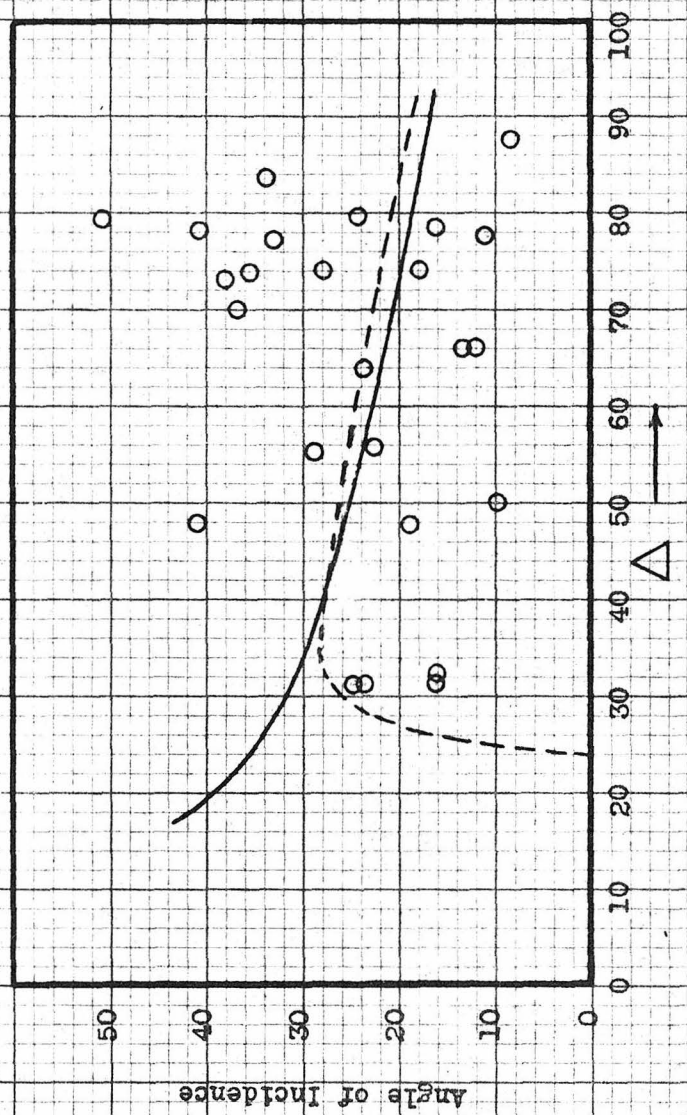


Fig. 31.- Angle of Incidence of S wave vs. Δ

○ Observed Angle of Vibration ($\theta_{\bar{4}}$)
 — Calculated Angle of Incidence ($i_{\bar{1}}$)
 - - - Calculated Apparent Angle of Incidence ($i_{\bar{0}}$)

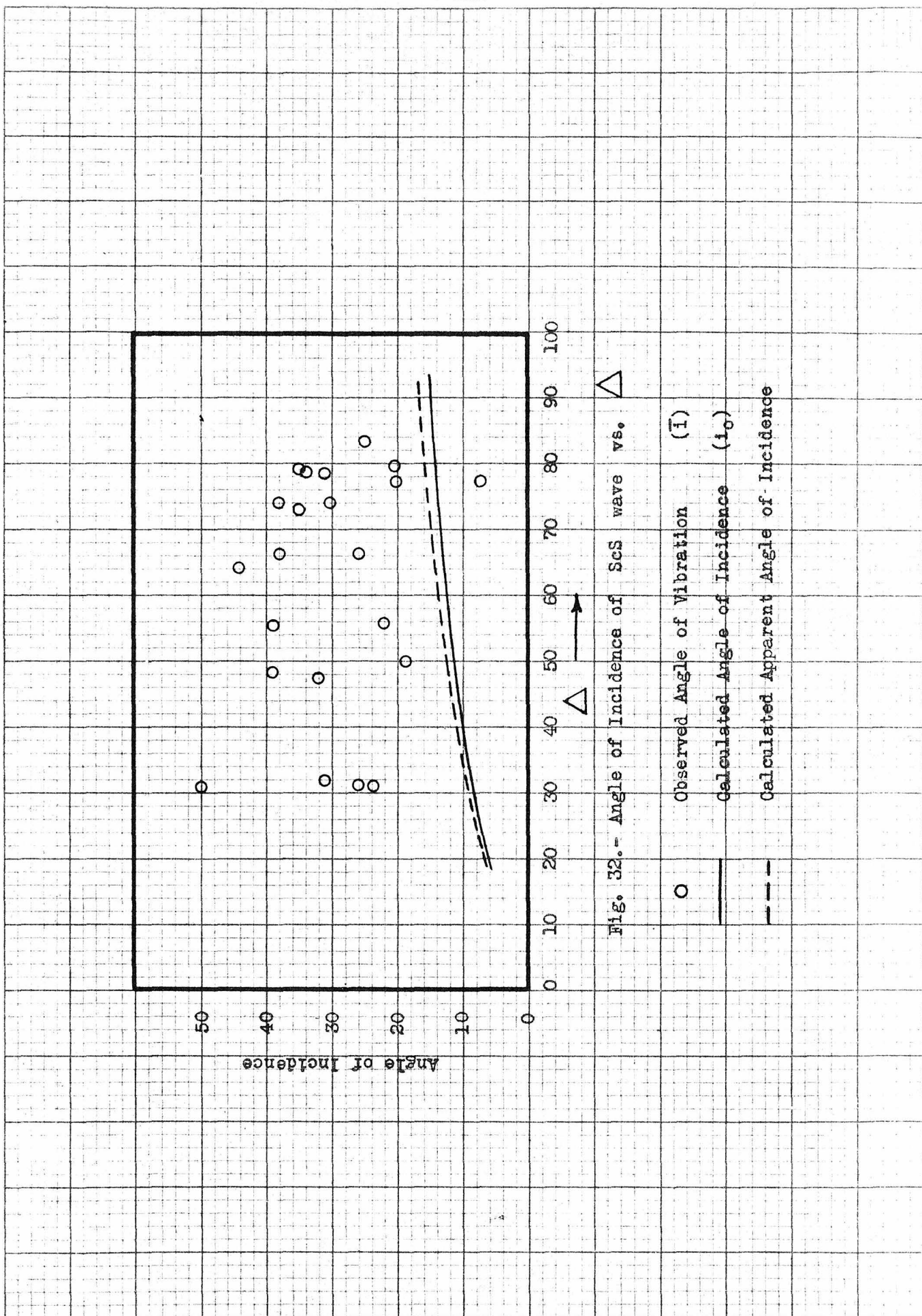


FIG. 32.- Angle of Incidence of SCS wave vs. Δ .

